DEVELOPMENT OF COMPOSITE HYDROGEL BASED BIOSENSORS USING NANOFILM BOUND BIOACTIVE MICRODOMAINS

A Dissertation

by

ANIKET BISWAS

Submitted to the Office of Graduate and Professional Studies of
Texas A&M University
in partial fulfillment of the requirements for the degree of

DOCTOR OF PHILOSOPHY

Chair of Committee,	Michael J. McShane
Committee Members,	Melissa A. Grunlan
	Akhilesh K. Gaharwar
	Victor M. Ugaz
Head of Department,	Michael J. McShane

December 2017

Major Subject: Biomedical Engineering

Copyright 2017 Aniket Biswas

ABSTRACT

Composite materials have recently been introduced as versatile systems for embedding functional microdomains within moldable hydrogels. Potential applications for these materials include optical biosensing, drug delivery, and anti-corrosion agent releasing smart coatings, wherein the microdomains comprise regions that contain active molecules bound by nanofilms that possess precisely-tailored transport properties.

In this work, composite hydrogels are investigated as sensing materials, with a focus on controlling analyte permeation into the internal microdomains. Transport of glucose across cross-linked PAH [poly (allylamine hydrochloride)] / PSS [poly (sodium 4-styrenesulfonate)] bilayers deposited on planar substrates was studied to evaluate the potential of ultrathin films to limit small-molecule diffusion. The nanofilm design was translated onto calcium carbonate colloidal templates to fabricate hydrogels that contain functional microdomains in order to demonstrate a "tunable" enzymatic biosensor. By varying the number of cross-linked and non-cross-linked bilayers deposited, the response characteristics of the hydrogel based sensors were successfully modulated; however, these sensors exhibited poor stability, prohibiting long term use.

Alginate microparticles containing either glucose sensing or lactate sensing chemistry coated with similar nanofilms were explored as an alternative colloidal template. Response of both glucose and lactate sensing hydrogels fabricated using alginate microparticles was evaluated at ambient oxygen levels and physiologically relevant low oxygen concentrations; this work demonstrated the operation of hydrogel

based enzymatic sensors at *in vivo* oxygen levels for the first time. Additionally, these sensors showed exceptional stability when used continuously, supporting their potential as long term implantable sensors. Furthermore, cooperative effect between biosensing micro- and macro- domains was carefully examined to study the limits of hydrogel based sensors for multiplexed and multianalyte sensing. Additionally, novel gold nanocluster containing microcapsules were explored as hydrogen peroxide sensors for potential coimmobilization in composite hydrogel based enzymatic sensors to monitor levels of hydrogen peroxide release over time; hydrogen peroxide is a byproduct produced in enzymatic glucose and lactate sensors that causes sensor failure.

The results demonstrate significant advances in the field of fully implantable composite hydrogel based devices; especially methods to control the permeation of analytes into bioactive microdomains in order to obtain stable sensor response at physiologically low oxygen levels. The knowledge gained from this study will serve as a guide to fine-tune and optimize composite biosensing hydrogels, after gaining additional information post-implantation in animal models.

ACKNOWLEDGEMENTS

I would like to thank my committee chair, Dr. McShane, for his continuous guidance and support throughout my tenure at Texas A&M University. I would also like to thank my committee members, Dr. Grunlan, Dr. Gaharwar, and Dr. Ugaz, for their support throughout the course of this research.

I acknowledge current and past members of the BioSym lab for their encouragement. In particular, I would like to thank Dr. Ashvin Nagaraja for teaching me research principles and for assisting me to develop both personally and professionally. I would like to extend my gratitude to Yil-Hwan You for SEM imaging and for having numerous helpful discussions with me. I would like to thank Lindsey Bornhoeft for her extensive contributions towards fabricating nanofilm coated alginate microparticles. I would also like to thank Dr. Swayoma Banerjee for confocal imaging. Finally, I would like to thank Maria Lyons for her assistance and for making life at graduate school a lot easier.

CONTRIBUTORS AND FUNDING SOURCES

Contributors

The work described in this dissertation was supervised by a committee consisting of Dr. McShane [advisor], Dr. Grunlan, and Dr. Gaharwar of the Department of Biomedical Engineering, and Dr. Ugaz of the Department of Chemical Engineering.

All scanning electron micrographs (figures 6, 7, and 18B) and confocal micrographs (figures 8,18C, 26, 36D, 36E, 36F, A2, A3A, and A4) were captured by Yil-Hwan You and Dr. Swayoma Banerjee respectively. The darkfield and hyperspectral images (figure 13) were captured by Byron Cheatham (CytoViva, Inc.). Nanofilm coated alginate particles used in Section 4 and Section 5 were fabricated by Lindsey Bornhoeft.

All other work conducted for the dissertation was completed by the author independently.

Funding Sources

This work was supported by the National Science Foundation (grant nos. 1066928, 1258696, and 1403002).

TABLE OF CONTENTS

Page

LIST OF FIGURES

Page

LIST OF TABLES

Page

1. INTRODUCTION

Chronic diseases have become one of the major causes of disability and death, with over 50% of the United States' adult population afflicted with one or more chronic conditions.[1] Cardiovascular diseases, cancer, obesity, diabetes, malignant neoplasms, and cerebrovascular diseases are some of the most common chronic conditions.[2] The financial burden of these diseases is tremendous with over 86% of healthcare dollars spent; cancer, heart conditions, and diabetes being the top contributors to healthcare spending.[3] There are a few key risk factors that contribute to these diseases, which include lack of physical activity, poor diet, tobacco use, excessive alcohol consumption, and uncontrolled hyperlipidemia and hypertension. [4, 5] Many of the risk factors and the resulting ailments can be addressed through policy changes, community programs, educational sessions, and technological innovations for monitoring biomarkers. Continuously monitoring biomolecules characteristic to chronic conditions using implantable biosensors can potentially mitigate the progression of such diseases and assist in better disease management especially when coupled with corrective therapeutic measures.

Invention of the Clark and Lyon's electrode based sensors marked the beginning of an era of biosensing.[6] Most of the biosensors had been initially used for laboratory purposes but with advances in commercial manufacturing and with active interest from big diagnostic and pharmaceutical companies, home-based consumer use of biosensors have become increasingly popular leading to over $13 billion US dollars in revenue.[7]

Glucose biosensors in particular dominate the biosensor market and are responsible for over 85% of the market share.[7] The most common method of home-based glucose sensing involves measuring blood glucose levels from blood drawn using a small lancet. Although this finger-prick method is highly sensitive and specific to glucose, it is marred by certain drawbacks. The finger-prick method only allows discrete glucose measurements revealing only a partial picture of diurnal glucose fluctuations that might lead to inaccurate therapeutic counter measures potentially resulting in life threatening glucose levels. Tracking glucose levels continuously using subcutaneous implantable sensors offer a better and more effective means to manage diabetes. Several such Food and Drug Administration (FDA) approved implantable electrode-based sensors have been commercialized.[8] However, the longevity of these needle-type implantable sensors are short lived requiring frequent replacements by users. This is primarily due to implant induced foreign body response, ultimately leading to complete sensor failure within a week of operation.[9]

Alternatively, hydrogel based fully implantable biosensing devices may be used for continuous biomarker tracking. Soft hydrogel based biosensors can potentially circumvent the problems associated with needle-type implantable sensors including repetitive tissue trauma, infections, and fibrous capsule induced sensor failure.[10, 11] Implanted hydrogels serve a dual purpose of housing sensing elements and of providing a biocompatible interface to minimize host response. However, it is imperative to consider the tradeoff between biocompatibility and analyte response characteristics. These biosensors are enzyme based catalytic devices that rely on the consumption of

glucose; therefore, any attempt to modify the hydrogel matrix to improve biocompatibility can adversely affect the passage of analytes making it extremely difficult to generate a reliable sensor response. Nevertheless, biocompatibility and analyte flux can be dealt with independently by segregating the sensing chemistry into micro-sized, nanofilm lined, bioactive domains that are then dispersed in an outer hydrogel matrix.

This unique hydrogel based nanocomposite architecture has been demonstrated for use as optical oxygen sensors using encapsulated phosphorescent dye.[12] Theoretically inclusion of an oxidoreductase enzyme (*e.g.* glucose oxidase, lactate oxidase) along with oxygen sensitive phosphors within nanofilm lined microdomains can transform these hydrogels into optical enzymatic sensors. However, the nanofilm design and composition requires special optimization specific to each analyte of interest. The high surface area to volume ratio of these microdomains makes the prevention of substrate diffusion challenging, as diffusion lengths are on the orders of nanometers. Furthermore, these devices depend upon local oxygen levels; as *in vivo* oxygen concentration is four times lower than ambient levels it makes analyte transport requirements even more stringent. Properly designed, these hydrogel based devices can be used as multianalyte and multiplexed sensors.

This dissertation has been organized to describe the development of novel hydrogel based enzymatic sensors for single analyte and multianalyte sensing. Section 2 provides a general background about glucose monitoring, particularly using enzymatic biosensors. Section 3 describes the use of crosslinked nanofilms to control the

permeation of glucose into composite hydrogel based glucose sensors, in order to manipulate the sensor's range and sensitivity; portions of this section have been published in *RSC Advances*. Section 4 and Section 5 explains the development of nanofilm bound alginate microsphere based composite hydrogels for stable detection of glucose and lactate at low physiological oxygen concentrations respectively. Portions of Section 4 have been published in *MDPI Biosensors*. Section 6 discusses and demonstrates the limitations and uses of composite hydrogel based enzymatic sensors for multianalyte and multiplexed sensing. Section 7 describes the development of a new method to fabricate gold nanocluster containing optical microcapsule sensors for hydrogen peroxide detection, which can be potentially used to monitor enzymatic reactions in hydrogel based biosensors; these microcapsules can also be used for intracellular hydrogen peroxide sensing that has been demonstrated and described in Appendix A. Portions of Section 7 and Appendix A have been published in *ACS Omega*. Finally, Section 8 discusses the major conclusion, limitations, and possible future direction.

2. BACKGROUND

2.1. Diabetes

Diabetes is a chronic condition characterized by the body's inability to regulate physiological blood glucose levels. An estimated 422 million adults globally and almost a tenth (~ 9.3%) of the US population are affected by diabetes; accounting for over $240 billion in healthcare costs in the US (2012).[13, 14] Insufficient production of insulin (a hormone that lowers blood glucose levels) or failure to successfully utilize insulin leads to diabetes. Type 1 diabetes is characterized by destruction of pancreatic beta cells by the body's immune system; beta cells are specialized cells that produce insulin. Type 1 diabetes is largely considered as a genetic disorder that is triggered by environmental factors. Type 2 diabetes is the most prevalent form and is due to insulin resistance, a situation where muscle, liver, and fat cells cannot efficiently utilize insulin. A combination of unhealthy lifestyle, lack of physical activity, and genetic predisposition contributes to Type 2 diabetes. Gestational diabetes is another common form of diabetes caused by insulin resistance that affects women during pregnancy. Uncontrolled and without proper management, diabetes can lead to life threatening circumstances over time. For example, incorrect medication dosage, stress, and exhaustion can decrease blood glucose (hypoglycemia) to dangerously low levels that might lead to loss of consciousness, seizures, or even coma. Hyperglycemia, on the other hand can trigger potentially fatal ketoacidosis or hyperosmolar coma. Additionally, sustained hyperglycemia can cause irreversible damage to nerves, kidneys, eyes, and heart.[15]

2.2. Monitoring diabetes

Proper control and management of blood glucose can prevent the progression of diabetes and its associated secondary complications. Effective glycemic control requires measuring blood glucose at regular intervals coupled with orally administered drugs (*e.g.* metformin, gliclazide) or injected insulin to maintain normal glucose levels (80 – 130 mg/dL). The most common method of home glucose monitoring involves drawing a drop of blood from the patient's fingertip using a lancet, followed by transferring the blood onto a disposable test strip that is ultimately inserted into a glucose meter to calculate glucose concentration. Although these devices are extremely accurate [16] they are unable to track changes in glucose throughout the day due to patient noncompliance. Cost of supplies and pain aversion are the main reasons that contribute to patient noncompliance. Thus, fully implantable continuous monitoring sensors provide a better alternative that does not require frequent manual measurements.

2.2.1. Commercially available continuous glucose monitoring system

Commercial available continuous glucose monitoring systems (CGMSs) consist of a tiny implantable metallic electrode coated with immobilized glucose oxidase (GOx); GOx catalyzes glucose to produce hydrogen peroxide that is amperometrically detected by the electrode.[17] These devices measure glucose every 1 – 5 min providing real-time information and therefore help preventing frequent episodes of hyperglycemia or hypoglycemia.[18, 19] Additionally, CGMSs have long term benefits of lowering HbA1c (glycated hemoglobin) levels.[20] Currently there are four FDA approved CGMSs

available to US consumers manufactured by Dexcom and Medtronic. Additionally, remote monitoring capability in CGMSs has been an emerging feature and can transform diabetes care; these devices can wirelessly transmit real-time data to physicians or relatives allowing even tighter glycemic control. [21, 22]

2.2.2. Foreign body response (FBR)

Foreign body response is the body's innate inflammatory response to an implanted sensor that ultimately leads to complete sensor failure. As soon as the device is implanted it causes local wounding and comes in contact with the host physiology initiating inflammation. The inflammatory response starts with accumulation of coagulated proteins and platelets, and progresses with the recruitment of inflammatory cells eventually leading to fibrosis. Inflammation may either lead to damage of sensor components or formation of a fibrous biomembrane that encapsulates the sensor. In order to be detected accurately an analyte should have unhindered access to the implanted sensor. However, formation of a biofouling membrane limits diffusion of the analyte of interest decreasing sensor performance over time eventually causing total sensor failure.[23] Although frequent calibrations may compensate for reduced sensor performance,[24] most sensors fail within 3 – 7 days.[9]

A number of strategies may be used to combat FBR and prolong a sensor's operational lifetime. The most common methods to extend a sensor's longevity involve coating the sensor surface with a biocompatible material (*e.g.* tetraglyme, phospholipid, albumin, hydrogel overlays, Nafion), manipulating the implanted sensor's surface

topology, or *via* the release of anti-inflammatory drugs (*e.g.* dexamethasone, nitric oxide).[25] Alternatively, completely hydrogel based fully implantable sensors that preclude the use of metallic electrodes have been gaining interest over the years. Owing to their low biofouling and biomimetic properties FBR is minimal[23, 26] engendering the use of hydrogels in the form of fibers, microparticles, and slabs [27-29] as biosensors.

2.3. Optical sensing

Advances in optical spectroscopy and optics instrumentation has led to rapid development of several optical sensing technologies that have been used for process control, remote sensing, and biomedical applications.[30] Optical sensors function *via* registering changes in at least one of the several optical parameters (refractive index polarization, scattering, reflectance, absorbance, fluorescence) in response to the analyte of interest. Infrared absorption spectroscopy,[31] thermal infrared measurements,[32] Raman scattering,[33] polarimetry,[34] and coherence tomography[35] are some of the non-invasive techniques that have been explored for use in glucose sensing. However, none of these methods have been successfully translated for commercial use due to their low signal-to-noise ratio and poor selectivity.[35] Fluorescence based techniques are highly sensitive and specific, offering a superior alternative. Unlike other methods, fluorescent based sensors are not affected by changes in intrinsic scattering or absorption properties of glucose. Moreover, the ready availability of cheap visible light emitting diodes and highly sensitive photodetectors have led to increased interest focused on developing fluorescent methods for sensing glucose and other relevant biomarkers. These sensors can be further

classified as bioaffinity or biocatalytic sensors based on their mode of glucose recognition.[36]

2.3.1. Bioaffinity based sensors

Bioaffinity sensors reversibly bind to an analyte of interest and produce a change in optical signal that is ultimately used to detect fluctuations in analyte concentration. A single fluorescent dye or a pair of fluorescent dyes can be employed to monitor such analyte mediated binding events.[37] Different receptors have been investigated to develop affinity based sensors; the most commonly used glucose receptors include apo-glucose oxidase,[38] glucose binding protein[39] and boronic acid derivatives.[40, 41] A subset of bioaffinity sensors are based upon competitive binding of a ligand (analyte) and a ligand analogue, to a ligand receptor; for example competitive binding of glucose and dextran to concanavalin A has been thoroughly studied for glucose sensing.[36, 42] Affinity based systems are independent of analyte diffusion rates, substrate consumption, or detrimental product formation making them attractive candidates for sensing. However, long term *in vivo* use of most of these systems with the exception of boronic acid derivatives are limited due to conformational instability over time. Senseonics recently demonstrated diboronic acid based highly sensitive and extremely accurate continuous glucose sensing in humans that lasted for 3 months.[43]

2.3.2. Biocatalytic (Enzymatic) sensors

Biocatalytic sensors are the most common forms of sensors that utilize either glucose oxidase or glucose dehydrogenase as the bioactive element to catalyze glucose. The sensing scheme may be direct or indirect; indirect sensing measures changes in pH, oxygen, or H_2O_2 with increase in glucose.

2.3.2.1. Direct sensing

Enzymatic optical sensors typically detect analyte levels indirectly by monitoring cosubstrate consumption or by-product formation; however, there are a few examples of direct fluorescence based enzymatic sensing. Direct enzymatic optical sensing utilizes either the intrinsic fluorescence of the analyte-catalyzing enzyme or the fluorescent properties of a probe attached to the enzyme. Hussain *et al.* demonstrated direct glucose sensing using intrinsic fluorescence of yeast hexokinase; hexokinase has inherent UV-fluorescence (excitation/emission at 295/330 nm) that is quenched in the presence of glucose. [44] Similarly, the fluorescence of flavin adenine dinucleotide (FAD) has been used for glucose sensing.[45, 46] FAD is a coenzyme of GOx, with strong green fluorescence (excitation/emission at 450/520 nm) that increases with glucose addition. Glucose dehydrogenase (GDH) was also reported for direct glucose sensing, where the blue fluorescence (excitation/emission at 340/460 nm) of its cosubstrate nicotinamide adenine dinucleotide (NADH) linearly increased with glucose.[47] Although these methods do not require the additional step of tagging the glucose-converting enzyme with a fluorescent probe, they are marred by low sensitivity and low signal-to-noise ratio

issues. These issues can be circumvented by attaching highly fluorescent probes to the enzymes. GOx has been derivatized with different fluorescent molecules for direct sensing applications. Coumarin tagged GOx has been shown to be responsive to glucose; GOx-coumarin's blue fluorescence increases with rise in glucose levels.[48] Alternatively, fluorescein labelled GOx that takes advantage of energy transfer between fluorescein and GOx's FAD group has also been demonstrated for sensing glucose.[49, 50]

2.3.2.2. Indirect sensing

Indirect enzymatic sensing consists of tracking co-substrates consumed or by-products formed as a result of enzymatic reactions. The enzymes involved are usually oxido-reductase in nature that catalyze reactions with high specificity, producing products or consuming reactants that can be detected using optical transducers. Such sensors have been developed for the detection of different bioanalytes (*e.g.* glucose, lactate, cholesterol, urea, ethanol) and have found use across various industries. The most extensively investigated enzymatic sensor oxidizes glucose in the presence of GOx *via* the following reaction: glucose + O_2 + H_2O $\rightarrow$ gluconic acid + H_2O_2. By monitoring the depletion of oxygen or the formation of products (*i.e.* gluconic acid or hydrogen peroxide) glucose concentrations can be indirectly inferred. Gibson *et al*. [51] described this reaction using the following set of reaction equations:

$$\mathrm{GOx_{ox}} + \mathrm{G} \overset{k1}{\rightarrow} \mathrm{GOx_{red}}\,\mathrm{GDL} \overset{\mathrm{k2}}{\rightarrow} \mathrm{GOx_{red}} + \mathrm{GDL}$$

$$\mathrm{GOx_{red}} + \mathrm{O_2} \overset{k3}{\rightarrow} \mathrm{GOx_{ox}H_2O_2} \overset{\mathrm{k4}}{\rightarrow} \mathrm{GOx_{ox}} + \mathrm{H_2O_2}$$

where G, GDL, O_2, H_2O_2, GOx_{ox}, GOx_{red}, and k_n represents glucose, glucono-δ-lactone, oxygen, hydrogen peroxide, oxidized form of GOx, reduced form of GOx, and the reaction rates respectively. Similarly, optical transduction can also be used to enzymatically detect lactate using lactate oxidase (lactate + O_2 + lactate oxidase + H_2O → pyruvate + H_2O_2). The kinetics of this reaction can also be represented by the following:

$$\mathrm{LOx_{ox}} + \mathrm{L} \overset{k1}{\rightarrow} \mathrm{LOx_{red}}\ \mathrm{pyruvate} \overset{\mathrm{k2}}{\rightarrow} \mathrm{LOx_{red}} + \mathrm{pyruvate}$$

$$\mathrm{LOx_{red}} + \mathrm{O_2} \overset{k3}{\rightarrow} \mathrm{LOx_{ox}H_2O_2} \overset{\mathrm{k4}}{\rightarrow} \mathrm{LOx_{ox}} + \mathrm{H_2O_2}$$

where L, O_2, H_2O_2, LOx_{ox}, LOx_{red}, and k_n represents lactate, oxygen, hydrogen peroxide, oxidized form of lactate oxidase, reduced form of lactate oxidase, and the reaction rates respectively.

2.3.2.2.1. Optical pH transduction

Changes in pH can be optically detected to transduce glucose levels; pH can be detected directly using an optical probe (*e.g.* dye, nanoparticle) or indirectly by monitoring hydrogel swelling kinetics using fluorophores. Hydroxypyrene trisulfonate (HPTS) a pH sensitive dye has been used for the development of optical fiber based and microcapsule based enzymatic glucose sensors.[52, 53] Similarly, fluorescein isothiocyanate (FITC) has also been used as a pH indicator coupled to GOx to fabricate optical fiber based sensors.[54] Recently, soft hydrogel based sensors that indirectly detect glucose using pH sensitive fluorescent dyes and pH sensitive Raman reporters have been

reported by McShane's group.[11, 55] When glucose enters these hydrogels glucose is oxidized by GOx, releasing gluconic acid that can be optically detected by SNARF or mercaptobenzonic acid capped gold nanoparticles. Alternatively, pH can swell or deswell a hydrogel that can be optically tracked and utilized to make enzymatic sensors; rhodamine derivative containing polyacrylamide gels that swell in response to a local decrease in pH uses this principle to detect glucose.[56] Fluorescence based detection of hydrogel swelling has also been demonstrated using energy transfer between tetramethylrhodamine (TRITC) and AlexaFluor 647, co-immobilized in chitosan hydrogel microspheres.[57]

2.3.2.2.2. Optical H_2O_2 transduction

Extremely low physiological H_2O_2 levels, allow H_2O_2 measurements with minimal background in biological samples.[58] In this context, it is worth mentioning that all FDA approved CGMSs available in the market today rely on amperometric detection of H_2O_2 using electrodes. Fluorescence based enzymatic sensing that rely on H_2O_2 fluctuations have also been developed, but are mostly irreversible and have been used as *in vitro* assays. For example, the conversion of non-fluorescent Amplex Red to fluorescent resorufin, was exploited to develop a glucose sensing assay; the H_2O_2 produced *via* GOx mediated glucose catalysis, is converted to superoxide radicals in the presence of a montmorillonite clay coated electrode that in turn reacts with Amplex Red.[59] Additionally, H_2O_2 sensitive quantum dots (QDs) and gold nanoclusters have been used to design irreversible sensing schemes. GOx conjugated to QDs (Mn-doped

zinc sulfide and CdTe) have been reported as glucose nanosensors.[60, 61] Protein capped gold nanoclusters that are sensitive to H_2O_2 have also been used by a number of research groups to develop glucose sensing assays.[62-64] Wolbeis et al. demonstrated the first and only reversible fluorescent H_2O_2 based enzymatic sensing. They reported a hydrogel based sensing system that contains GOx and europium tetracycline (EuTC); EuTC binds reversible to H_2O_2 with an increase in phosphorescence that is used for indirect glucose detection.[65]

2.3.2.2.3. Optical transduction of oxygen

The most widely used method of indirect optical enzymatic sensing, utilizes oxygen sensitive fluorophores. The first report of such a sensor describes the use of an optical fiber coated with two layers: a GOx containing nylon membrane and decacyclene containing silicone layer.[66] Using a blue excitation source, glucose could be easily detected in the range 0.1 – 20 mM with a response time of 1 – 6 min; the response time was further decreased by crosslinking GOx with glutaraldehyde.[67] A fiber optic based flow injection analysis system capable of indirectly detecting glucose and lactate using oxygen sensitive decacyclene was also demonstrated.[68] Although the use of decacyclene was very popular for almost a decade it was rapidly replaced by ruthenium complexes and metallo-porphyrins, owing to their large Stokes' shift, high quantum yield, and long phosphorescence lifetimes. For the first time, ruthenium bipyridyl coupled to silica and immobilized in a GOx containing silicone matrix was demonstrated for use as an optical fiber based sensor.[69] Similarly, other ruthenium complexes (*e.g.* ruthenium

phenanthroline, ruthenium di phenyl phenanthroline) in conjunction with oxido-reducatase enzymes coated on optical fiber tips have also been used to develop sensors.[70-72] This sensing scheme was successfully translated to fabricate implantable subcutaneous sensors; a dual sensor consisting of a glucose responsive unit and an oxygen reference was used to monitor physiological glucose levels (up to 20 mM).[73, 74] A few ruthenium based subcutaneous sensors have also been patented by companies including Becton Dickinson, Minimed Inc., and Baxter.[75-77] Palladium and platinum porphyrins are another major class of oxygen sensitive probes that have been used in enzymatic sensing. These porphyrin dyes offer a better alternative than ruthenium probes because of their higher sensitivity to oxygen and longer excitation/emission wavelengths. Papkovsky demonstrated glucose sensing using optical fibers coated with GOx and platinum porphyrin containing polystyrene membrane; by monitoring changes in phosphorescence lifetime or intensity glucose was detected in the range 0.2 – 20 mM.[78] Bayer successfully patented a similar sensing system based on porphyrin dyes.[79]

2.4. Oxygen indicators

Oxygen sensitive fluorophores are collisionally quenched in the presence of molecular oxygen. Quenching is usually represented by the Stern-Volmer equation:

$$\frac{I_0}{I} = \frac{\tau_0}{\tau} = 1 + k_q \tau_0 [Q] = 1 + K_{SV}[Q]$$

Fluorescence/phosphorescence intensities in the absence and presence of oxygen are denoted by I_0 and I respectively, whereas lifetimes in the absence and presence of

oxygen are represented by τ_0 and τ respectively. Additionally, k_q is the biomolecular quenching constant and Q is the concentration of oxygen. The product of k_q and τ_0 is typically denoted by a single variable K_{sv}, the Stern-Volmer quenching constant. The biomolecular quenching constant (k_q) can be further described using the Smoluchowski equation as:

$$k_q = 4\pi Np(D_f + D_q)(R_f + R_q) \times 10^{-3}$$

In this equation, the diffusion coefficients of the fluorophore and the quencher (oxygen) are denoted by D_f and D_q respectively, the collision radii of the fluorophore and the quencher (oxygen) are represented by R_f and R_q respectively, the Avogadro's number by N, and the probability of collision by p. For a single dye-single quencher system all the variables described by the Smoluchowski equation remains constant with the exception of the diffusion coefficients, which are dependent on the dye immobilization technique used and the surrounding matrix.[80] Diffusion coefficient variability warrants the empirical determination of K_{SV} values for discrete dye-matrix combinations by measuring intensity or lifetime values with varying oxygen levels. A plot of intensity/lifetime against oxygen concentration is typically linear as describe by the Stern-Volmer equation; however, in reality there are cases where the relationship deviates from linearity. A Stern-Volmer plot with a downward curvature is due to unequal access of dye populations to the quencher whereas, an upward curved Stern-Volmer plot results from a combination of static and dynamic quenching.[80]

Nonmetallic organic compounds and organometallic compounds have been used as luminescent oxygen sensitive probes. Nonmetallic organic compounds include

decacyclene compounds and polycyclic aromatic hydrocarbons (*e.g.* pyrene, quinolone); these compounds are characterized by short wavelength excitation and short decay lifetimes that leads to low signal-to-noise ratio and low oxygen sensitivity respectively, making them unsuitable for *in vivo* use.[81] Organometallic compounds can be further classified as transition metal complexes and metalloporphyrins. Transition metal complexes or metal ligand complexes (MLCs) typically consists of a transition metal (*e.g.* ruthenium (II), Osmium (II), Iridium (III), rhenium (I)) complexed to one or multiple diamine ligands. The most commonly used ligands include 2, 2'–bipyridine and tris (4, 7–diphenyl–1, 10–phenanthroline). In these MLCs, electrons are transferred from metal orbitals to ligand orbitals when excitation photons are absorbed. This transfer takes place from a singlet to a triplet state *via* intersystem crossing, contributing to longer lifetimes when the excited complex state decays predominantly by non-radiative pathways. MLCs can have lifetimes ranging from 100 ns to 10 μs. When in the excited triplet state MLCs can be easily quenched by molecular oxygen with the formation of singlet oxygen.

Metalloporphyrins have similar electron transfer properties with longer lifetimes (100 μs to 1 ms) making them highly sensitive to oxygen. Porphyrins are naturally occurring macrocyclic compounds, containing four pyrrole rings connected by methine linkers; porphyrin rings coordinate with transition metal atoms to form metalloporphyrins. Pt- and Pd- porphyrins in particular have been widely popular for sensing oxygen due to their high quantum yield (~10–20%), high oxygen sensitivity, and long wavelength excitation / emission. The Pt- and Pd- porphyrins are a class of highly

stable metalloporphyrins, which can withstand extremes of temperature, pH, and salt concentrations while retaining their phosphorescent properties.[82] Metalloporphyrins usually have three absorption peaks one around 400 nm (the Soret band) and two around 500 – 650 nm (Q band) providing greater latitude while designing sensing schemes. In general, Pt- porphyrins are more sensitive as they have 10 times longer lifetimes than Pd- porphyrins; however, they have marginally shorter excitation / emission peaks making Pd- porphyrins more amenable for *in vivo* use.

2.5. Mass transport limiting membranes

As explained previously, enzymatic sensors typically consist of oxidoreductase enzymes coupled to a transduction system, which can be either optical or electrochemical in nature. These transduction systems indirectly monitor analyte concentration by tracking changes in local oxygen, pH, or by-product (*i.e.* H_2O_2) levels. Enzymatic sensors require a delicate balance between the diffusion rates of both oxygen and analyte entering the sensor core and the enzymatic reaction kinetics. An ideal sensor is analyte-limited; the relative diffusion rate of analyte into the sensor is extremely low compared to that of oxygen. Under analyte-limited conditions the sensor response is linear, as the enzymatically consumed oxygen is rapidly replenished. However, as glucose levels continue to rise, oxygen concentration decreases to the point that it cannot be replenished anymore (oxygen-limited) and the sensor reaches saturation. Thus to maintain analyte-limited sensor behavior over a desired analyte range, a diffusion barrier

that regulates the relative diffusion rates of both oxygen and analyte is usually employed.[83]

For electrochemical sensors, control over the substrate fluxes has been achieved by using materials like Nafion [84] and silicone-based coatings. [85] However, application of these coatings is limited to relatively large surfaces because of the procedures required, such as casting and dip-coating. Alternatively, self-assembly coating techniques are useful for modifying smaller (micro or nano-scale) structures, which may be used as optical biosensors. [86-89] At these scales, the necessity to curb substrate diffusion becomes even greater as diffusion lengths are on the order of nanometers [90] and effective surface area relative to sensor volume is greatly increased.

Layer-by-layer (LbL) self-assembly is an attractive approach to address the analyte flux-control issue for these devices. Since Decher introduced the versatile LbL ultrathin film fabrication technique in the early 1990s,[91] it has been used with a variety of polyelectrolytes and applied across many different fields. Among these, LbL-coated micro/nanoparticles and capsules enabled by the foundational work of Sukhorukov et al. [92] have been explored intensively for various applications [93, 94] including biochemical sensing. [95, 96] The wide range of possible materials and conditions for LbL film fabrication allows fine-tuning of the resulting nanofilm properties. Despite this versatility and promise of tailorable features, the study and application of small-molecule transport control with these LbL nanofilms has been limited to a few cases. Bruening systematically investigated the transport of small uncharged solutes like glucose across LbL polyelectrolyte multilayers (PEMs)[97-99] using various

polyelectrolytes such as, poly (diallyldimethylammonium chloride) (PDADMAC), poly (sodium 4-styrenesulfonate) (PSS), poly (acrylic acid) (PAA) and poly (allylamine hydrochloride) (PAH). The findings from Bruening's experiments suggested that glucose diffusion across PAH/PSS bilayers was orders of magnitude lower than PDADMAC/PSS bilayers. Moreover, Bruening also demonstrated that glucose diffusion could be further reduced by including PAA/PAH bilayers in the nanofilm architectures. The results also indicated that PSS-terminated bilayers are more effective in restricting glucose diffusion.

Despite these studies, none of the LbL designs have been able to finely-tune the movement of small molecules across LbL coated microcapsules; a capability that is desirable for various applications including biosensing, drug delivery, and anti-corrosive agent release.

2.6. Hydrogels based sensors

The McShane group strives to overcome the limitations posed by metallic electrode based sensors by using fully implantable hydrogels. Roberts *et al*. demonstrated the use of biocompatible hydrogels containing immobilized sensing chemistry for potential use as fully implantable optical glucose sensors.[29] This work established luminescence based indirect glucose sensing mediated by oxygen-sensitive (palladium (II) meso-tetra (4-carboxyphenyl) porphyrin) and pH-sensitive (seminaphtharhodafluor-4F 5-(and 6) - carboxylic acid)) fluorophores. Furthermore, the effect of biofouling on these sensors' sensitivity and analytical range was also examined

in a later work; changes in diffusion characteristics and sensor response, when exposed to rat serum and after implantation in rats were thoroughly examined.[100] Banking on these promising preliminary results, preclinical studies were performed by subcutaneously implanting red-light excitable hydrogel based sensors in pigs.[101] Although these sensors showed glucose response 2 h after implantation, they failed to register any response a week after implantation; this sensor failure can be attributed to depleting local oxygen levels over time. Based on this same sensing scheme, lactate sensors were also developed by Andrus *et al*.; however, these sensors also failed to operate at low oxygen.[102]

An alternative approach to fabricate functional hydrogel based devices involves embedding micro- or nano- sized spherical reactors within the hydrogel matrix. An introductory proof of concept study was conducted by Roberts *et al*.; microcapsules fabricated *via* LbL were used to develop composite hydrogels.[103, 104] Building upon this work, Biswas *et al*. also demonstrated, the use of LbL nanocapsules containing oxygen-sensitive porphyrin dye to construct oxygen sensing composite hydrogels.[12] Enzyme containing spherical microdomains can be represented by a set of six equations that describe the reaction-diffusion kinetics using the standard partial differential equation:

$$\frac{\partial C_i}{\partial t} + \frac{1}{r^2}\frac{\partial}{\partial r}\left(-D_i\, r^2\, \frac{\partial C_i}{\partial r}\right) = R_i$$

where D_i and R_i represent the diffusion coefficient and the reaction rates of one of the nine reaction species including analyte concentration, oxygen, enzyme concentration, hydrogen peroxide levels *etc*, r denotes the radius of the microdomains.[105, 106] These

equations can be solved to predict the spatio-temporal distribution of the analytes and the products. As oxido-reductase enzymes act catalytically, the Thiele modulus (ϕ) [107-109] given by

$$\Phi_s = \sqrt{\frac{k_{cat}[E]}{D_s[s]}}\, l$$

is usually used to describe the reaction-diffusion balance of the system; where E is the concentration of enzyme (GOx, LOx), k_{cat} is the catalytic turnover rate of the enzyme, S is the concentration of the analyte (glucose or lactate), D_s is the diffusion coefficient, and l is the length of the reaction matrix. High Thiele modulus (ϕ) values (>1) are characteristic of diffusion limited systems, while values < 0.3 [109-111] are indicative of reaction-limited systems. Furthermore, as these enzymatic reactions depend on the availability of oxygen, the Thiele modulus ratio ϕ_r :

$$\Phi_r = \frac{\Phi_o}{\Phi_s} = \sqrt{\frac{D_s[s]}{D_o[O]}}$$

between oxygen (ϕ_o) and the analyte (ϕ_s) in question allows a better understanding of the system; prior studies have shown that a ϕ_r value that lies between 2 and 100 is suitable for a sensor with desirable parameters (longer range with a high sensitivity).[112]

All prior works have failed to demonstrate the successful operation of a hydrogel based enzymatic sensor at physiologically lower oxygen levels. Subsequent chapters of this dissertation will describe the development and testing of nanocomposite hydrogel based enzymatic sensors that operate at low oxygen.

2.7. Multianalyte sensing and multifunctional composite devices

Several chronic conditions and metabolic disorders are characterized by fluctuations in multiple biomarkers; engendering an increased interest for the development of multianalyte sensors. [113, 114] Ideally a multianalyte sensor produces discrete signals characteristic to individual analytes with minimal interference. In case of optical sensors distinct signals can be achieved by using fluorescence reporters with non-overlapping spectra or by using temporal lifetime separation techniques. Additionally, multiple optical transduction modes (*e.g.* luminescence intensity, luminescence lifetime, Raman scattering) can also be used for multianalyte detection, making signal separation easier. Apart from multianalyte sensors, multifunctional composite sensing systems have also been gaining interest amongst researchers. A possible use of a multifunctional system aims to sense biomarkers and to release therapeutic agents simultaneously. These therapeutic agents may have a localized effect (*e.g.* reduce inflammation) to curb host response or a more systemic effect (*e.g.* regulate glucose by releasing insulin) that maintains body homeostasis. Both, multianalyte and multifunctional systems have the potential to revolutionize chronic disease management; however, such hydrogel based sensing systems have not been studied.

2.8. Summary

This work describes the development of composite hydrogel based enzymatic sensors that can continuously track relevant biomolecules (*e.g.* glucose, lactate). A stringent design requirement was to fine-tune the movement of analytes into bioactive

microreactors entrapped in hydrogel matrices, in order to make the sensor response diffusion limited. LbL deposited PAH/PSS bilayers were chosen as polymeric materials to coat the outer surface of the hollow microreactors; interlayer and interlayer crosslinking of PAH/PSS with glutaraldehyde was emphasized as a facile method to control analyte permeation rates. Further work was devoted to improving the sensor's operational lifetime and response at low oxygen conditions by using solid alginate microspheres. Additionally, the modular nature of the composite hydrogel sensor was demonstrated by adapting the design to sense lactate at physiologically low oxygen levels. Subsequent sections study the limits of composite hydrogel based sensors for multianalyte and multiplexed sensing and the development of novel gold nanocluster based H_2O_2 microcapsule sensors for potentially monitoring enzymatic reactions in hydrogel sensors.

3. CROSS-LINKED NANOFILMS FOR TUNABLE PERMEABILITY CONTROL IN A COMPOSITE MICRODOMAIN SYSTEM *

3.1. Introduction

Microcapsule technology plays a critical role in numerous applications for biotechnology, food, agriculture, cosmetic, and pharmaceutical industries.[1-3] A capsule shell acts as a barrier between the payload material and the external microenvironment; functioning to modulate specific surface interactions and to selectively control permeability.[4-6] An abundance of technology exists for the encapsulation of materials *via* entrapment, adsorption, or diffusional loading,[7-12] where the preferred method for a given application is chosen based on the properties of the cargo being encapsulated and the desired function of the capsule. The interaction of the colloid-cargo composite with its environment may then be further modified by tuning the physical and the chemical properties of the capsule exterior.

Layer-by-layer (LbL) self-assembly provides a versatile route to modulate the surface properties of an assortment of template materials in a precise manner using a very simple process that may nevertheless result in a highly complex multifunctional coating.[13] The deposition of these nanofilms is driven by a combination of chemical and physical interactions such as electrostatics, covalent bonding, hydrogen bonding, or

* Reprinted with permission from "Cross-linked nanofilms for tunable permeability control in a composite microdomain system" by Biswas. A., Nagaraja. A.T., McShane. M.J. *RSC Advances* 2016, *6, 71781-71790*. Copyright 2016 by The Royal Society of Chemistry.

bioaffinity;[14] these may be adjusted by engineering the deposition conditions and the multilayer composition itself. Fortuitously, a large set of molecules are available for use in constructing these materials. The ability to achieve nanoscale architectural precision makes LbL uniquely suited to construct coatings that selectively control molecule permeation through the capsule wall for applications such as drug delivery,[15] self-healing smart coatings,[16] or biosensing.[17] The nanofilm coating can be used to match burst/sustained release profiles of active agents (drugs, anticorrosive substances) or to gate diffusion into the capsule interior for selective biomolecular sensing. For the special case of enzymatic bioreactors, the nanofilm coating can be used as a diffusion-limiting barrier for finely tuning substrate flux and hence substrate consumption. In enzymatic biosensors, this controls the reaction-kinetics of the sensor chemistry which manifests as changes in the sensor analytical range and sensitivity.[18]

LbL has been employed to make nanofilms for gas barrier coatings and separation membranes by the inclusion of high-aspect-ratio materials such as inorganic clay platelets (*e.g.* Laponite, vermiculite, or montmorrilonite) and graphene.[19-22] These platelets are assembled to align parallel to each other within the nanofilm layers (normal to the direction of analyte flux) to create a highly tortuous path for molecules diffusing through the layers. However, the use of platelet LbL to regulate molecular permeation rates has been more effective on planar films than on colloidal templates. There have been a few examples of capsules fabricated with platelet-based nanofilm layers[23-26] but the reduction in observed diffusion was substantially lower compared to the planar

equivalent. An innovative approach to reduce permeability of capsule walls involves the introduction of preformed nanoparticles or *in situ* nucleation and growth of nanoparticles within the polymer shell.[27-29] These methods produce structurally stable microcapsules with stimuli responsive burst release capabilities; however, they still face a challenge in achieving reproducible and controlled reduction of permeability.[27]

In addition to the compositional route, permeability through soft material nanofilms may also be controlled by changing the number of layers or the thickness and structure of these layers using different deposition conditions. Electrostatic deposition of polyelectrolytes can be controlled with a high degree of reproducibility and precision by controlling pH and salt concentration.[30-32] These methods have been shown to be effective on planar films[33, 34] but face challenges for replication in capsule formation due to tedious process flow and quality control issues ascribed to colloidal destabilization.[35] UV, thermal, or chemical cross-linking of polyelectrolyte multilayer (PEM) films have also been demonstrated as an effective means to affect film permeability while also varying structural properties. UV cross-linked diazoresin / poly (styrene sulfonate) microcapsules that are extremely stable to solvents and osmotic pressure fluctuations, have exhibited reduced permeability to enzymes.[36, 37] Carbodiimide-activated or thermally-induced cross-linking between amine and carboxylic acid groups present in PEMs have also been reported to produce capsules with enhanced physical stability and decreased permeability.[38-41] Another promising approach to fabricate high diffusion barrier nanofilms is to cross-link amine containing polyelectrolytes using glutaraldehyde. Grunlan's group reported that glutaraldehyde cross-linking of an amine-

containing polyelectrolyte polyethylenimine (PEI) could reduce the diffusion of oxygen across planar nanofilms below detection limits.[42, 43] It has been established that glutaraldehyde cross-linked planar nanofilms can limit the diffusion of monovalent and divalent cations;[44] glutaraldehyde cross-linked polymeric microcapsules have also been shown to possess better chemical, thermal, and mechanical stability, with reduced permeability to larger macromolecules (460 - 2000 kDa FITC - Dextran) compared to non-cross-linked microcapsules made from similar amine-containing PEMs.[45-47]

Although there has been considerable progress in LbL technology to forge capsules with enhanced stability and stimuli-sensitive switchable permeability characteristics,[48, 49] advancement related to finely tuning diffusion of analytes in/out of polymeric capsules has been scarce and limited to methods involving irreversible enzymatic degradation of the microcapsule shell.[50, 51] This is somewhat surprising given that capsule permeability control is especially vital in payload release and biosensing applications that demand precise diffusion control to achieve desired functionality.[17, 52]

In this study we explored the use of glutaraldehyde cross-linked PAH [poly (allylamine hydrochloride)] / PSS [poly (sodium 4-styrenesulfonate)] bilayers to provide accurate and reproducible control over the diffusion of a model analyte glucose. The controlled reduction in glucose permeation rate is examined by varying the number of cross-linked PAH/PSS bilayers deposited on planar Anopore membranes. The cross-linked nanofilm constructs were translated onto sacrificial calcium carbonate templates to construct microcapsule-based enzymatic reactors for glucose oxidation, which were also functionalized with a phosphor for optical readout. These micron-sized glucose sensors

were ultimately dispersed in an alginate hydrogel matrix. Flux-based enzymatic microcapsule sensors immobilized in a matrix act in an ensemble fashion, thus any change to substrate permeation properties of individual microcapsules manifests as substantial shifts in bulk sensor properties. This provides a powerful tool to probe substrate diffusion across the microcapsule wall towards the engineering of a tunable biosensing hydrogel device, which may be used as a fully implantable soft-material enzymatic sensor to monitor physiologically relevant biomarkers.

3.2. Experimental section

3.2.1. Chemicals

Sodium carbonate (Na_2CO_3), calcium chloride ($CaCl_2$), poly (sodium 4-styrenesulfonate) (PSS, average Mw 70000 Da), poly (diallyldimethylammonium chloride) (PDADMAC, average Mw 100000-200000 Da), poly(allylamine hydrochloride) (PAH, average Mw 15000 Da), glutaraldehyde solution (grade II, 25% in H_2O), alginic acid sodium salt from brown algae (100-300 cP, 2% at 25 °C), and buffer salts ($NaHCO_3$, MES, $C_2H_3NaO_2$, and TRIS) were obtained from Sigma and were used as received without further purification. Glucose oxidase (GOx) from *Aspergillus niger* (257 U/mg, BBI solutions) and Pd-meso-tetra (4-carboxyphenyl) porphine (PdTCPP, Frontier Scientific) suspended in DMSO (10 mM) solution were used in all experiments. Glucose used for all sensor response studies was obtained from Macron Fine Chemicals.

3.2.2. Layer-by-layer assembly on planar substrate

Nanofilms were deposited on Whatman Anopore inorganic aluminum oxide membrane filters (25 mm diameter, 0.02 μm pore size) placed in an open-face filter holder (Pall Co.). The open face of the filter membrane was exposed to oppositely charged polyelectrolyte solutions 20 mg/mL PDADMAC (pH 8), 20 mg/mL PAH (pH 8), 20 mg/mL PSS (pH 7.2) alternately with wash steps (5 mM $NaHCO_3$) between each polyelectrolyte exposure step. A primer coating consisting of [PSS]-[PDADMAC/PSS]$_5$ was deposited to achieve complete surface coverage[53] before depositing the desired number of PAH/PSS bilayers (Figure 1A). After depositing the target number of PAH/PSS bilayers, the nanofilms were exposed to 0.1 M glutaraldehyde solution for 30 minutes to cross-link the amine groups on PAH (Figure 5A). Excess glutaraldehyde was removed by washing the nanofilms with 5 mM $NaHCO_3$ (pH 7.2). All polyelectrolyte solutions were prepared in 5 mM $NaHCO_3$.

To fabricate interspersed cross-linked PAH layers (Figure 1B), a PSS/PDADMAC layer was deposited between successive PAH/PSS bilayers. Cross-linking of the interspersed layers was performed using the same protocol to cross-link non-interspersed PAH/PSS bilayers. It should be noted that when depositing PAH/PSS bilayers wash steps were performed using 5 mM $NaHCO_3$ (pH 7.2), and while depositing PDADMAC/PSS bilayers 5 mM $NaHCO_3$ (pH 8) was used for the washing steps, to ensure that the polyelectrolytes were sufficiently ionized while deposition.

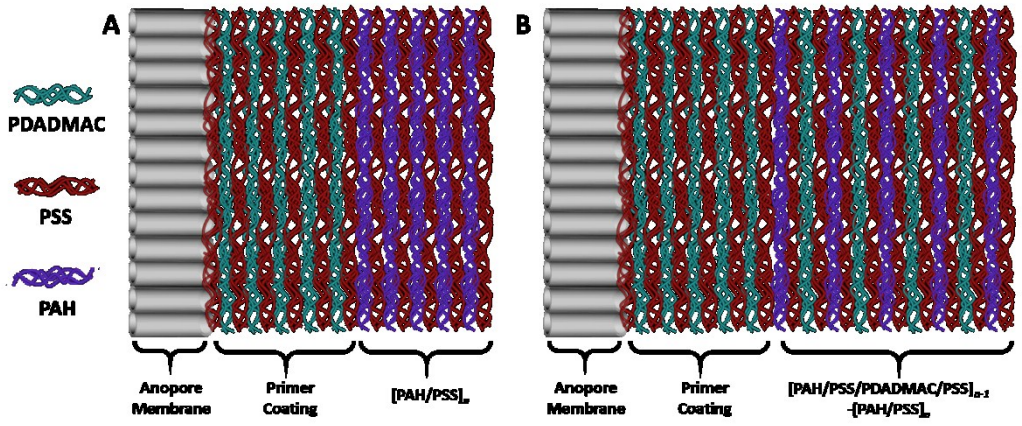

Figure 1. (A) $[PAH/PSS]_n$ nanofilms and the primer coating ($[PSS]$-$[PDADMAC/PSS]_5$) deposited on Anopore membrane, (B) $[PSS/PAH/PSS/PDADMAC]_{n-1}$-$[PAH/PSS]$ nanofilms and the primer coating ($[PSS]$-$[PDADMAC/PSS]_5$) deposited on Anopore membrane.

3.2.3. Permeability measurements

Nanofilms fabricated on Anopore membrane filters, were placed between the feed and the permeate chambers of a side-by-side diffusion cell (Permegear Inc.). The feed chamber was filled with 7 mL of 5 mM $NaHCO_3$ (pH 7.2) containing 1 g/L glucose and the permeate chamber was filled with 7 mL of 5 mM $NaHCO_3$ (pH 7.2). Samples were collected from both the feed and the permeate sides at regular time intervals, and the glucose concentration of the samples were measured using a YSI biochemistry analyzer (2700 Select). The rate of increase in concentration over time in the permeate chamber (dC/dt) was calculated by linear regression for the different nanofilm formulations.

3.2.4. Nanofilm coated microparticles with encapsulated sensing chemistry

PdTCPP and GOx containing calcium carbonate ($CaCO_3$) microparticles were synthesized using the co-precipitation method, [115] with minor modifications. Briefly, 200 μL of 10 mM PdTCPP solution was added to 8 mL of 0.2 M Na_2CO_3 containing 64 mg of GOx under continuous stirring (800 RPM). After 5 mins, 8 mL of 0.2 M $CaCl_2$ was added rapidly and the reaction was allowed to continue for 10 mins. Nanofilms were deposited on the PdTCPP and GOx containing microparticles, by alternately exposing the particles to polyelectrolyte solutions (20 mg/mL PDADMAC (pH 8), 20 mg/mL PAH (pH 8), 20 mg/mL PSS (pH 7.2)) with intermediate wash steps. The wash solutions used were the same as describe above for making nanofilms on planar substrates. After depositing the desired number of nanofilms, 3.3 mg of nanofilm-coated microparticles was suspended in 10 mL, 3 M glutaraldehyde solution for 30 min. Excess glutaraldehyde was removed by washing the microparticles with 5 mM $NaHCO_3$ (pH 7.2). The amount of glutaraldehyde used for the microcapsules was based on the ratio of [nanofilm surface area]:[mass of glutaraldehyde]. Hollow microcapsules were made from the PEM lined, payload containing microparticles, by exposing them to 0.2 M sodium acetate buffer at pH 5.1.

3.2.5. Microporous alginate composite (MPAC) hydrogels

MPAC hydrogels were made using a modified version of the protocol described by Roberts et al.[55] Briefly, microcapsules fabricated using 3.3 mg of PEM coated $CaCO_3$ microparticles were suspended in 75 μL of deionized water, non-coated $CaCO_3$

microparticles (25 μL of 33.3 mg/mL), 3% alginate solution (200 μL), and MES (100 μL, 0.5 M, pH 6.1) were mixed to make a slow-gelling hydrogel precursor. The precursor was then poured between two glass slides separated by a 1.5 mm Teflon spacer, and allowed to gel for 24 hours.

3.2.6. Characterization

Confocal fluorescence and differential interference contrast (DIC) microscopy images were captured using an inverted laser spinning-disk confocal microscope (Olympus IX81, Yokogawa CSU-X1). Hydrogel samples excited at 488 nm were viewed through 40 X and 100 X oil immersion objectives. Images were analyzed using ImageJ 1.48 v software.

SEM images of nanofilm coated microparticles, microcapsules and MPAC hydrogels were captured using a JEOL 7500 scanning electron microscope. A diluted sample of either nanofilm coated microparticles or microcapsules was placed on a silica wafer and was allowed to dry overnight. To prepare a hydrogel sample for SEM imaging, a 5 mm X 5 mm hydrogel was placed on a silica wafer and dried overnight. All samples were sputter-coated with 2.5 nm of palladium/platinum before imaging. SEM images were analyzed using ImageJ 1.48 v software.

3.2.7. Sensor response testing

Hydrogel discs (4 mm radius) were excised from the hydrogel slab using a biopsy punch. Each sample was placed in a liquid flow cell (Figure 2), and changes in

lifetime with varied glucose and oxygen concentrations were recorded using a custom time-domain lifetime measurement system as described elsewhere.[56]

The response to oxygen was evaluated by flowing buffer having varied dissolved oxygen concentrations (0 - 206.8 μM). The dissolved oxygen concentration of 10 mM TRIS (pH 7.2) containing 10 mM $CaCl_2$ was changed by purging air and nitrogen with mass flow controllers (type 1179A, MKS).

To determine the response to glucose, solutions containing different concentrations of glucose (0 - 400 mg/dL) dissolved in 10 mM TRIS (pH 7.2) with 10 mM $CaCl_2$ were flowed over the hydrogel samples. The response parameters were calculated from each of the obtained response curves. The limit of detection (*LOD*) was estimated by calculating the glucose concentration at which the response was 10 % higher than the response at 0 mg/dL glucose concentration. Similarly, the maximum differentiable glucose concentration (*MDGC*) was estimated by calculating the glucose concentration at which the response was 10% lower than response at 400 mg/dL glucose concentration. The range of the sensor was defined as $R = MDGC\text{-}LOD$, while the sensitivity was defined as the percent change in the maximum and minimum response observed per unit range of the sensor.

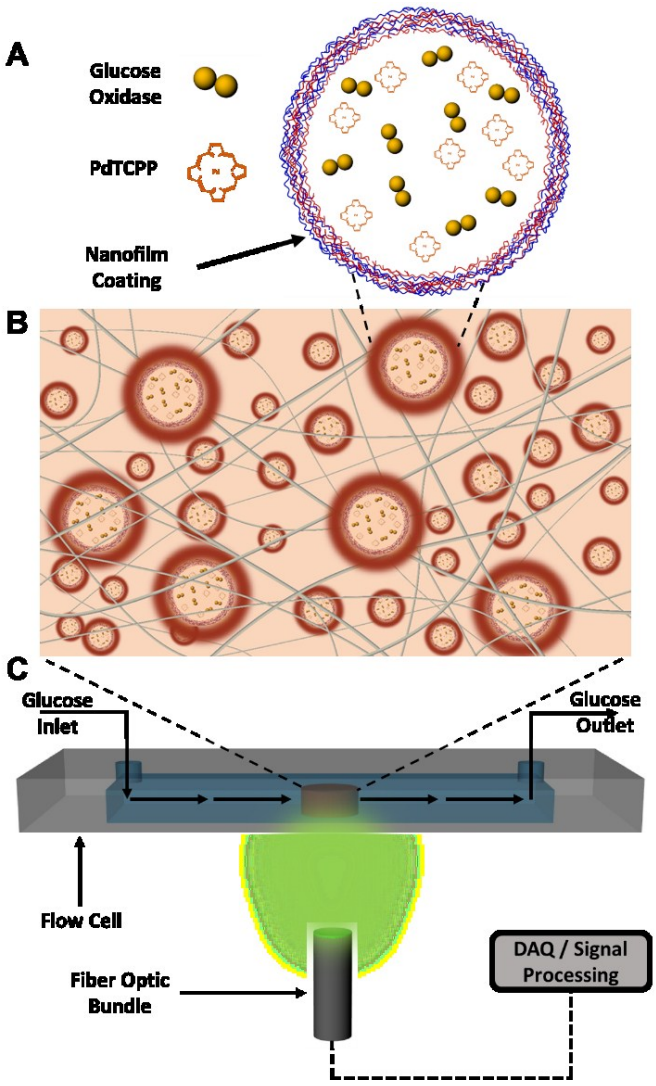

Figure 2. Schematic diagram of (A) enzyme/dye containing microdomain bound by nanofilm coating, (B) a section of the microdomain containing hydrogel and (C) the experimental setup consisting of the flow through cell and the time-domain lifetime measurement system used to evaluate sensor response.

In order to test the long term stability of MPACs, MPACs containing cross-linked $[PDADMAC/PSS]_5$-$[PAH/PSS]_9$ bound microdomains were continuously

exposed to 400 mg/dL glucose and lifetime of the sensors were measured every 5 min. With increase in glucose, the baseline lifetime (~133 μs) of the sensors rose and achieved steady state; this steady state lifetime (~310 μs) is considered to be 100% signal retention and subsequent drop in lifetime is reported with respect to this value.

3.3. Results and discussion

3.3.1. Permeation studies on planar nanofilm

The effect of glutaraldehyde cross-linking of PAH/PSS bilayers on the diffusion of glucose was evaluated by measuring the rate of glucose diffusion across PAH/PSS nanofilm constructs deposited on Anopore membranes. PAH/PSS bilayers were deposited on the primer coating (PSS-$[PDADMAC/PSS]_5$) to fabricate PSS-$[PDADMAC/PSS]_5$-$[PAH/PSS]_n$ multilayers, where n was varied from 1 to 10. The glucose diffusion across different nanofilm formulations was evaluated by calculating the linear slope of the glucose concentration change dC/dt (where C is the concentration of glucose (g/L) and t is time (hours)) on the permeate side of the diffusion cell. The data presented in Figure 3 shows the decrease in dC/dt for both the cross-linked and non-cross-linked PAH/PSS bilayers as the number of layers is increased. It is quite clear that the decrease in dC/dt is much more pronounced in the case of the cross-linked PAH/PSS bilayers. Specifically, the glucose permeation rate through non-cross-linked PAH/PSS bilayers decreases by ~ 46 % when n is increased from 3 to 9, whereas the dC/dt of cross-linked PAH/PSS bilayers decreases by ~ 98% for the same number of bilayers. It is evident from this that the cross-linked films more effectively prohibit the free

diffusion of glucose compared to the native nanofilm constructs. For the same number of bilayers, cross-linking significantly decreases the *dC/dt* across the multilayer constructs. Comparing the glucose permeation rates through cross-linked and non-cross-linked PEMs when n = 3, 5, and 9, the *dC/dt* of glucose through the cross-linked PEMs was found to be less than the corresponding non-cross-linked PEMs by ~ 71%, ~ 88% and ~ 99%, respectively. Extrapolating fitted data (Figure 4), revealed that 124 non-cross-linked PAH/PSS bilayers would be required to achieve the glucose permeation rate obtained when using 9 bilayers of cross-linked PAH/PSS. The first five cross-linked bilayers decrease the glucose permeation rate drastically; however, further increase in the number of cross-linked bilayers has a proportionally lower effect. The *dC/dt* values for glucose through the cross-linked PEMs change by ~ 39% when comparing diffusion rates between n = 1 and n = 2, whereas the decrease was only ~ 15% when comparing n = 5 and n = 6. This is believed to simply be a function of the percentage of total film thickness represented by the additional layers; in the first case, doubling the thickness of cross-linked layers is a more substantial increase in thickness than adding one layer to five already deposited (15-20% increase).

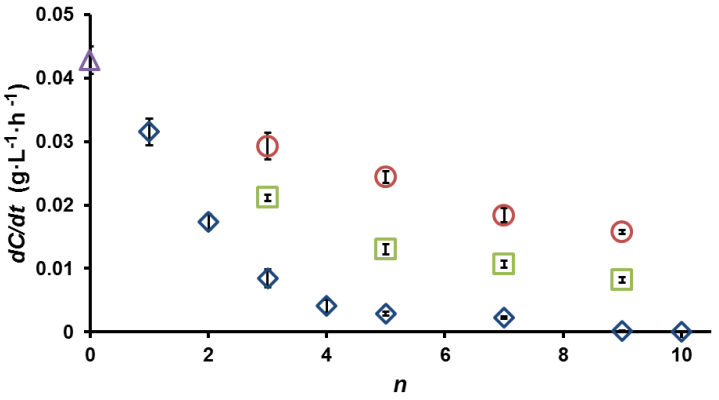

Figure 3. The glucose permeation rate (*dC/dt*) through PAH/PSS bilayers composed of cross-linked PSS-[PDADMAC/PSS]$_5$-[PAH/PSS]$_n$ (blue ◊), cross-linked PSS-[PDADMAC/PSS]$_5$-[PSS/PAH/PSS/PDADMAC]$_{n-1}$-[PAH/PSS] (green □), non-cross-linked PSS-[PDADMAC/PSS]$_5$-[PAH/PSS]$_n$ (red ○), and the primer coating PSS-[PDADMAC/PSS]$_5$ where $n = 0$ (purple Δ). Error bars represent 95% confidence intervals for three separate nanofilm constructs.

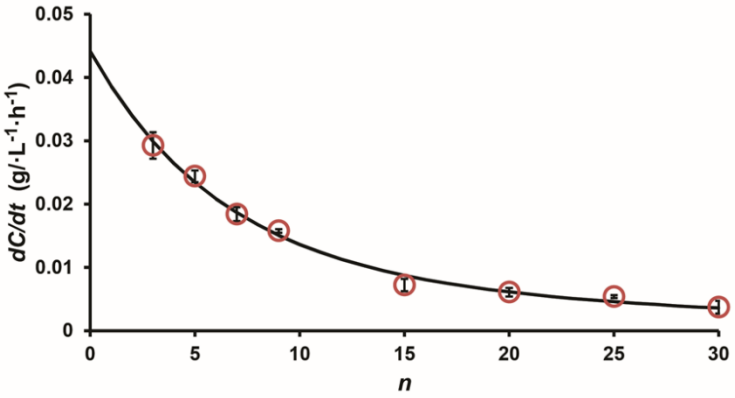

Figure 4. The glucose permeation rate (*dC/dt*) through PAH/PSS bilayers composed of non-cross-linked PSS-[PDADMAC/PSS]$_5$-[PAH/PSS]$_n$ (red ○). Error bars represent 95% confidence intervals for three separate nanofilm constructs.

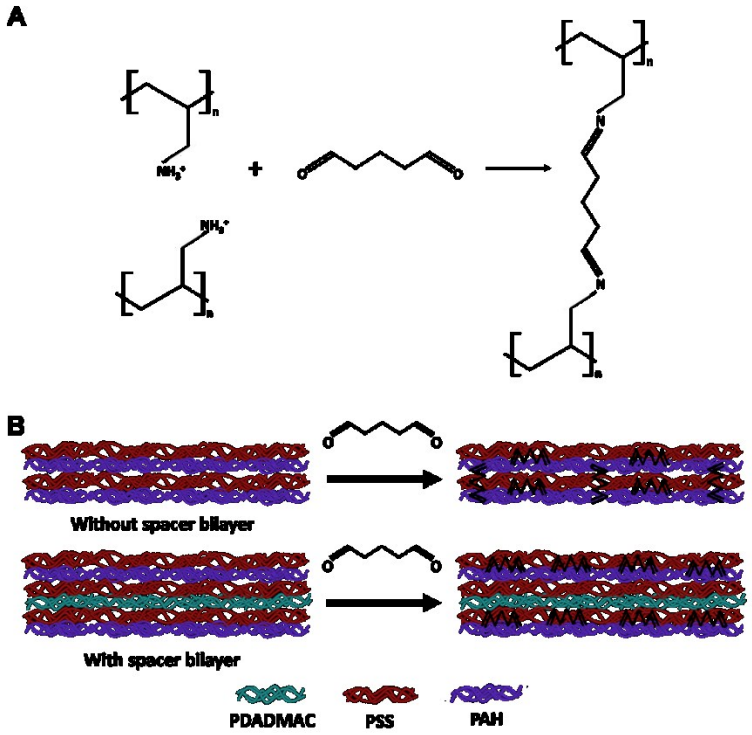

Figure 5. (A) Cross-linking of poly (allylamine hydrochloride) (PAH) by glutaraldehyde. (B) Glutaraldehyde cross-linked PAH/PSS nanofilm constructed without and with a PDADMAC/PSS spacer bilayer.

The drastic decrease in permeability to glucose when the $-NH_2$ groups of the PAH layer are cross-linked (Figure 5A) in the presence of glutaraldehyde may be attributed to the decrease in free volume present in the PEMs.[42, 43] Apart from cross-linking the $-NH_2$ groups of PAH in an individual PAH layer, the possibility also exists to have cross-linked $-NH_2$ groups present in successive PAH layers due to the interpenetrating nature of LbL assembled PEMs.[57] This led us to question the extent of interlayer and intralayer cross-linking and the corresponding influence on glucose diffusion. To investigate this, nanofilms were designed with a spacer bilayer

PSS/PDADMAC introduced between successive PAH/PSS bilayers (Figure 5B). The spacer containing PEMs fabricated are represented by PSS-[PDADMAC/PSS]$_5$-[PSS/PAH/PSS/PDADMAC]$_{n-1}$-[PAH/PSS]. The spacer containing cross-linked PAH/PSS bilayers were found to limit glucose diffusion to a greater extent than non-cross-linked nanofilms but less than cross-linked PAH/PSS nanofilms without spacer bilayers (Figure 1). Introduction of the PSS/PDADMAC spacer bilayer allowed glucose to diffuse through the nanofilm coatings more freely as compared to glucose diffusion across non-spacer containing successively cross-linked films with the same total number of PAH layers. For n = 3, 5, and 9 the dC/dt of cross-linked P PSS-[PDADMAC/PSS]$_5$-[PSS/PAH/PSS/PDADMAC]$_{n-1}$-[PAH/PSS] was 2.5, 4.5, and 81 times greater, respectively, than their cross-linked counterparts without the spacers (PSS-[PDADMAC/PSS]$_5$-[PAH/PSS]$_n$). It is important to recognize that the metrics used are of glucose permeation rate and are not normalized by film thickness. Thus, even though the cross-linked spacer-containing PEMs contain more layers and are overall thicker, the total glucose diffusion barrier is less than the cross-linked PEMs without the spacer bilayers. This increase in dC/dt is ascribed to the reduced interlayer cross-linking by the introduced spacer bilayer that decreases the interpenetration of neighboring PAH layers. Once the glucose permeation rate effects were determined with the planar multilayers, the nanofilm architectures were translated to microparticle template coatings as a way to fabricate microcapsule based optical glucose sensors. The expectation was that the varying glucose permeation rate of the different nanofilms would result in correspondingly shifted glucose sensor behavior (sensitivity and response range). In

these enzymatic glucose sensors, GOx catalyzes the oxidation of glucose in the presence of molecular oxygen, ultimately producing gluconic acid (glucose + O_2 + glucose oxidase + H_2O $\rightarrow$ gluconic acid + H_2O_2). If the enzyme is in excess, and the reaction is not limited by oxygen supply then the decrease in molecular oxygen should be proportional to the amount of glucose oxidized. Thus measuring the decrease in molecular oxygen using an oxygen sensitive phosphorescent dye (PdTCPP) enables the indirect measurement of glucose concentrations. The design described, places severe demands on transport control. In a generic enzymatic biosensor, a diffusion-limiting coating is used to restrict the amount of substrate entering the enzyme module per unit time, effectively making the system substrate-transport limited rather than reaction-kinetics limited.[58] It is important to appreciate that the overall range and the sensitivity of an enzymatic biosensor can be tailored by controlling the rate of substrate diffusion.[59]

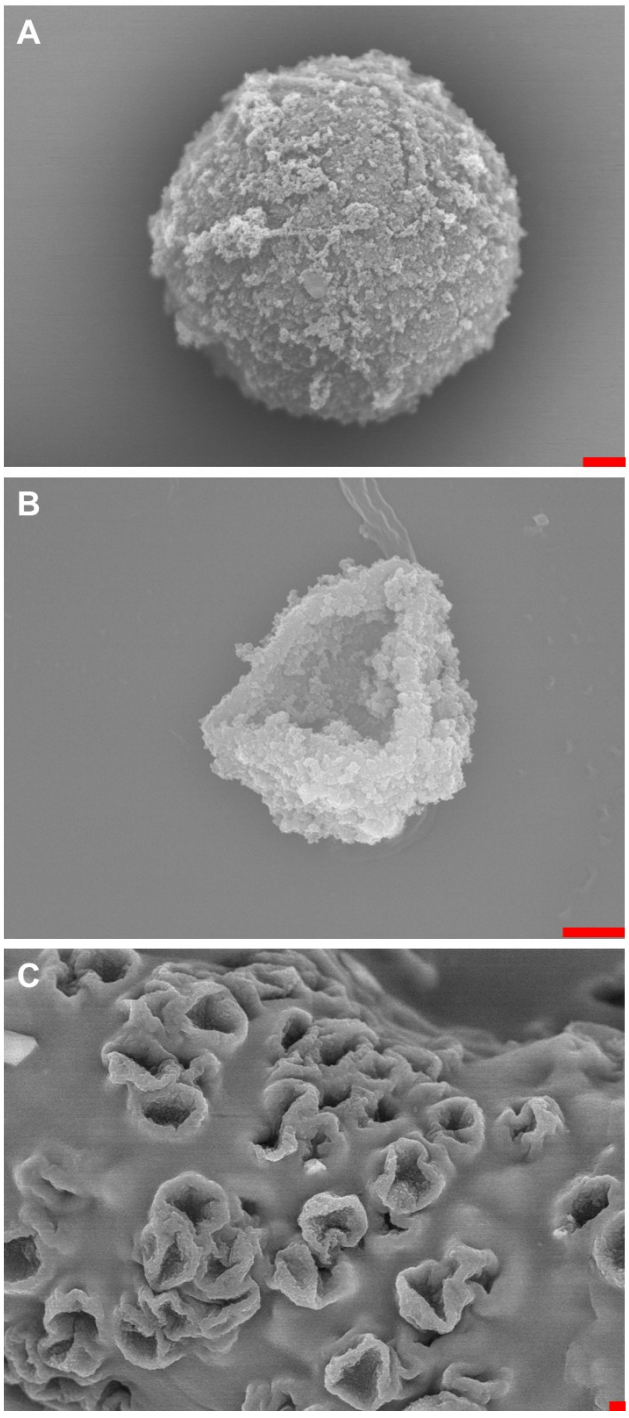

Figure 6. SEM images of sputter-coated (A) cross-linked $[PDADMAC/PSS]_5$-$[PAH/PSS]_9$ coated microparticle (B) cross-linked $[PDADMAC/PSS]_5$-$[PAH/PSS]_9$ bound microcapsule (C) MPAC containing cross-linked $[PDADMAC/PSS]_5$-$[PAH/PSS]_9$ bound microdomains. Scale bars correspond to 1 µm.

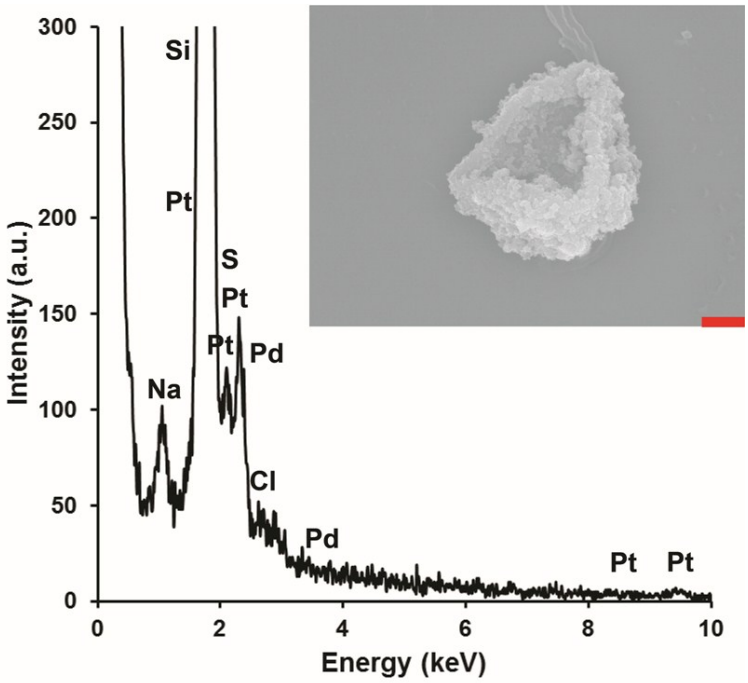

Figure 7. Energy Dispersive X-ray Spectroscopy (EDS) spectra for sputter coated (4nm of palladium/platinum) cross-linked $[PDADMAC/PSS]_5$-$[PAH/PSS]_9$ microcapsule samples, prepared on silicon substrates. Absence of calcium in the spectra confirms complete dissolution of $CaCO_3$. Platinum, palladium, and silicon peaks result from the silicon substrate and the sputter-coated film.

3.3.2. Characterization of nanofilm coated microparticles, microcapsules, and nanocomposite hydrogels

The cargo containing microparticles and capsules were first characterized by optical and electron microscopy to confirm that the desired products were produced in the fabrication process. SEM images of cross-linked $[PDADMAC/PSS]_5$-$[PAH/PSS]_9$ coated microparticles (Figure 6A) revealed the spherical morphology of the $CaCO_3$ microparticles bound by fuzzy PEMs. The average diameter of the coated particles is estimated to be about 3.6 μm. Elemental analysis carried out using an EDS system

attached to the SEM (Figure 7) confirmed that $CaCO_3$ was no longer present in the microcapsules after dissolution of the $CaCO_3$ core. The hollow microcapsules (Figure 6B) appear as collapsed structures, which occurs when specimens are dried during sample preparation for SEM. The SEM image of the cross-linked PAH/PSS coated microparticles are similar to those reported by Volodkin et al.[3] However, the cross-linked PAH/PSS microcapsules appear to have capsule walls that collapse less than the cross-linked PAH/PSS microcapsules fabricated by Tong et al.[45] and Wang et al.[47] This minor difference is attributed to the greater number of cross-linked bilayers and increase in overall coverage by the PAH/PSS bilayers compared to prior studies. Images of the microcapsules entrapped in MPAC hydrogels (Figure 6C) reveal a wrinkled microporated morphology for the hydrogel when dried, which is characteristic of microcapsule-containing MPAC gels.[55]

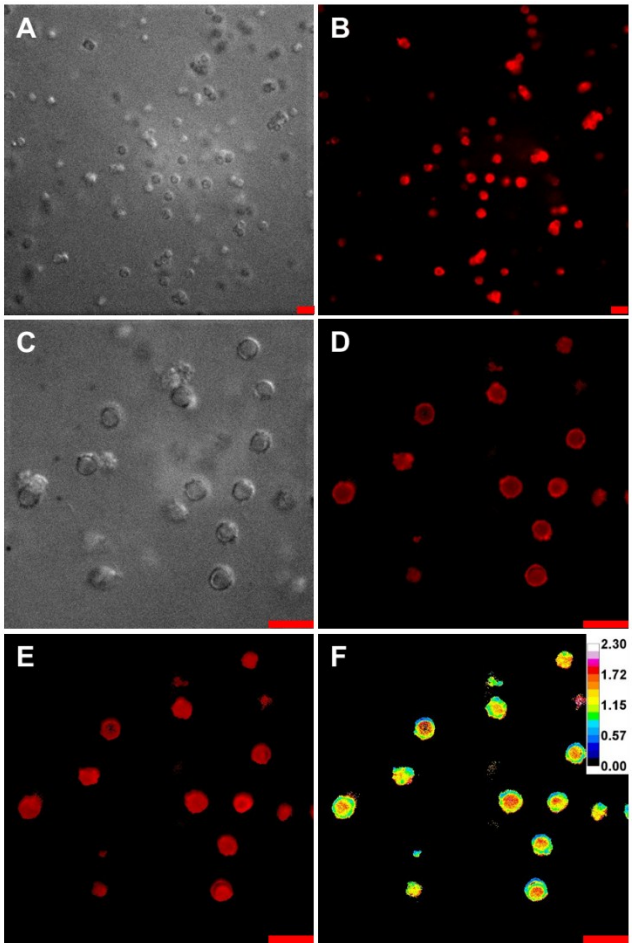

Figure 8. DIC images of MPAC hydrogels containing cross-linked microcapsules ([PDADMAC/PSS]$_5$-[PAH/PSS]$_9$) at (A) 40 X magnification and (C) 100 X magnification. Fluorescence microscopy images of microcapsule containing MPAC gels at (B) 40 X magnification, (D) 100 X magnification (ambient oxygen), (E) 100 X magnification (reduced oxygen) and the intensity ratio of the MPACs under reduced oxygen to ambient oxygen (F). Scale bars correspond to 10 µm. Color coded scale corresponds to intensity ratios of PdTCPP containing microdomains (reduced oxygen : ambient oxygen).

Differential interference contrast (DIC) micrographs (Figure 8A and Figure 8C) revealed that the cross-linked microcapsules containing GOx and PdTCPP were uniformly distributed when immobilized in MPAC hydrogels. The average diameter of

the microcapsules entangled in the MPAC gels was estimated using ImageJ software to be 4.0 ± 0.4 μm, which is comparable to the size of the corresponding nanofilm-coated microparticle templates viewed by SEM. The slightly larger estimated size of the microcapsules viewed by DIC images may be attributed to the hydrated state of the samples relative to the dried samples used for SEM. In the confocal micrographs (Figure 8B and Figure 8D) the phosphorescent dye PdTCPP is clearly localized in the spherical microdomains, which is expected as the dye is confined within the nanofilm boundary. The MPAC hydrogels were imaged under ambient (Figure 8D) and reduced oxygen (Figure 8E) conditions, while keeping the camera settings constant to obtain a ratio image (Figure 8F). An intensity ratio (reduced oxygen : ambient oxygen) corresponding to > 1 depicts that the PdTCPP intensity has increased under reduced oxygen. While not absolutely quantitative, these images show that the dye remains localized within the capsules and retains its response to oxygen after glutaraldehyde cross-linking and immobilization in the hydrogel.

Alginate matrices containing GOx/PdTCPP microdomains can potentially function as enzymatic biosensors. GOx contained in these microdomains oxidizes glucose, reducing local oxygen concentrations proportional to the glucose permeation rate. We envisioned to tune the analytical range and sensitivity of the hydrogel based sensor by decreasing glucose permeation rate into the microdomains, eventually making it a truly glucose-diffusion limited system. However, it is imperative to understand that glucose-limited behavior is achieved only if the influx of oxygen is much higher than or

equivalent to the influx of glucose; requiring the nanofilms to preferentially decrease glucose diffusion rates over oxygen diffusion rates.

The response of the MPAC hydrogels containing PdTCPP and GOx loaded microdomains to changing oxygen concentrations was evaluated to ascertain whether cross-linking of PAH/PSS bilayers affects oxygen diffusion. As a control, the oxygen sensor response of MPAC hydrogels containing non-cross-linked $[PDADMAC/PSS]_5$-$[PAH/PSS]_9$ microcapsules was also determined. Figure 9 (inset) represents the Stern-Volmer normalized lifetime (lifetime at zero oxygen concentration divided by lifetime at given oxygen level) against varying oxygen concentrations. K_{SV} values were calculated using the Stern-Volmer equation $\tau_0/\tau = 1+K_{SV}[O_2]$, and found to be $0.030 \pm 0.002\ \mu M^{-1}$ on an average. All the hydrogel samples having different nanofilm compositions showed a high sensitivity to oxygen at levels less than 100 μM, and a decreased sensitivity at higher oxygen concentrations, characteristic of oxygen-sensitive palladium porphyrin dyes.[60-62] The similar oxygen response characteristics show that cross-linking of the nanofilms in the hydrogel does not affect the kinetics of oxygen diffusion.

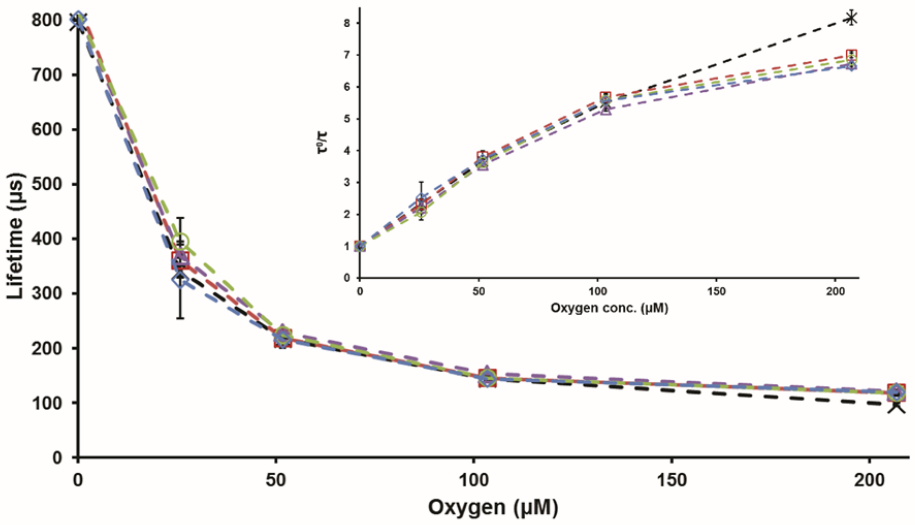

Figure 9. Quenching curves. Lifetime and (Inset) normalized lifetime (normalized to the lifetime at zero oxygen concentration) against varying oxygen concentrations for MPAC hydrogels containing microdomains bound by different nanofilm architectures. The cross-linked nanofilm architectures are represented by $[PDADMAC/PSS]_5$-$[PAH/PSS]_n$ where n = 3 (red □) , n = 5 (purple Δ), n = 7 (green ○), n = 9 (blue ◊) and non-cross-linked nanofilm architecture $[PDADMAC/PSS]_5$-$[PAH/PSS]_9$ (black ×). Error bars represent 95% confidence intervals for three separate MPAC hydrogels. The dashed lines are provided only as a guide to the eyes.

3.3.3. Sensor response of hydrogels

The glucose sensing characteristics of MPACs containing non-cross-linked $[PDADMAC/PSS]_5$-$[PAH/PSS]_n$ nanofilm bounded microdomains were examined to establish that cross-linking of PAH/PSS bilayers was necessary to alter the sensor characteristics significantly. The phosphorescence lifetime of MPAC hydrogels containing PdTCPP and GOx loaded microdomains was recorded as the materials were exposed to buffer solutions containing varied concentrations of glucose (0 - 400 mg/dL). The normalized sensor response curves for MPACs containing non-cross-linked

[PDADMAC/PSS]$_5$-[PAH/PSS]$_n$ nanofilm bounded microdomains are illustrated in Figure 10A, where the change in lifetime is calculated relative to the lifetime obtained at maximum glucose concentration (refer to Figure 10C for non-normalized lifetime response curves). A coherent trend was observed in terms of sensitivity and range of the sensors as the number of bilayers was increased. This was anticipated since altering the transport properties of the microcapsule directly influences the sensor characteristics.[63] With an increase in the number of PAH/PSS bilayers from $n = 3$ to $n = 9$, the analytical range increases by ~ 106% while the sensitivity over the same range decreases by ~ 59%. This inverse relationship between range and sensitivity is characteristic of flux-based sensors.[59] Table 1 summarizes the sensor parameters for non-cross-linked microcapsule-containing hydrogels. The decrease in the flux of glucose diffusing into the microdomains as the number of bilayers are increased accounts for the changed sensor response characteristics. Although the analytical range increases as the number of bilayers are increased, the analytical range achieved for the materials using non-cross-linked nanofilms still does not encompass the usual operational range for glucose sensors (0 - 400 mg/mL).[64] All of the sensor formulations made using non-cross-linked PEMs were highly sensitive to glucose changes in the hypoglycemic range (< 70 mg/dL),[65] but they failed to detect glucose concentration changes above 98 mg/dL. This suggests that the glucose flux into the microdomains is too high, which either overwhelms the enzyme or consumes oxygen too fast. These findings indicate that the diffusion of glucose into the discrete microdomain sensors should be decreased further, to make the composite hydrogel system glucose-diffusion limited.

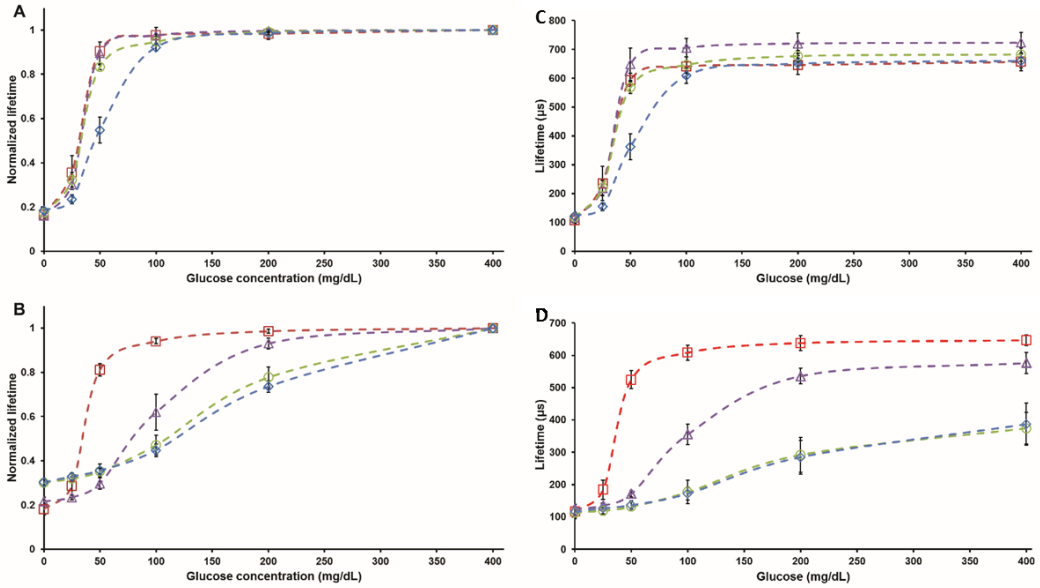

Figure 10. (A) Sensor response curves of MPACS containing non-cross-linked $[PDADMAC/PSS]_5$-$[PAH/PSS]_n$ nanofilm bounded microdomains when $n = 3$ (red □), $n = 5$ (purple Δ), $n = 7$ (green ○) or $n = 9$ (blue ◊). (B) Sensor response curves of MPACs containing cross-linked $[PDADMAC/PSS]_5$-$[PAH/PSS]_n$ nanofilm bounded microdomains when $n = 3$ (red □) , $n = 5$ (purple Δ), $n = 7$ (green ○) or $n = 9$ (blue ◊). Error bars represent 95% confidence intervals for three separate MPAC hydrogels. The dashed lines are provided only as a guide to the eyes.

Table 1. Calculated sensor parameters for MPACs containing non-cross-linked and cross-linked [PDADMAC/PSS]$_5$-[PAH/PSS]$_n$ nanofilm-bounded microdomains [a]

	LOD [b] ***(mg/dL)***	***MDGC*** [c] ***(mg/dL)***	***Range*** [d] ***(mg/dL)***	***Sensitivity/range (% per mg/dL)***
Non-cross-linked				
[PAH/PSS]$_3$	12.0 ± 6.8	54.4 ± 3.2	40.7 ± 8.8	13.0 ± 4.5
[PAH/PSS]$_5$	15.6 ± 0.1	54.6 ± 4.9	39.8 ± 4.5	13.2 ± 0.6
[PAH/PSS]$_7$	11.5 ± 2.3	62.5 ± 2.1	51.0 ± 4.3	9.4 ± 1.6
[PAH/PSS]$_9$	14.4 ± 2.0	98.2 ± 7.4	83.8 ± 5.5	5.3 ± 0.5
Cross-linked				
[PAH/PSS]$_3$	14.3 ± 5.0	65.4 ± 7.3	52.2 ± 11.1	12.5 ± 3.4
[PAH/PSS]$_5$	24.3 ± 4.8	170.8 ± 23.4	168.0 ± 13.4	2.0 ± 0.4
[PAH/PSS]$_7$	32.9 ± 3.7	296.4 ± 28.9	271.4 ± 23.0	0.9 ± 0.1
[PAH/PSS]$_9$	33.2 ± 9.7	321.2 ± 8.2	292.7 ± 9.5	0.8 ± 0.1

[a] In each case, data from three separate MPAC hydrogels were used to calculate mean values (95% confidence). [b]*LOD,* limit of detection; [c]*MDGC,* maximum differentiable glucose concentration; [d]Range*, MDGC-LOD*.

Having demonstrated that non-cross-linked nanofilm containing sensor formulations are not effective in controlling sensor dynamics considerably, the sensor response of formulations containing glutaraldehyde cross-linked microdomains were evaluated (refer to Figure 10D for non-normalized response curves). As expected, with an increase in the number of cross-linked PAH/PSS bilayers in the nanocomposite hydrogels, the analytical range of the sensors increases and the sensitivity decreases (Figure 10B). The analytical range increases by ~ 461% while the sensitivity over the range decreases by ~ 94%, as *n* is increased from 3 to 9. The analytical range and sensitivity of MPAC hydrogels containing cross-linked $[PDADMAC/PSS]_5$-$[PAH/PSS]_9$ was found to be ~ 227% more and ~ 85% less respectively than MPAC hydrogels containing non-cross-linked $[PDADMAC/PSS]_5$-$[PAH/PSS]_9$. Thus, cross-linking of PAH/PSS bilayers is crucial to significantly decrease *dC/dt* of glucose into the sensor and alter sensor response parameters considerably. However, as discussed previously, the rate of change of *dC/dt* decreases with the increase in the number of cross-linked bilayers that consequently affects how the sensor characteristics change as number of bilayers are increased. The analytic range increases by ~ 8% and the sensitivity over the range decreases by ~ 8% when the number of cross-linked bilayers is increased from 7 to 9. This change is insignificant compared to the change in response between sensors fabricated from 3 cross-linked bilayers and 5 cross-linked bilayers. Sensor figures of merit for cross-linked microcapsule-containing hydrogels are summarized in Table 1.

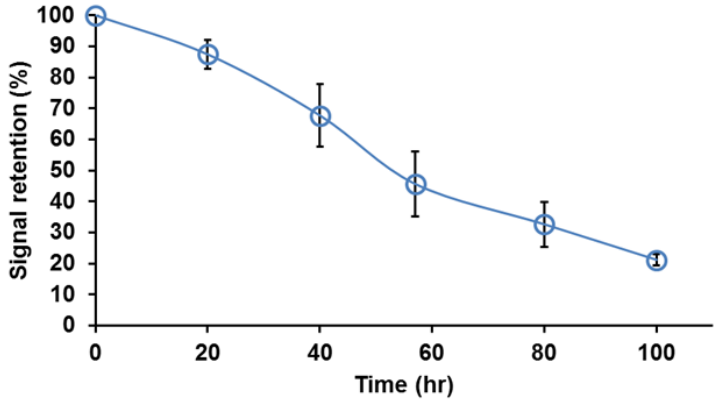

Figure 11. Plot depicting decrease in lifetime signal of MPACs containing cross-linked [PDADMAC/PSS]$_5$-[PAH/PSS]$_9$ nanofilm bounded microdomains when continuously exposed to 400 mg/dL glucose. Error bars represent 95% confidence intervals for three separate MPAC hydrogels.

Finally, to examine the long term stability of the glucose sensors, the hydrogels were continuously exposed to 400 mg/dL glucose; at 400 mg/dL glucose, the sensor response is completely saturated because GOx converts glucose at the maximum rate possible. This simulates an extreme scenario when a sensor is exposed to very high levels of glucose. The signal retention of the sensor gradually decreased (Figure 11) over time (~ 50% loss in 48 h) indicating loss in GOx activity. As GOx becomes less active it loses its ability to oxidize glucose resulting in less consumption of local oxygen that is manifested as loss in sensor response. This result prompted the search for alternative GOx immobilization techniques (discussed in the next section) in order to improve the sensors operational lifetime.

3.4. Conclusion

This work demonstrates the utility of glutaraldehyde cross-linked LbL nanofilms for precise diffusion control and the application of this technology for the development of glucose sensors. The diffusion control of cross-linked films was first investigated using planar films to develop a method capable of providing a large diffusion barrier, while also considering the design constraints needed for eventual use in engineering microcapsules. Cross-linking just a few bilayers of nanofilms reduced glucose permeation rate to levels, which could only be theoretically achieved using hundreds of non-cross-linked bilayers. The effect of cross-linking was further probed by the introduction of spacer bilayers as it was expected that the nanofilm cross-linking was a combination of interlayer and intralayer cross-linking due to the fuzzy nature of the interpenetrating PEMs. Spacer bilayers lessen the degree of diffusion restriction, which could be useful for achieving more specific permeation rates or for the diffusion modulation of larger molecules. The cross-linking scheme was adapted for colloidal templates using glucose as a model analyte and microcapsules containing encapsulated glucose sensor chemistry. Cross-linked nanofilms preferentially restricted glucose movement over oxygen transport across the microcapsule walls, which manifested as an extension in the analytical range of the hydrogel based composite biosensors.

We anticipate that similar results will be observed by cross-linking other amine containing components (*e.g.* peptides, enzymes, polysaccharides) which are commonly used to fabricate LbL nanofilms. This technology can be used to tailor the functionality of flux-based biosensors for a variety of small-molecule analytes (*i.e.* urea, lactate, *etc.*)

and we expect it can also play a role in controlled-release systems for applications such as drug delivery and self-healing coatings. Having the ability to differentially control the release or intake of molecules, opens the possibility to formulate multiplexed and multifunctional nanocomposite devices. Although, we demonstrated the use of composite hydrogels to sense glucose in the physiological range, additional modifications to the design scheme are necessary for *in vivo* operation. Implantable *in vivo* sensors mandate greater operational stability and reliable sensor response at physiologically low oxygen conditions. In the next chapter, modifications to our sensor design for operation under in vivo conditions will be discussed. Future work will also focus on the development of these unique microcapsule enabled hydrogel based devices for multi-analyte sensing and theranostic applications.

4. COMPOSITE HYDROGELS WITH ENGINEERED MICRODOMAINS FOR OPTICAL GLUCOSE SENSING AT LOW OXYGEN CONDITIONS *

4.1. Introduction

Fully-implantable bioresponsive materials offer potential to overcome issues associated with minimally-invasive, electrochemical sensors; however, devices proposed for implantation carry stringent requirements. Any sensing material that is completely implanted should satisfy the following basic criteria: (1) soft biomaterial possessing small form factor and mechanical properties similar to the surrounding tissue;[116] (2) high-fidelity response over the biologically relevant range;[117] and (3) long-term stability.[118] Insensitivity to electromagnetic interference (EMI) and low/zero-power operation with facile recharging are additional desirable properties.[119] To meet these requirements in an approach that offers the additional advantage of avoiding the use of implanted electronics, our group has recently developed bioresponsive materials that respond to lactate and glucose by covalently immobilizing oxidoreductase enzymes and an oxygen-sensitive metalloporphyrin dye within biocompatible hydrogel matrices. [101, 102] These unique materials transduce chemical concentration into optical information (phosphorescence intensity or lifetime). While these materials were found to exhibit the desired response characteristics in benchtop testing, it was observed that the response

* Reprinted with permission from "Composite Hydrogels with Engineered Microdomains for Optical Glucose Sensing at Low Oxygen Conditions" by Bornhoeft. L.R., Biswas. A., McShane. M.J. *MDPI Biosensors* 2017, *7(1), 8*. Copyright 2017 by Multidisciplinary Digital Publishing Institute.

often saturated at relatively low analyte concentrations when used in vivo; this undesired outcome has been attributed primarily to low tissue oxygen levels which have been found to be ~ 3 times lower than air-equilibrated aqueous solutions. [120, 121] These low oxygen concentrations disrupt the function of the bioresponsive material because they were designed and lab-proven based on a diffusion-reaction equilibrium expecting higher oxygen concentrations. Modification of the materials to address this issue requires drastic reduction of analyte flux; this is essential because enzymatic bioresponsive materials require a delicate balance between analyte diffusion and reaction to produce a signal that varies sensitively over the entire analyte concentration range of interest.[122, 123] The use of PEMs to form responsive microdomains dispersed in hydrogel matrices to control glucose diffusion was recently demonstrated as an effective means to "tune" the optical response; these responsive materials are capable of preferentially reducing glucose flux while not affecting oxygen diffusion kinetics.[55, 124] However, the relatively low enzyme stability (Figure 11) in the hollow microdomains of these materials was insufficient to support use in long-term sensing applications as described in Chapter 3. In contrast, ionically-crosslinked alginate, a polysaccharide with mild encapsulation and gelation techniques, was chosen as an improvement in the material to enhance enzyme stability.[125, 126]

In this work, the same principle of transport control *via* nanofilm coatings on microdomains mentioned above was adapted for application to alginate microparticles that were subsequently embedded in alginate hydrogels. We hypothesized that the sensitivity to different oxygen concentrations could be influenced by the composition of

the nanofilm coating and that there would be a substantial increase in stability by protecting and immobilizing enzymes within alginate microparticles. This design was expected to leverage the advantages of different systems studied in our previous work, providing enzyme stability along with the capability to fine-tune the optical response of the material for different applications/environments; together, these properties give a level of engineering control over the sensing figures of merit that, to our knowledge, has not been demonstrated before.

4.2. Experimental section

4.2.1. Chemicals

All chemicals were reagent-grade and used without further purification. Alginic acid sodium salt (250 cP, 2% @ 25°C), buffer salts (TRIS, 2-(N-morpholino) ethanesulfonic acid)), calcium carbonate ($CaCO_3$), 2,2,4-trimethylpentane (isooctane), poly (allylamine hydrochloride) (PAH, average MW 15 kDa), poly (sodium-4-styrenesulfonate) (PSS, average MW 70 kDa), dimethyl sulfoxide (DMSO), and glutaraldehyde (grade II, 25% in deionized water) were obtained from Sigma Aldrich. β-D-glucose and calcium chloride ($CaCl_2$) were obtained from Macron Fine Chemicals. Surfactants sorbitan trioleate (SPAN 85) and polyoxyethylene sorbitan trioleate (TWEEN 85) were obtained from Tokyo Chemical Company and Sigma Aldrich, respectively. Pd-meso-tetra (4-carboxyphenyl) porphyrin (PdTCPP) was obtained from Frontier Scientific. Glucose oxidase (284 U/mg, *Aspergillus Niger*) and catalase (6500

U/mg, bovine liver) were obtained from BBI Solutions and Calzyme Laboratories, Inc., respectively.

4.2.2. Alginate microparticle synthesis

Alginate microparticles containing encapsulated PdTCPP, glucose oxidase (GOx), and catalase (Cat) were synthesized following a previously reported emulsion method with minor modifications [86]. Briefly, 5 mL of aqueous solution containing 3 w/v % alginic acid, 500 µL of 1:1 molar ratio GOx (11.7 mg) and Cat (18.3 mg) in 50 mM TRIS buffer (pH 7.2), and 500 µL of 10 mM PdTCPP in DMSO were added drop-wise and emulsified in a solution containing 10.8 mL isooctane (99%) with 170 µL SPAN 85 (1.55 v/v %) using a homogenizer (IKA T25, S25N18G dispersing tool) operating at 8000 rpm for 2 min. A second surfactant solution containing 1.5 mL isooctane (99%) with 96 µL TWEEN 85 (6 v/v %) was added and homogenized at the same speed for 1 min. For external gelation of alginate microparticles, 4 mL of 10% w/v $CaCl_2$ solution was added and the emulsion was stirred gently in a round bottom flask for 20 min. Alginate microparticles were washed with deionized water and collected after centrifugation (2000g for 2 min).

4.2.3. Layer-by-Layer (LbL) deposition on alginate microparticles

Nanofilms were deposited on alginate microparticles by alternately adding 1 mL of 20 mg/mL PAH (pH 8) and 1 mL of 20 mg/mL PSS (pH 7.2) to microparticles and washing between each deposition with 10 mM TRIS buffer (pH 8 and pH 7.2, respectively) until the desired number of layers were applied. Studies of diffusion

inhibition by the nanofilms have been previously performed to evaluate the relationship between the number of layers and flux of glucose and oxygen; [124] based on those findings, 10 bilayers were used for this work. Covalent crosslinking of the PAH amine groups was performed by mixing 4.4 mg of LbL-coated alginate microparticles with 20 mL of 3 M glutaraldehyde and gently stirring for 30 min at room temperature. Particles were washed with deionized water and stored at 4°C in a solution containing 10 mM TRIS (pH 7.2) and 10 mM $CaCl_2$.

4.2.4. AnA fabrication: alginate microparticles embedded in alginate hydrogel

The alginate hydrogel fabrication process was based on a previously reported internal gelation method with minor modifications.[103] Briefly, alginate microparticles (75 μL, 8.8 mg) were mixed with 200 μL of 3 w/v% alginate and 25 μL of 33.3 mg/mL $CaCO_3$. Dissolution of $CaCO_3$ was initiated by addition of 100 μL of 10 mM MES buffer (pH 6.1). The solution was vortexed and quickly transferred to a 1.5 mm-thick Teflon and glass mold and allowed to gel for 15 min. AnA hydrogels were then punched into discs (4 mm diameter, 1.5 mm thick, Fig. 1c) using a biopsy punch. All materials were stored in a solution containing 10 mM TRIS (pH 7.2) and 10 mM $CaCl_2$ and allowed to equilibrate overnight before use.

4.2.5. Diffusion measurements

LbL polyelectrolyte nanofilms were deposited on 0.2 μm filters (Anapore) by alternately adding 1 mL of 20 mg/mL PAH (pH 8) and 1 mL of 20 mg/mL PSS (pH 7.2)

to the filters while washing between each deposition with 10 mM TRIS buffer (pH 8) until the desired number of layers were applied. Covalent crosslinking of the nanofilms was performed by adding 1 mL of 3 M glutaraldehyde for 30 min at room temperature followed by rinsing with deionized water. The nanofilm-coated Anapore filters were placed in a side by side permeate chamber (Permegear Inc.) with the feed chamber containing 7 mL of a 1 g/L glucose solution and the permeate chamber containing 7 mL of a 10 mM TRIS buffer (pH 7.2). Samples were taken at regular time points from both chambers and analyzed with an YSI Biochemistry Analyzer (Model 2700). The change in concentration over time (dC/dt) was calculated using linear regression.

4.2.6. Oxygen and glucose challenges

AnA hydrogels were immobilized in a custom-built flowcell previously reported elsewhere.[124] Oxygen challenges were performed by exposing the AnA hydrogels to varying dissolved oxygen concentrations (0-206.8 μM, 37 °C). The oxygen concentration was adjusted using mass flow controllers (1179A, MKS). Glucose challenges were performed by exposing the AnA hydrogels to varying physiologically relevant glucose concentrations (0-400 mg/dL in 10 mM TRIS with 10 mM $CaCl_2$, 37°C) at fixed oxygen concentrations (206.8 μM for ambient and 70 μM for interstitial oxygen concentration).[120] The oxygen concentration was regulated by a vacuum degasser (9000-1118, Systec). All optical measurements were recorded using a custom-built time domain phosphorescence lifetime measurement instrument with a 530 nm excitation source described elsewhere. [101, 102] The combination of the AnA hydrogel

(bioresponsive material) with the lifetime measurement unit (detector) will be referred to as the "sensing system." The glucose challenge data of phosphorescence lifetime versus concentration were fit using a sigmoidal function in MATLAB (version R2015a). The upper and lower limits of detection (*ULOD* and *LLOD*, respectively) used to calculate the dynamic range (*ULOD-LLOD*) for each glucose challenge were calculated by using the 3-σ method described elsewhere.[12] The sensitivity was calculated by dividing the difference in phosphorescence lifetime values at the *ULOD* and *LLOD* by the dynamic range. All statistical tests were performed using GraphPad Prism (version 7.0a).

4.2.7. Scanning electron microscopy of alginate

Bare and nanofilm-coated alginate microparticles were imaged using a scanning electron microscope (SEM, JEOL 7500, 15 kV). Samples were prepared by pipetting 2 μL of a 1:20 dilute solution of microparticles onto a silicon wafer and drying in a vacuum desiccator overnight. The samples were sputter coated with Pd/Pt (2.5 nm) prior to image acquisition.

4.2.8. Darkfield and hyperspectral imaging of AnA hydrogels

AnA hydrogels (4 mm biopsy punch) were used for darkfield and hyperspectral imaging using a research grade optical microscope (BX51, Olympus, 60x oil, variable NA iris, aluminum quartz halogen source lamp) equipped with an enhanced darkfield illumination condenser system. Hyperspectral image acquisition was obtained with a diffraction grating hyperspectral imager, integrated CCD, and line scan or "pushbroom"

system. CytoViva software (customized ENVI hyperspectral image software, nanoscale analysis) was used for all image processing.

4.3. Results and discussion

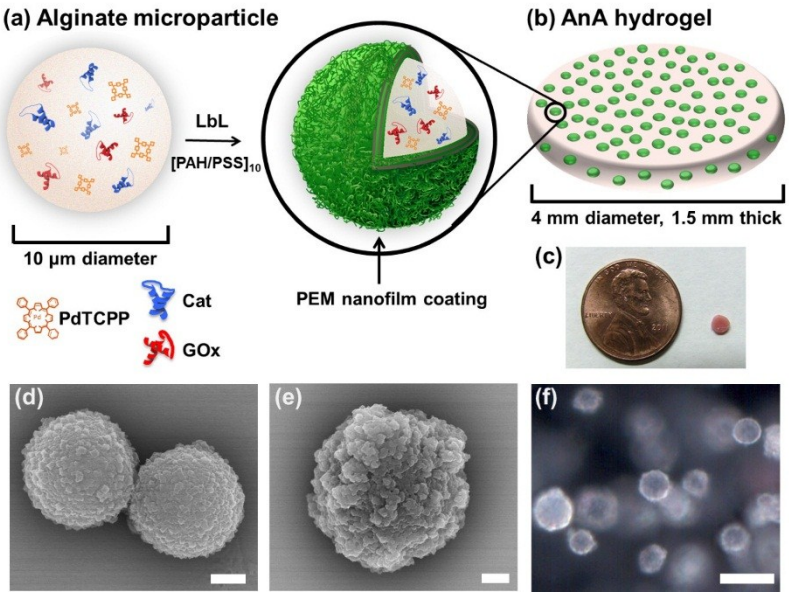

Figure 12. AnA hydrogels: composition and microscopic imaging. (A) Illustration of an alginate microparticle containing PdTCPP, GOx, and Cat coated with 10 bilayers of PAH and PSS. (B) AnA hydrogel with embedded PEM-coated alginate particles. (C) Photograph of AnA hydrogel next to a penny. SEM micrograph of (D) uncoated and (E) coated alginate microparticles, respectively. Scale bars = 1 μm for both micrographs. (F) Darkfield optical image of the AnA hydrogel containing alginate microparticles distributed throughout an alginate matrix. Scale bar = 10 μm.

4.3.1. Characterization of the AnA hydrogels

Fig. 1a-b illustrate an alginate microparticle, synthesized by a water-in-oil emulsion method, containing PdTCPP, GOx, and Cat before and after LbL nanofilm

deposition of 10 bilayers of PAH and PSS (denoted as $[PAH/PSS]_{10}$). The bare and coated microparticles were imaged to reveal morphological differences using SEM, as shown in Figure. 12 D-E, respectively. The textured surface of the uncoated microparticles resulted from residual $CaCl_2$ salt but was much smoother than the LbL-coated spheres, which exhibit increased surface roughness. After characterization of the alginate microparticles, the AnA hydrogel (Figure 12C) was fabricated by the internal gelation method described above. Darkfield microscopy of the AnA hydrogel (Figure 12F) shows individual alginate microparticles distributed throughout the 1.5 mm thick alginate hydrogel. The reflectance spectrum and hyperspectral imaging of Figure 12F showed an absence of signal in areas of the hydrogel where there was an absence of sensing microdomains indicating confinement of PdTCPP to the nanofilm bound microparticles. (Figure 13)

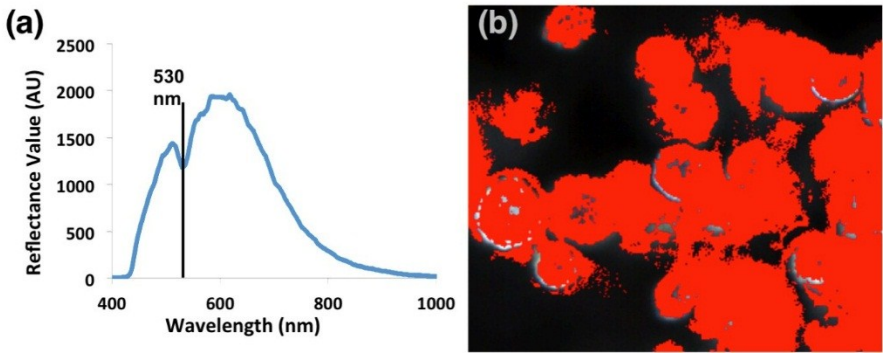

Figure 13. (A) Reflectance spectrum of encapsulated PdTCPP embedded within the AnA hydrogel. The decrease in the reflectance value, indicated by a black line at 530 nm, correlates to the excitation wavelength of PdTCPP. (B) Hyperspectral map of a section of the AnA hydrogel with false red color identifying encapsulated PdTCPP at multiple focal planes. Scale bar = 10 μm.

4.3.2. AnA hydrogel response

Following synthesis and characterization of the alginate microparticles and AnA hydrogels, performance of the full system was evaluated. The sensing capability of this system is governed by the following well-known enzymatic reaction in the presence of GOx: glucose + O_2 + H_2O → gluconic acid + H_2O_2. Glucose and molecular oxygen diffuse into the sensing material, and glucose is catalytically converted into gluconic acid and hydrogen peroxide by the oxidoreductase enzyme GOx. This reaction results in the consumption of and decrease in local glucose and oxygen concentrations. The co-immobilized phosphorescent porphyrin dye (PdTCPP) is collisionally quenched by molecular oxygen, resulting in phosphorescence intensities and lifetimes that are inversely proportional to the local oxygen concentration.[127] As oxygen decreases, PdTCPP is quenched less; with the co-substrate reaction scheme, this results in increasing phosphorescence lifetimes that are directly correlated with glucose concentrations within the AnA hydrogel. As a result, the systems employing enzymatic AnA hydrogels are flux-based, where performance relies on the ability to control relative diffusion of oxygen and glucose.

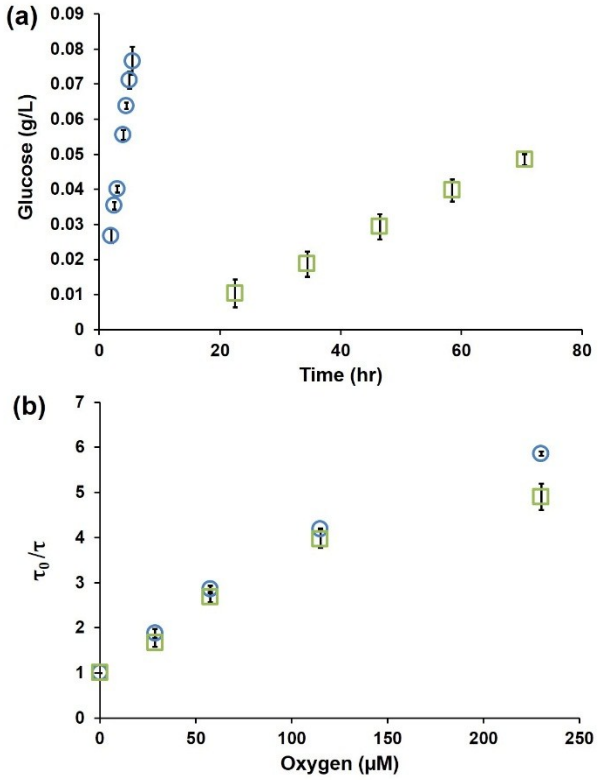

Figure 14. (A) Plot showing the difference in the rate of glucose permeation through 10 bilayers of PAH/PSS without (blue ○) and with (green □) glutaraldehyde crosslinking. (B) The phosphorescence lifetimes of AnA hydrogels containing 10 bilayers of PAH/PSS plotted against oxygen concentrations for particles without (blue ○) and with (green □) glutaraldehyde crosslinking. Error bars for both plots represent 95% confidence intervals for three separate samples.

To tune the sensitivity of AnA hydrogels under different oxygen conditions, we aimed to control the nature of the diffusion-limiting coatings on the surface of the alginate microparticle. Glutaraldehyde crosslinking of the amine groups on PAH has been shown as an effective method to significantly reduce glucose permeation; therefore, AnA hydrogels containing alginate microparticles without and with crosslinking were synthesized.[124] We quantitatively assessed the effect crosslinking has on the diffusion of

glucose across planar Anapore filters containing 10 bilayers of PAH/PSS and found a 179% decrease in the glucose permeation rate when crosslinking was introduced (Figure 14A). Next, we evaluated the optical phosphorescence lifetime response when oxygen concentrations were varied by using the Stern Volmer relationship: $\tau_0/\tau = 1 + K_{SV}[O_2]$. The normalized phosphorescence lifetime ($\tau 0/\tau$) was plotted against oxygen concentration ($[O_2]$) in order to calculate the Stern Volmer quenching constant (KSV), summarized in Table 2 below. We found no statistical difference between AnA hydrogels without and with crosslinking at oxygen levels lower than 115 μM ($p > 0.05$, Figure 14B), which represents the expected operating conditions (<100 μM $[O_2]$) for an in vivo implantable glucose bioresponsive material. With this system, we control the analyte flux only, while the oxygen concentration remains unperturbed; this is especially key for environments that are limited in oxygen supply.

Figure 15A is a graph of the phosphorescence lifetime response to glucose concentration changes, which clearly presents the biosensing capability of this system. The AnA hydrogels were tested at physiologically relevant glucose concentrations (0-400 mg/dL) and at two different oxygen levels, ambient (206.8 μM) and interstitial (70 μM). Calibration curves were generated for each response, and the *ULOD* and *LLOD* were calculated in order to determine the dynamic range and sensitivity for each AnA hydrogel. At ambient conditions, the AnA hydrogels containing non-crosslinked microparticles respond over a wide dynamic range of 5.7-330 mg/dL with a sensitivity of 0.80 ± 0.11 μs dL mg-1. In contrast, AnA hydrogels containing crosslinked LbL coated microparticles under ambient conditions exhibit only a slight increase in the

optical response with phosphorescence lifetimes of 115-150 μs correlating to a dynamic range of 87-350 mg/dL and low sensitivity of 0.075 ± 0.013 μs dL mg-1 when exposed to glucose. This difference observed at ambient conditions is due to an imbalance in the analyte diffusion kinetics, where the low glucose flux relative to oxygen flux results in a lack of sensitivity when using crosslinked LbL coated microparticles within the AnA hydrogels. Specifically, glucose diffusion through AnA hydrogels with crosslinked microparticles is so slow relative to oxygen that the reaction does not effectively deplete oxygen locally. At low oxygen levels, however, a decrease in glucose diffusion is necessary in order to prevent saturation of the signal. AnA hydrogels containing non-crosslinked particles immediately saturated when exposed to the lowest concentration of glucose. Alternatively, AnA hydrogels containing crosslinked microparticles have a linear response at physiologically-relevant glucose and oxygen concentrations with a dynamic range of 2.6-350 mg/dL and sensitivity of 0.97 ± 0.054 μs dL mg-1. The sensing figures of merit are summarized in Table 2 for AnA hydrogels containing either non-crosslinked or crosslinked microparticles at ambient and low oxygen. These results demonstrate the ability to control the desired optical response by carefully engineering the diffusion-limiting coating on alginate microparticles; this is extremely important when translating this bioresponsive composite hydrogel design to in vivo applications. We note some of our parallel efforts specifically address some of the questions pertaining to subcutaneous deployment of such responsive materials. Specifically, we have performed studies with live subjects (animal and human models) to assess the potential for successful in vivo application of similar materials. These comparable

sensing systems consisting of implantable hydrogel based materials with longer-wavelength benzoporphyrin phosphors (with red-light excitation, compared to the green-excited phosphors used here) and along with a complementary phosphorescence detection instrument with red LED and filters matching the long wavelength emission.[101, 128] These studies describe a strategy that appears effective for in vivo use and should be applicable to the AnA hydrogels described here, but they will similarly require a shift to longer-wavelength phosphors to enable the deeper tissue penetration.

To better understand the AnA hydrogel performance and further underscore the necessity to tune the sensitivity and dynamic range, we compared a numerical simulation of glucose finger prick measurements with predicted AnA hydrogel response values. Figure 15 B-C present graphs of reference glucose values overlaid on a plot of predicted AnA hydrogel response values that would be expected from non-crosslinked or crosslinked microparticles calibrated and operated at ambient and low oxygen. The glucose values represent measurements from finger prick blood glucose measurements. The predicted optical response values were extrapolated from the calibration curves generated from Figure 15A and are associated with each individual glucose measurement. Figure 15B shows that incorporation of non-crosslinked microparticles at ambient oxygen concentrations correlate relatively strongly with simulated glucose values ($r = 0.810$), indicating that the oxygen concentrations at ambient conditions are high enough that they do not necessitate an increased diffusion barrier and decrease in analyte flux. Although AnA hydrogels containing crosslinked microparticles also correlate remarkably well with glucose when tested at ambient oxygen ($r = 0.998$, Figure

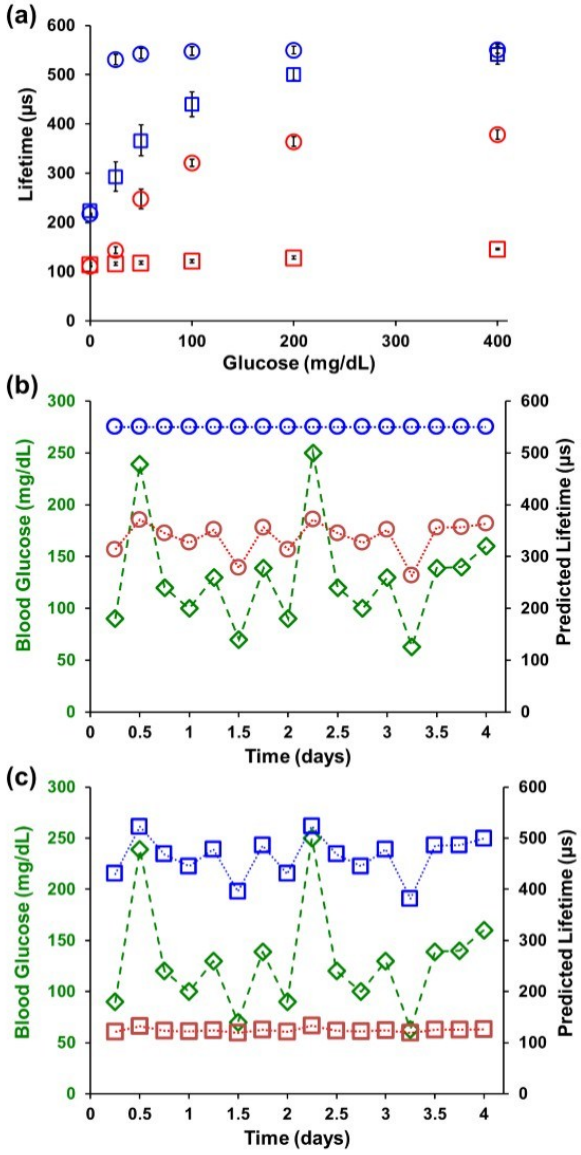

Figure 15. Calibration and performance stability of AnA hydrogels. (A) AnA hydrogel response to varying glucose concentration (0-400 mg/dL) for non-crosslinked (blue ○ or red ○, ambient and low oxygen, respectively) and crosslinked (blue □ or red □, ambient and low oxygen, respectively) microparticles. Error bars represent 95% confidence intervals for three separate samples of the same formulation. (B,C) Simulated blood glucose levels (green, left axis) collected over time and predicted response of each AnA hydrogel (blue and red, right axis). The predicted values indicate estimated responses from calibration of materials containing either non-crosslinked (blue ○ or red ○, ambient and low oxygen, respectively) or crosslinked (blue □ or red □, ambient and low oxygen, respectively) microparticles.

15B), the sensitivity is too low to distinguish between the phosphorescence lifetime values for most practical applications. Alternatively, the AnA hydrogels with non-crosslinked microparticles tested at low oxygen generate a constant, saturated response; here, no correlation between predicted phosphorescence lifetime values and input glucose values is expected. Crosslinked microparticles are essential for a robust response at low oxygen levels; these predictions show dramatically improved correlation with reference glucose values (r = 0.904, Figure 15C).

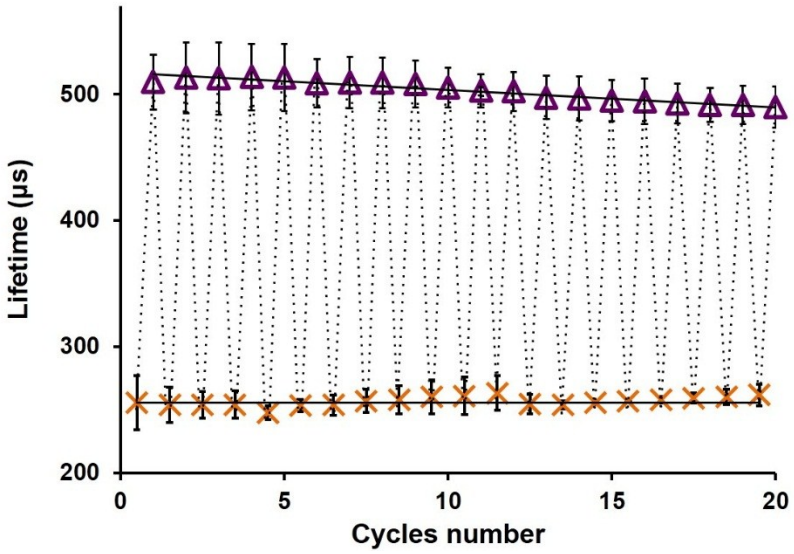

Figure 16. Stability of the AnA hydrogel. Cyclic testing of AnA hydrogel consisting of crosslinked microparticles tested at interstitial oxygen levels over 2 days. Glucose was varied between 0 mg/dL (orange X) and 400 mg/dL (purple Δ). Error bars represent 95% confidence intervals for three separate samples.

Table 2. Figures of merit calculated for AnA hydrogels with and without crosslinked microparticles at ambient and low oxygen.[a]

	Non-crosslinked	**Crosslinked**
τ_0 (μs)	603 ± 16.3	588 ± 22.3
K_{sv} (O_2 %)	1.9 ± 0.072	2.3 ± 0.017
Ambient O_2		
Dynamic Range (mg/dL)	5.7-330	87-350
Sensitivity (μs × dL/mg)	0.80 ± 0.11	0.075 ± 0.013
Low O_2		
Dynamic Range (mg/dL)	[b]---	2.6-350
Sensitivity (μs × dL/mg)	[b]---	0.97 ± 0.054

[a] Data is calculated based off of three separate AnA hydrogels from the same formulation with 95% confidence intervals. [b] AnA hydrogel saturated immediately after first glucose concentration; Metrics not determined.

4.3.3. AnA hydrogel stability

Biosensing materials containing a bioactive enzyme often loose function over time due to enzyme degradation by various mechanisms, including spontaneous enzyme denaturation and peroxide poisoning [129, 130]. Catalase is an enzyme found in many organisms utilized for the catalysis of hydrogen peroxide into water and oxygen and has been incorporated into enzymatic glucose responsive hydrogels to mitigate peroxide

poisoning [110, 131]. By co-immobilizing catalase with glucose oxidase in our microparticles, the stability was expected to increase with respect to sensors not having catalase; this has been extensively demonstrated by multiple research groups over the last couple of decades.[105, 132-134] Indeed, Figure 16 shows the remarkable stability of the AnA hydrogel containing crosslinked alginate microparticles tested at an interstitial oxygen concentration (70 μM [O_2]). The hydrogels were tested repeatedly over the course of two days at the extreme physiological values of 0 and 400 mg/dL. The phosphorescence lifetime data points for each glucose concentration (0 and then 400 mg/dL) were fit with a linear regression line. Although there appears to be a slight increase and decrease in the phosphorescence lifetime values at 0 and 400 mg/dL, respectively, there was no statistically significant difference in optical response from start to end at either of the two concentrations studied ($p > 0.05$). Using linear regression to predict the rate of degradation, it was estimated that the AnA hydrogel when exposed to these extreme, cyclic glucose concentrations would lose 50% of optical signal (phosphorescence lifetime, ~315 μs) at cycle 173; this translates to a functional working lifespan of ~ 2 weeks.

4.4. Conclusion

Alginate hydrogels embedded with alginate microparticles containing oxygen-sensitive phosphors and oxidoreductase enzymes were demonstrated as stable optical bioresponsive materials. This combination offers a number of attractive features. In terms of performance, these materials exhibit precisely-controlled diffusion of glucose

and oxygen into the discrete biosensing domains, which is necessary for accurate sensing at low, physiologically relevant oxygen concentrations. The AnA hydrogels were designed for *in vivo* sensing applications where long-term stability is necessary; here, we showed remarkable stability even after two days of cyclic exposure to extreme glucose concentrations. The sensors lose 50% of its optical signal in two weeks, supporting the possibility for use as an implantable sensing material. The stability is attributed to the supportive environment of the alginate microparticles wherein the enzyme is physically trapped. This demonstration of effective control of sensitivity and dynamic range by adjusting the properties of nanofilm coatings on microscale inclusions opens the door for application of a new class of engineered materials for sensing. The same approach will be applicable when adapting these materials for sensing with other oxidoreductase enzymes for the monitoring of different chronic conditions; the next chapter demonstrates the use of this modular design to develop lactate sensors.

5. NANOCOMPOSITE HYDROGELS CONTAINING BIOACTIVE MICROREACTORS FOR OPTICAL ENZYMATIC LACTATE SENSING

5.1. Introduction

As discussed in earlier sections enzymatic biosensors commonly contain an oxidoreductase enzyme (oxidase or dehydrogenase) that catalyzes the enzymatic utilization of the substrate accompanied by a specific product formation; substrate depletion and/or byproduct formation is then monitored optically or electrochemically.[135] In Section 4 the use of nanofilm coated alginate microparticles (AlgMPs) containing specific sensing chemistry was demonstrated for use as glucose sensors that operate at physiologically low oxygen. It was hypothesized that the microparticle sensors are modular in nature and that by replacing the glucose oxidase with other oxidoreductase enzymes the functionality of the sensors could be easily altered; in this section we demonstrate the application of AlgMPs for use as lactate sensors. Lactate, a primary byproduct of anaerobic metabolism has been an analyte of interest among researchers due to its relevance in the food industry, sports medicine, and critical care.[136-138] Monitoring blood lactate concentrations in patients with severe ketoacidosis is essential, to prevent muscle damage and potential heart attack. [139] Additionally, lactate tracking can be used to identify patients requiring resuscitative care in the event of significant blood loss.[140]

Nearly all enzymatic lactate sensors described to date have been based on planar or cylindrical transducers (*e.g.* wires, optical fibers, patterned electrodes, or waveguides)

with a coating applied to the outer surface to control analyte transport.[141-144] These devices require physical connections for measurements and have a narrow range of possible mechanical properties, limiting their potential use in many applications especially in the biomedical space. Here, we describe a unique lactate sensing platform relying on the combined effect of a population of microdomains dispersed within a hydrogel matrix to generate a measurable change in an optical property (phosphorescence). In this format the microdomains (Figure 17A) contain bioactive lactate oxidase and a reporter dye, and are lined by polyelectrolyte multilayers (PEMs); the PEM coating provide a means to control local diffusion properties and to alter sensor response. Optical sensors based on these active domains embedded within a soft hydrogel are suitable for aqueous analysis, including potential use as implantable devices if an appropriately biocompatible matrix is employed.

In enzymatic lactate sensors, LOx (lactate oxidase) catalyzes the oxidation of lactate in the presence of molecular oxygen, ultimately producing pyruvate (lactate + O_2 + lactate oxidase + H_2O $\rightarrow$ pyruvate + H_2O_2); just like the glucose sensors described, these lactate sensors should be substrate-transport limited rather than reaction-kinetics limited. [83] In this work we hypothesized that PEM lined microreactors entrapped in an outer hydrogel matrix can be used as optical lactate biosensors that work reversibly at physiologically relevant oxygen conditions. For the first time, we fabricated nanofilm-bounded LOx and phosphor-containing microreactors using alginate microparticle templates, which were ultimately dispersed in an alginate matrix to be used as nanocomposite hydrogel based lactate sensors. We evaluated the response of these

sensors to lactate at ambient and low oxygen concentrations and furthermore, we examined the stability of these sensors to repeated cyclic lactate exposure.

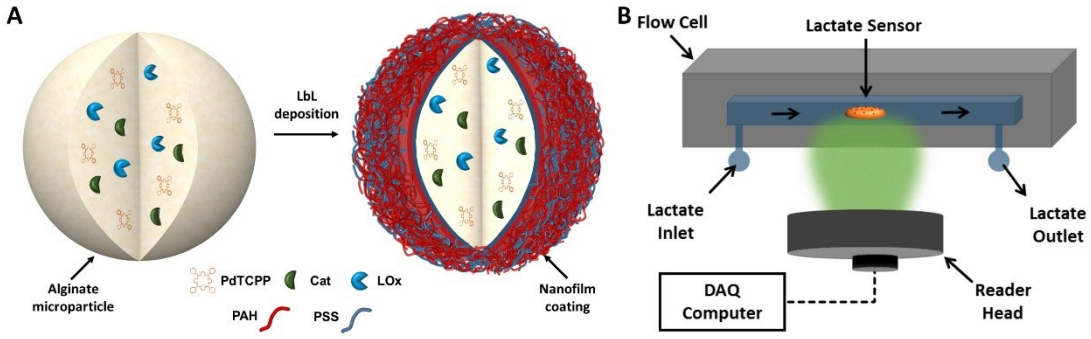

Figure 17. (A) Representation of lactate sensing AlgMPs coated by LbL nanofilm coating (B) flow through system and reader head used to test the hydrogel based lactate sensors.

5.2. Experimental section

5.2.1. Chemicals

Sodium L-lactate, calcium carbonate ($CaCO_3$), poly (sodium-4-styrenesulfonate) (PSS, average MW 70 kDa), poly (allylamine hydrochloride) (PAH, average MW 15 kDa), alginic acid sodium salt (250 cP, 2% @ 25°C), buffer salts (TRIS, MES), polyoxyethylene sorbitan trioleate (TWEEN 85), 2,2,4-trimethylpentane (isooctane), dimethyl sulfoxide (DMSO), and calcium chloride ($CaCl_2$) were obtained from Sigma Aldrich. Pd-meso-tetra(4-carboxyphenyl) porphyrin (PdTCPP), lactate oxidase (*Aerococcus viridians*), and catalase (Bovine Liver) were obtained from Frontier

Scientific , AG Scientific and Calzyme Laboratories respectively. All chemicals were used as received.

5.2.2. Alginate microparticle (AlgMP) and hydrogel sensor fabrication

Lactate oxidase (LOx), catalase (Cat), and PdTCPP containing alginate microparticles (AlgMPs) were fabricated using a slightly modified emulsification method. [86] Alginic acid (5 mL, 3% wt), enzyme solution (14 mg LOx and 21.9 mg Cat suspended in 500 µL, 50 mM TRIS buffer (pH 7.2)), and PdTCPP solution (10 mM in DMSO) were added dropwise to a round bottomed flask containing a mixture of 10.8 mL iso-octane (75 g) and 170 µL of SPAN 85 (1.7 g), and emulsified at 8000 rpm for 2 min using a homogenizer (IKA T25, S25N18G). After 2 min 96 µL of another surfactant TWEEN 85 (0.904 g) dissolved in 1.5 mL isooctane (5 g) was added and further homogenized for an additional minute. To the resulting mixture 4 mL of $CaCl_2$ (10% w/v) solution was added and gently stirred for 20 min to allow ionotropic gelation of the AlgMP sensors. The AlgMPs were washed thoroughly (3 times) with DI water before further use.

To deposit PEM nanofilms the AlgMPs were alternately exposed to 1 mL PAH (20 mg/mL, pH 8) and 1 mL PSS (20 mg/mL, pH 7.2) and washed with 10 mM TRIS buffer (pH 8) between each PEM deposition step, until the desired number of bilayers are achieved. Nanocomposite hydrogel sensors containing nanofilm coated AlgMPs were fabricated using a previously reported protocol.[115, 124] Briefly, 8.8 mg of nanofilm coated AlgMPs, 0.8 mg of $CaCO_3$ particles, 200 µL of alginate (3 w/v %), and 100 µL of

10 mM MES buffer (pH 6.1) were mixed to make a slow gelling mixture. The gelling mixture was then poured between two glass slides separated by a 0.06' Teflon spacer and allowed to gel for 30 min to make the hydrogel sensor slabs. The hydrogel slabs were stored in 10 mM TRIS (pH 7.2) containing 10 mM $CaCl_2$ and allowed to equilibrate overnight before use.

5.2.3. Characterization

Zeta potential data was collected using a Zeta Sizer Nano Series ZEN 3600 Spectrometer (Malvern Instruments Ltd.). For all zeta potential measurements, 1/1000 diluted stock in 5 mM TRIS pH 9 buffer containing 1 mM $CaCl_2$ was used.

Scanning electron microscopy (SEM) images of nanofilm lined AlgMPs and nanocomposite hydrogels were obtaining using a JEOL 7500 SEM. The AlgMP stock was diluted to 1/1000, and 2 μL of the diluted solution was placed on a silica wafer and dried overnight before imaging.

Fluorescent micrographs of hydrogels containing AlgMPs were obtained using an Olympus IX81 inverted laser spinning-disk confocal microscope. Samples were excited at 488 nm and viewed using a 40X oil immersion objective. Pseudo colored ratiometric image was obtained by dividing the AlgMP pixel intensities at reduced oxygen and AlgMP pixel intensities at ambient oxygen. All images were analyzed using ImageJ 1.48v software.

5.2.4. Sensor testing

Lactate sensor discs (4 mm) excised from the hydrogel sensor slabs, were affixed in a custom made flow cell (Figure 17B)and exposed to varying concentrations of dissolved oxygen (0 – 103.4 μM) and lactate (0-40 mg/mL). Dissolved oxygen concentration of buffer was controlled using mass flow controllers (1179A, MKS). Lactate challenges at physiologically low oxygen concentrations were performed by using a vacuum degasser (9000-1118, Systec). Lifetime response of the sensors were collected using a custom made time domain system with a 530 nm LED excitation source that has been described previously.[102] Lower limit of detection (*LOD*) and maximum differentiable lactate concentration (*MDLC*) were determined using the 3-σ method. [115] The analytical range was defined as $R = MDLC\text{-}LOD$ and sensitivity was calculated using the percentage change of maximum and minimum response of the sensor per unit analytical range.

5.3. Results and discussion

5.3.1. Characterization

PEMs were deposited on LOx/CAT/PdTCPP containing AlgMPs using the LbL approach that involves coating the AlgMPs with oppositely charged polyelectrolyte layers. The zeta potential (Figure 18A) of the AlgMPs was measured to confirm successful surface charge reversal after deposition of each PEM. The polyelectrolyte

lined AlgMPs exhibited a high degree of colloidal stability owing to its high surface charge; -20.6±2.4 for PSS coated AlgMPs and 49.7±5.2 for PAH coated AlgMPs. After deposition of 10 bilayers, the nanofilm coated AlgMPs were used to fabricate lactate sensing nanocomposite hydrogels. SEM images revealed the morphology of both the nanofilm coated AlgMPs (Figure 18B) and the nanocomposite lactate sensing hydrogels (Figure 18C). The $[PSS/PAH]_{10}$ coated AlgMPs were spherical and covered by a fuzzy outer layer, characteristic to PEM coated colloidal particles. [145, 146] SEM images of the hydrogel depicts multiple AlgMPs with a wrinkled architecture entrapped within an outer hydrogel matrix. DIC images were used to determine the mean diameter of the $[PSS/PAH]_{10}$ coated AlgMPs as ~8 μm. From the confocal image (Figure 18D) it can be clearly seen that the phosphorescent PdTCPP dye is restricted within the PEM lined alginate microreactors which is expected as the nanofilm coating localizes the macromolecules (LOx, Cat, and PdTCPP) within the spherical microdomains. Furthermore, fluorescence intensity based ratiometric imaging (Figure 18E) was used to confirm that the lactate sensing bioreactors were sensitive to changes in oxygen; an intensity ratio >1 ratifies that the phosphorescence of PdTCPP in the microreactors increases with a decrease in oxygen level.

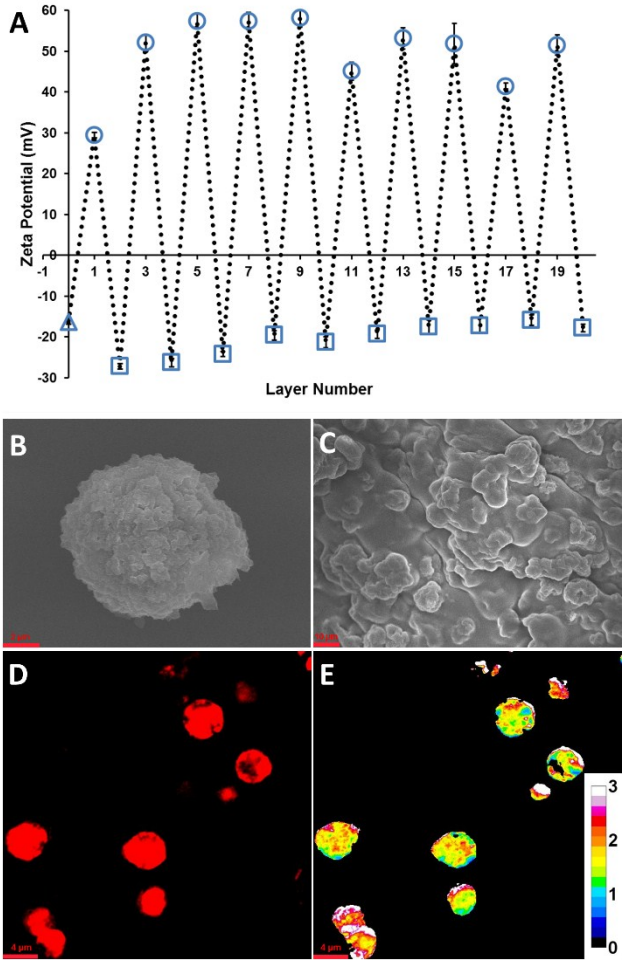

Figure 18. (A) Change in zeta potential change with increase in the number of polyelectrolyte layers coated on alginate microparticles. Δ = bare alginate microparticles, ○ = PAH and □ = PSS. Error bars represent 95% confidence intervals for three separate batches. Scanning electron micrographs of (B) nanofilm coated alginate microparticle, (C) alginate hydrogel containing dispersed bioactive PEM lined alginate microparticles. Fluorescence microscopy images of alginate hydrogel containing dispersed bioactive PEM lined alginate microparticles at ambient oxygen (D) and ratiometric intensity image (E) under reduced oxygen to ambient oxygen.

5.3.2. Response to oxygen and lactate

To quantitatively evaluate the oxygen response, the nanocomposite hydrogels were exposed to varying concentrations of oxygen. The lifetime response of the hydrogels (Figure 19A) increases with a decrease in oxygen; plotting the normalized lifetime against oxygen (Figure 19A inset) and using the Stern Volmer equation $\tau_0/\tau = 1+K_{SV}[O_2]$ the mean K_{SV} was calculated to be $0.04 \pm 0.001\ \mu M^{-1}$ that is not statistically different ($p > 0.01$) from previously reported values.[147] It should be noted that at higher oxygen concentrations there is a decrease in linearity attributed to oxygen's unequal accessibility to the dye molecules.[148]

Having established that the LOx/Cat/PdTCPP loaded microreactors are sensitive to oxygen, the response of the hydrogels to lactate was examined. We hypothesized that composite hydrogels containing embedded LOx/Cat/PdTCPP microdomains can function as enzymatic lactate biosensors; as lactate enters the bioactive reactors it is oxidized accompanied with a reduction in local oxygen that can then be optically monitored. However, the hydrogel based sensors registered no significant change ($p>0.01$) in lifetime response (Figure 19B) with increasing lactate concentrations at ambient oxygen (~ 21%). Investigating the permeation of lactate (Figure 20A) across planar $[PSS/PAH]_{10}$ nanofilms deposited on porous Anopore substrates revealed that 10 bilayers of PSS/PAH were readily permeable to lactate. Thus, there is no significant changes in lifetime response even though lactate is readily available to LOx contained in the microreactors. Additionally, when lactate was added to a highly concentrated

suspension (32 mg/mL) of LOx/Cat/PdTCPP containing microparticles a ~1.8 X increase in phosphorescence

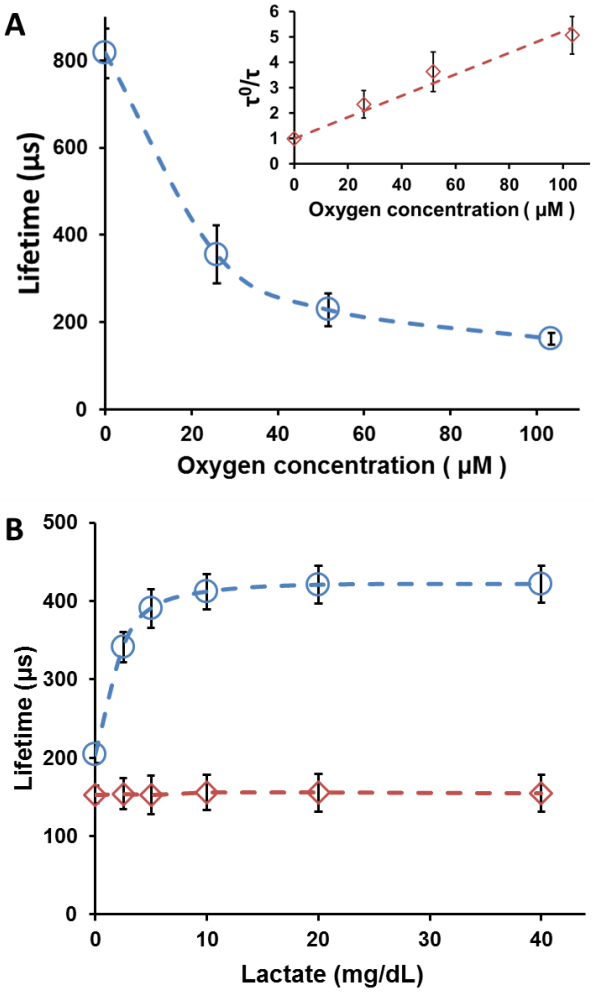

Figure 19. (A) Plot of lifetime against increasing dissolved oxygen concentration. Inset: Data representing change in normalized lifetime (lifetime/lifetime at zero oxygen) with increasing dissolved oxygen concentration. (B) Response of bioactive AlgMP containing hydrogels to increasing concentrations of lactate at ambient (red ◊) and low oxygen (blue ○) condition. Error bars represent 95% confidence intervals for three separate batches of bioactive AlgMP containing hydrogels.

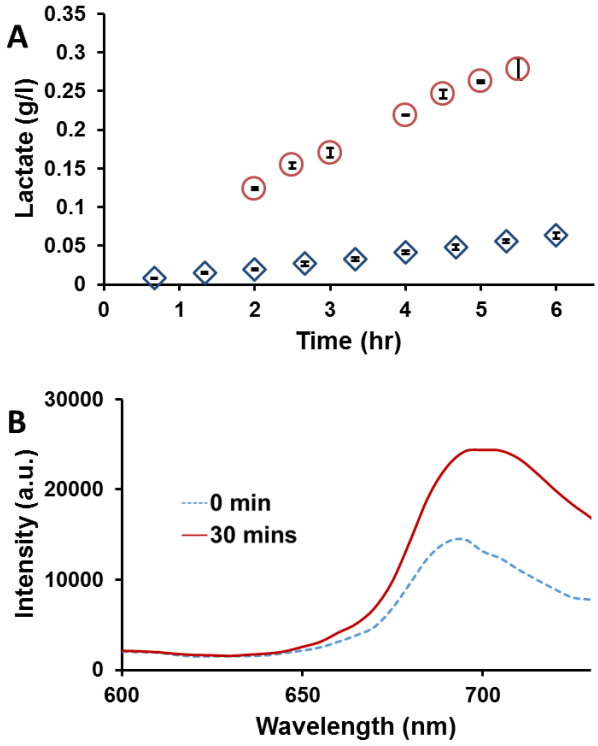

Figure 20. (A) Plot depicting the rate of lactate permeation across 10 bilayers of non-cross-linked (red circle) and cross-linked (blue diamond) PAH/PSS layers deposited on Anopore membrane, (B) increase in phosphorescence intensity of LOx/CAT/PdTCPP AlgMPs suspended in a cuvette, when exposed to lactate.

intensity at 700 nm (Figure 20B) was observed; indicating that active LOx was present in the AlgMPs catalyzing lactate oxidation; thus, increasing the number of particles within the hydrogel would engender a response at ambient oxygen but we found that increasing the particle concentration above what has been used for the hydrogels is not a practical option. We speculate that the non-responsive behavior of the AlgMPs containing nanocomposite hydrogel is due to PdTCPP's low sensitivity at higher

ambient oxygen concentrations; PdTCPP is unable to respond considerably to minute fluctuations in local oxygen with changing lactate concentrations at ambient oxygen.

5.3.3. Sensor stability

Next, we lowered the oxygen concentration to physiologically relevant ~ 5.5% and evaluated the response of the hydrogels to lactate. From the results reported in Figure 19B it can be seen that the hydrogel sensors are highly sensitive when exposed to lactate at low dissolved oxygen condition. The response profile of the sensor fits well to a sigmoidal function (R^2=0.99) that was used to calculate the sensor parameters. Using the 3-σ method, the *LOD*, *MOLC*, and analytical range (*R*) were calculated as 0.053 ± 0.043 mg/dL, 9.3 ± 0.81 mg/dL, and 9.2 ± 0.83 mg/dL respectively. Additionally, the mean sensor sensitivity was estimated to be 11 ± 0.90 % change per unit range. It is important to recognize that this highly sensitive response is desirable for detection of low physiological levels (4.50-13.5 mg/dL) of lactate[149]; these findings demonstrate the principle of using lactate sensing AlgMPs immobilized in an alginate matrix for potential application as implantable hydrogel based lactate biosensors. Finally, reversibility and stability of the sensors were evaluated by alternately exposing the sensors to high (40 mg/dL) and low (0 mg/dL) levels of lactate; the concentrations of lactate were chosen to simulate extreme conditions. Enzymatic sensors that produce hydrogen peroxide as a by-product are prone to peroxide mediated enzyme denaturation, that ultimately leads to sensor failure over time.[105] This is a well-established occurrence that has been extensively studied in the context of enzymatic sensors; these studies have also shown that the effect of H_2O_2 can be easily mitigated by the incorporation of Cat.

[105, 132-134, 141] Presence of co-immobilized Cat in the AlgMPs engenders the catalytic degradation of by-product peroxide and enhances the stability of the lactate sensors. The baseline lifetime response at 0 mg/dL lactate and the sensor response at 40 mg/dL showed no significant difference ($p > 0.01$) even after 20 cycles of repeated lactate exposure (Figure 21) corroborating the highly stable and reversible nature of the biosensors.

5.3.4. Effect of crosslinking PAH/PSS coated AlgMPs

Finally, in an attempt to increase the analytical range of the hydrogel sensors we crosslinked the PAH/PSS coating on the AlgMPs. In case of the glucose sensing AlgMPs, crosslinking PAH/PSS layers decrease analyte diffusion and alter the sensor range and sensitivity; thus, we speculated that we would observe similar effects in case of lactate sensing AlgMPs. We observed (Figure 22) that crosslinking the nanofilm coated AlgMPs with different concentrations (0.375 – 3 M) of glutaraldehyde decreased (4X) lactate permeation drastically (Figure 20 A) reducing sensitivity to the extent that the sensors were unusable. The hydrogels containing non-coated AlgMPs showed a sensitivity of ~110.4% whereas the hydrogels containing AlgMPs exhibited an average sensitivity of ~8% (FEAS 24) and ~2.3% (GRN 1) when tested using two different reader heads that house the excitation source and the detector, FEAS24 and GRN1 respectively.

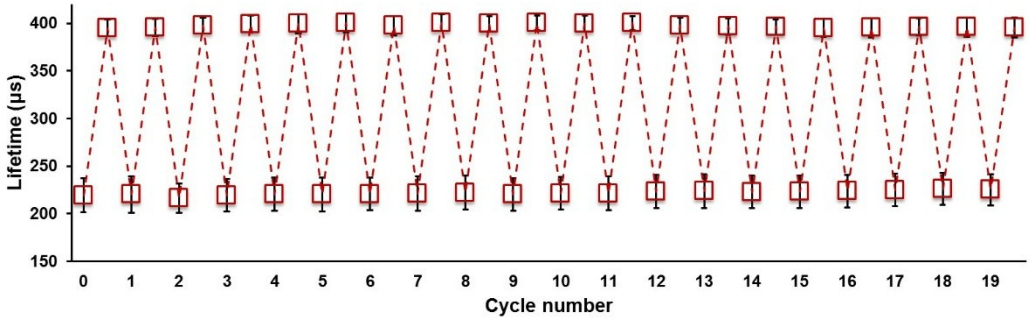

Figure 21. Cyclic testing of lactate sensors when alternately exposed to 0 mg/dL and 40 mg/dL lactate at low oxygen. Error bars represent 95% confidence intervals for three separate batches of bioactive AlgMP containing hydrogels.

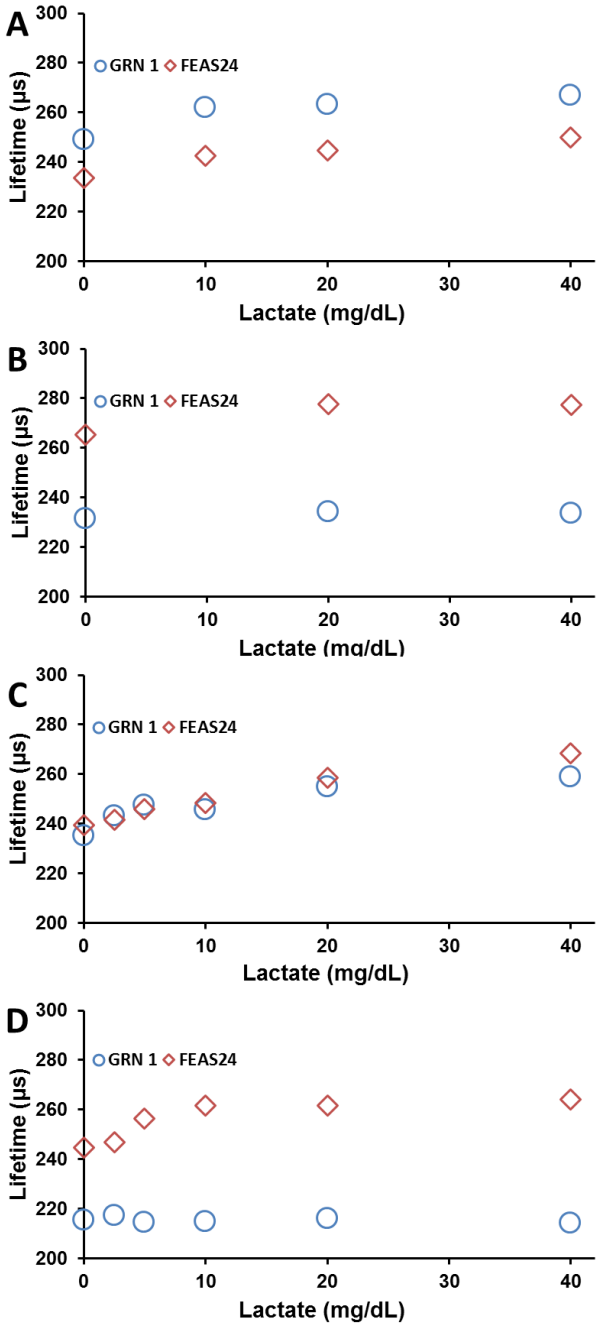

Figure 22. Response of cross-linked PAH/PSS coated AlgMP containing nanocomposite hydrogels to lactate (0 mg/dL - 40 mg/dL) at low oxygen.

5.4. Conclusion

This work has shown the ability to use nanocomposite hydrogels as reversible and stable optical lactate sensors; these hydrogels are embedded with PEM lined bioactive AlgMPs that contain encapsulated enzyme and oxygen sensitive porphyrin dye. The LbL nanofilms were able to fine-tune the transport of oxygen and lactate into the bioactive microreactors for successful lactate sensing. We demonstrated that these sensors were highly sensitive (~ 101.2%) in the range 0.05 – 9.3 mg/dL when operated at physiologically low oxygen levels, which is necessary for *in vivo* sensing. Additionally, these sensors exhibited extraordinary stability when repeatedly exposed to high lactate levels further supporting possible long term *in vivo* use. The high degree of stability is ascribed to enhanced GOx stability due to: (1) the presence of co-immobilized Cat that removes detrimental H_2O_2 and (2) stabilization of GOx's tertiary structure due to interaction with the surrounding polymer matrix.[150] This nanocomposite hydrogel based sensor design can be easily modified to sense other chronic disease biomarkers (*e.g.* cholesterol, urea) by switching the oxidoreductase enzyme. In future, we will be using our sensors for implantation in animal models to evaluate *in vivo* sensor response. The next chapter focusses on how microdomains embedded in hydrogels behave in a cooperative manner to produce a changes in sensor response. Additionally, the limits of hydrogel based sensors for use as multianalyte and multiplexed sensors are also discussed.

6. INVESTIGATING COOPERATIVE EFFECT IN COMPOSITE HYDROGEL BASED ENZYMATIC SENSORS

6.1. Introduction

As explained in the preceding chapters chronic diseases have emerged as the leading cause of mortality worldwide; as many chronic diseases are characterized by multi-metabolite concentration fluctuations, research focused on multiplexed (multianalyte and multimodal) analysis has been steadily gaining momentum.[39 151-153] The majority of prior developments toward sensor multiplexing has been in the field of amperometric sensors, which is particularly challenging; requiring complex and tedious techniques (electrodeposition, photolithographic patterning, and electro-polymerization) for spatially separated immobilization of multiple biorecognition elements (enzyme) onto individual electrodes. [154, 155] These limitations have driven interest into alternative sensor platforms, including optical systems, with flexible opportunities for optical multiplexing, facile fabrication options and no requirement for physical electrical connections.

Recently, hydrogel based implantable oxygen biosensors have been demonstrated for long term monitoring of subcutaneous tissue oxygen levels. [156, 157] These oxygen-sensing hydrogels contain covalently crosslinked metallo-porphyrins that have been already extensively studied and proven quite reliable for sensing and diagnostic applications due to their moderately high quantum yield (~ 10-20%), highly stable phosphorescence, and their inherent dynamic quenching property in the presence of

molecular oxygen. [158, 159] Their innate long lifetime phosphorescence in the red to near-infrared region make them ideal for *in vivo* applications, as there is negligible long-lifetime auto-fluorescence from the surrounding environment and greater optical penetrability engendered by their long wavelength excitation and emission. [160] Such hydrogel based systems have been further modified and used as enzymatic sensors. Along these lines, we have developed and reported two effective designs for these hydrogel based biosensors; the use of microdomains to fabricate nanocomposite sensors or hydrogel based sensors with the sensing chemistry covalently attached to the matrix. [101, 102, 55, 124]

Optical sensors can be multiplexed (multifunctional or multianalyte) either by dispersing micro-sized sensing units, capable of detecting multiple analytes in a binder matrix or by segregating macro-sized multiple analyte sensing regions within an outer matrix. [161] Exploiting these strategies, there have been a few examples of optical fiber based multiplexed phosphorescence sensors. [162-165] However, multiplexed hydrogel based optical enzymatic sensors have not been reported or examined. The target analyte of enzymatic hydrogel based biosensors can be easily altered by substituting the oxidase enzyme; hypothetically, a single hydrogel system containing discrete sensing units opens up the possibility for multiplexing. The key aspects to consider when developing such a multiplexed sensor are analyte specificity and spectral cross-talk of the reporter dye. The spectral cross-talk conundrum can be circumvented by selecting appropriate reporter dyes with non-overlapping excitation and emission spectra, coupled with suitable instrumentation. Spectral cross-talk can also be eliminated by temporal separation

techniques using frequency-domain or time-domain dual lifetime acquisition. [166] The use of enzymes make enzymatic-biosensors highly specific to the biomolecule of interest. However, since most enzymatic sensors operate *via* transduction of a product formed or a co-substrate consumed, a cooperative product formation or cooperative co-substrate consumption interferes with potential multiplexing.

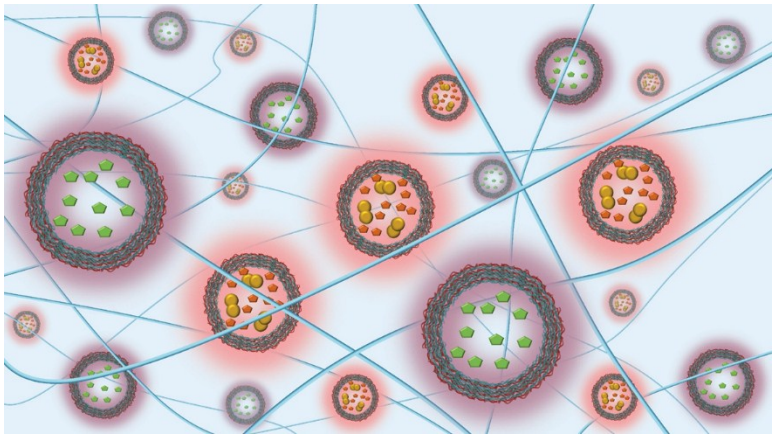

Figure 23. An illustration showing a section of a hydrogel containing a mixed population of microdomains.

In this work, we examined the cooperative depletion of co-substrate oxygen in the vicinity of different formats of micro- and macro-sized sensors to develop and understand the bounds of hydrogel based multiplexed enzymatic optical sensors. Using cross-linked and non-crosslinked nanofilm-lined oxygen-sensing and glucose-sensing microdomains entrapped in the same hydrogels (Figure 23) we measured the changes in phosphorescence lifetime from the different microdomains with increase on glucose

levels to assess the extent to which micro- sensors behave cooperatively; *i.e.* where enzymatic reaction in one microdomain affects the oxygen concentrations of adjacent non-reactive microdomains. We further examined cooperative oxygen depletion between two separate, adjacent macro-sized oxygen/glucose sensing regions (Figure 24B) entrapped within a single encompassing hydrogel matrix ("gel-in-gel" format), as the size of the enzyme containing glucose macro- sensor was varied. Finally, using this gel-in-gel (GIG) design, we fabricated and tested multiplexed glucose sensors and multi-analyte glucose/lactate sensors for their sensitivity compared to independent sensors as a proof of concept to evaluate their potential as multianalyte sensing implants.

Nanocomposite hydrogel based glucose sensors fabricated from vaterite calcium carbonate particles [124] and lactate sensors made by covalently attaching sensing chemistry to hydrogel matrices [102] were used in this study.

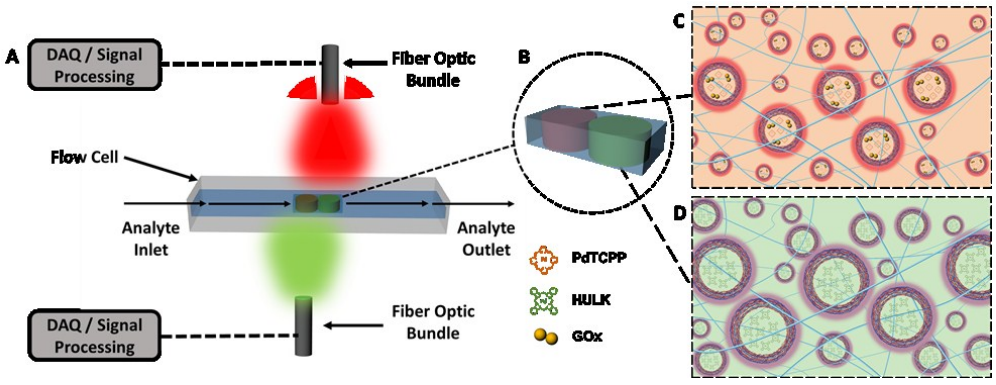

Figure 24. Schematic diagram of (A) sensor testing set-up: time-domain lifetime acquisition system and the flow cell, (B) representative glucose oxygen GIG'em sensor, (C) section of the glucose sensing macrodomain containing PEM lined glucose sensing microdomains, (D) section of the oxygen sensing macrodomain containing PEM lined oxygen sensing microdomains.

6.2. Experimental section

6.2.1. Chemicals

Calcium chloride ($CaCl_2$), sodium carbonate (Na_2CO_3), poly (allylamine hydrochloride) (PAH, average Mw 15000 Da), poly (diallyldimethylammonium chloride) (PDADMAC, average Mw 100000-200000 Da), poly (sodium 4-styrenesulfonate) (PSS, average Mw 70000 Da), glutaraldehyde solution (grade II, 25% in H_2O), alginic acid sodium salt from brown algae (100-300 cP, 2% at 25 °C), 1-ethyl-3-[3-dimethylaminopropyl] carbodiimide hydrochloride (EDC), N-hydroxy sulfosuccinimide sodium salt (NHS), 2,2-dimethoxy-2-phenyl-acetophenone (DMAP), ethylene glycol, buffer salts (TRIS, MES and $NaHCO_3$) and sodium lactate were obtained from Sigma Aldrich. Tetra (ethylene glycol) methacrylate (TEGDMA) and 2-hydroxyethyl methacrylate (HEMA) were purchased from Polysciences Inc. Pd-meso-tetra (4-carboxyphenyl) porphyrin (PdTCPP, Frontier Scientific), Pd-meso-tetra (sulfophenyl) tetrabenzoporphyrin (HULK, Frontier Scientific) and methacrylated palladium benzoporphyrin (PdBP, donated by Profusa, Inc.) suspended in DMSO (10 mM) were used for all experiments. Lactate oxidase from *Aerococcus viridians* (LOx), and acrylamide (Aam) were obtained from A.G. Scientific. Glucose oxidase (GOx) from *Aspergillus niger* and glucose were purchased from BBI solutions and Macron fine Chemicals respectively. All chemicals were used as received without further purification.

6.2.2. Encapsulation of sensing elements in microparticles and synthesis of microcapsules

Calcium carbonate ($CaCO_3$) microparticles containing sensing chemistry were synthesized using the co-precipitation method. [167] 200 µl of 10 mM PdTCPP was added to 8 ml solution of Na_2CO_3 (0.2 M) containing 64 mg of GOx and stirred (700 rpm) for 5 min using a wedge edged stir bar. 8 ml of $CaCl_2$ (0.2 M) was rapidly added to the solution of Na_2CO_3 containing GOx and PdTCPP and allowed to react for 10 min to fabricate GOx/PdTCPP loaded $CaCO_3$ microparticles. The GOx/PdTCPP microparticles serve as templates to synthesize glucose sensing microcapsules. Microparticle templates for HULK containing glucose sensing microcapsules were made in a similar fashion with the only exception that 200 µl of 10 mM HULK was added to 8 ml Na_2CO_3 (0.2 M) containing 64 mg of GOx. Microparticle templates for oxygen sensing capsules were also made using the same principle with minor modifications; 200 µl of 10 mM HULK was added to 8 ml solution of Na_2CO_3 (0.2 M) and stirred (700 rpm) for 5 min followed by the rapid addition of 8 ml of $CaCl_2$ (0.2 M), and the reaction was allowed to continue for 10 min.

Microparticle templates were alternately exposed to oppositely charged polyelectrolyte solutions PDADMAC (20 mg/ml, pH 8, containing 5 mM $NaHCO_3$) / PSS (20 mg/ml, pH 7.2, containing 5 mM $NaHCO_3$) or PAH (20 mg/ml, pH 8, containing 5 mM $NaHCO_3$) / PSS (20 mg/ml, pH 7.2, containing 5 mM $NaHCO_3$) with wash steps in between to coat the microparticles with polyelectrolyte multilayer (PEM) nanofilms. Irrespective of the encapsulated cargo content, all microparticles were first

coated with $[PDADMAC/PSS]_5$ to ensure a contiguous nanofilm primer coating. [168] Following the deposition of the primer coating, GOx/PdTCPP microparticle templates and GOx/HULK microparticle templates were coated with $[PAH/PSS]_9$ bilayers whereas HULK microparticle templates were coated with $[PAH/PSS]_5$. To fabricate cross-linked nanofilm coated GOx/PdTCPP microparticles, ($[PDADMAC/PSS]_5$-$[PAH/PSS]_9$) coated microparticles containing GOx/PdTCPP (3.3 mg) was added dropwise to 3 M glutaraldehyde solution and allowed to react for 30 min, to cross-link the amine groups contained in PAH ensuring that the nanofilm coating restricts the free diffusion of glucose. To fabricate macromolecule-containing microcapsules, the $CaCO_3$ microparticle cores were dissolved by exposing the microparticle templates to a low pH buffer solution. Specifically 3.3 mg of nanofilm coated CaCO3 templates were suspended in 0.2 M MES buffer at pH 5.8 for 60 min.

6.2.3. Fabrication of glucose / oxygen sensing microporous alginate composite (MPAC) hydrogels

Microporous alginate composite (MPAC) hydrogels were fabricated according to the principle described by Roberts et al.[103] Nanofilm coated $CaCO_3$ microparticles containing co-precipitated cargo (3.3 mg suspended in 75 µl of deionized water), 3% alginate solution (200 µl), non-coated $CaCO_3$ microparticles (25 µl of 33.3 mg/ml) and 100 µl of MES (0.5 M, pH 6.1) were mixed to make a slow-gelling hydrogel precursor. The precursor was then poured between two glass slides separated by a 0.06" Teflon spacer, and allowed to gel for 30 min.

6.2.4. Fabrication of lactate sensing hydrogels

Lactate sensors were made according to the protocol described by Andrus et al. [102] Briefly, 125 µl of enzyme solution (molar ratio LOx : Catalase :: 10:1, dissolved in PBS, pH 7.4), 5 µl TEGDMA, 50 µl PdBP (10 mM dissolved in DMSO), 187.5 µl HEMA, 62.50 µl Aam (dissolved in DMSO 67.2 *v*/*v* %), 90 µl ethylene glycol and 2.5 mg DMAP were mixed to make a hydrogel precursor that was then poured between two glass slides separated by a 0.03" Teflon spacer, and allowed to gel by exposing the glass slides to UV light for 3 min on either side. After UV curing the gel was taken out of the mold and exposed to PBS buffer containing a mixture of EDC and sulfo-NHS (40 ml PBS containing 15 mg sulfo-NHS and 6.6 mg EDC) to cross-link the enzyme mixture to the hydrogel matrix.

6.2.5. Fabrication of gel in gel enzymatic multiplexed (GIG'em) sensors

Circular hydrogel disks excised from glucose/oxygen sensing MPACs or lactate sensing hydrogels, were placed in a circular mold (radius = 1 cm, thickness = 1.5 mm). A slow gelling alginate precursor was made by mixing 250 µl of a 3% alginate solution, 62.5 µl of non-coated $CaCO_3$ microparticles (33.3 mg/ml), 437.5 µl deionized water and 250 µl of MES buffer (0.5 M, pH 6.1). The slow gelling alginate precursor was then gently poured into the mold containing two circular hydrogel punches capable of sensing either glucose, lactate or oxygen, ensuring that the circular hydrogel punches are always in contact with each other at the edges.

6.2.6. Characterization

An inverted laser spinning-disk confocal microscope (Olympus IX81) was used to obtain confocal fluorescence and differential interference contrast (DIC) microscopy images of micro domain containing MPAC hydrogels. Micro domains containing PdTCPP were excited with a 488 nm laser whereas micro domains containing HULK were excited with a 445 nm laser. Image J software was used to analyze all images.

6.2.7. Sensor testing setup

Hydrogel samples were placed in a custom flow-through system (Figure 24) and exposed to varying concentrations of glucose (0-400 mg/dl), lactate (0-40mg/dl), and dissolved oxygen (0-206.8 μM). Two separate custom-made time-domain lifetime measurement systems that have been described elsewhere [101, 169] were alternately used to record changes in lifetime of the sensors; all data acquisition parameters were same as described in the previous works. Sensors containing HULK or PdBP were illuminated with a 630 nm LED, whereas the PdTCPP containing sensors were excited with a 530 nm LED [169] to measure their respective luminescent lifetime responses.

Two mass flow controllers (type 1179A, MKS) were used to mix nitrogen and compressed air, in order to control the dissolved oxygen concentration (0-206.8 μM) of buffer (10 mM TRIS, 10 mM $CaCl_2$) flowing through the flow chamber during Stern-Volmer experiments. Different concentrations of glucose (0-400 mg/dl) or lactate (0-40mg/dl) dissolved in buffer (10 mM TRIS, 10 mM $CaCl_2$) were flowed over the hydrogel sensors to measure glucose and lactate response respectively. The response

curves obtained were used to extract relevant sensor response parameters: limit of detection (*LOD*), maximum differentiable glucose concentration (*MDGC*), analytical range (*R=MDGC-LOD*), and sensitivity. The *LOD* and *MDGC* were calculated using a 3σ approach. The sensitivity of the sensor was assessed by computing the difference of the maximum and minimum response per unit analytical range.

6.3. Results and discussion

6.3.1. Characterization of microdomains

To demonstrate the existence of cooperative co-substrate (oxygen) depletion in composite hydrogel based enzymatic biosensors, we fabricated two different kinds of microcapsules: glucose sensing microcapsules and oxygen sensing microcapsules. Glucose sensing microcapsules were composed of $[PDAMAC/PSS]_5$ -$[PAH/PSS]_9$ nanofilm bound microdomains containing PdTCPP and GOx, whereas oxygen sensing microcapsules were made by encapsulating HULK in $[PDAMAC/PSS]_5$-$[PAH/PSS]_5$ bound microdomains. We studied the emission characteristics of the microcapsules before using them to examine cooperative effect. Figure 25A shows the emission spectra of both glucose sensing and oxygen sensing microcapsules when excited by 530 nm individually, while Figure 25B shows the emission spectra of the capsules when excited by 630 nm separately. Figure 25A reveals that at 530 nm excitation wavelength, GOx/PdTCPP containing microcapsules have a strong emission peak around 710 nm; however, the emission from HULK containing microcapsules around 710 nm is almost negligible. Similarly, at 630 nm excitation wavelength, HULK containing microcapsules

emit intensely around 810 nm; conversely, the GOx/PdTCPP containing microcapsules have insignificant emission at 810 nm.

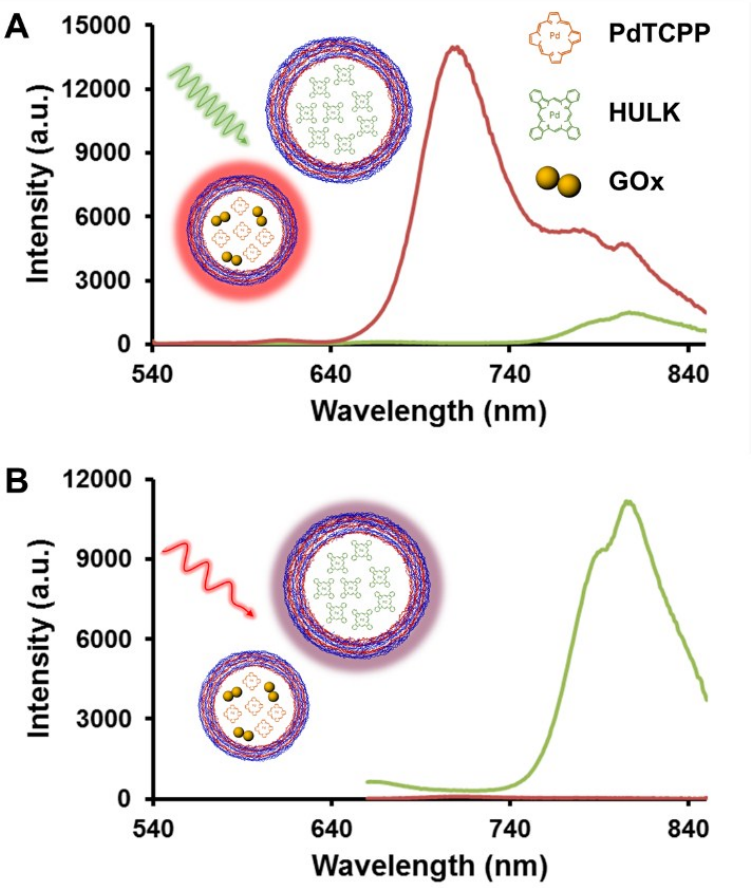

Figure 25. (A) Emission spectra of PdTCPP/GOx containing capsules and HULK containing capsules when excited at 530 nm, (B) emission spectra of PdTCPP/GOx containing capsules and HULK containing capsules when excited at 630 nm.

Having established that the emission peak wavelengths of the glucose sensing capsules and the oxygen sensing capsules are spectrally separated, and that there is

negligible cross-excitation when microcapsules are discretely excited at either 530 nm or 630 nm, MPAC hydrogels containing a mixture of glucose sensing and oxygen sensing microcapsules were fabricated. Observing the changes in lifetime of both the glucose sensing and the oxygen sensing microdomains with changing glucose concentrations would help understand how the microdomains behave in a cooperative manner, where lifetime response of one microdomain is affected by its neighboring microdomains. In all following experiments, we recorded the lifetime emission data around wavelengths 710 nm and 810 nm when excited at 530 nm and 630 nm respectively using custom-made lifetime-domain systems. [101, 169]

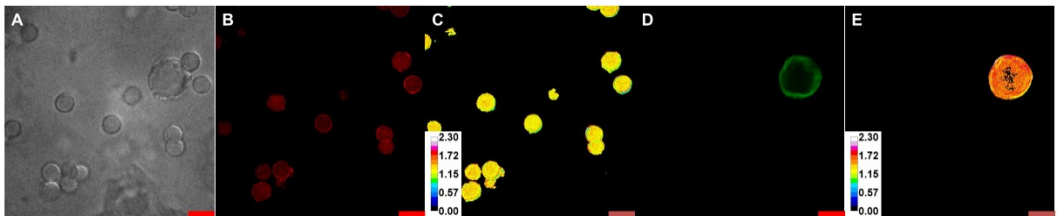

Figure 26. Nano-composite hydrogels containing both glucose and oxygen sensing Microdomains. (A) DIC image at 100 X magnification, (B) confocal image of GOx / PdTCPP containing microdomains [red], (D) confocal image of HULK containing microdomain [green], (C) intensity ratio image of GOx and PdTCPP containing microdomains under reduced oxygen to ambient oxygen, (E) intensity ratio of HULK containing microdomains under reduced oxygen to ambient oxygen. Scale bars correspond to 10 µm. Color coded scale relates to intensity ratios of GOx and PdTCPP containing microdomains (reduced oxygen: ambient oxygen).

We imaged the MPAC hydrogels using confocal microscopy (Figure 26) to verify the co-localization of the glucose sensing and the oxygen sensing microdomains.

The DIC micrograph (Figure 26A) shows a mixed population of microdomains immobilized inside the MPAC hydrogel. However, individual populations of either GOx/PdTCPP containing microdomains (Figure 26B) or HULK containing microdomains (Figure 26D) luminesce at their characteristic wavelengths when excited appropriately. Using confocal images of glucose sensing and oxygen sensing microdomains captured under ambient and reduced oxygen conditions we constructed intensity ratio images to confirm qualitatively that the oxygen quenching property of PdTCPP and HULK, encapsulated in the microdomains was unaffected. Intensity ratios in both cases increased (Figure 26C, Figure 26E), indicating that entrapped PdTCPP and entrapped HULK were quenched in the presence of molecular oxygen.

MPAC hydrogels containing GOx/PdTCPP microdomains and HULK containing microdomains were exposed to buffer solutions having different concentrations of dissolved oxygen, to quantitatively evaluate their oxygen response when co-immobilized. A plot of the normalized lifetimes (normalized to the lifetime at zero oxygen concentration) of both the microdomains, against changing oxygen concentrations is represented in Figure 27. Using linear least-squares regression and the Stern-Volmer equation ($\tau_0/\tau = 1+K_{SV}[O_2]$) the K_{SV} value of the GOx/PdTCPP loaded microdomains was calculated to be $0.046 \pm 0.002\ \mu M^{-1}$ and the K_{SV} value of the HULK microcapsules in the MPAC hydrogel was calculated as $0.015 \pm 0.001\ \mu M^{-1}$. The response of both PdTCPP and HULK microdomains was noticeably linear, something inherent to oxygen sensitive porphyrin phosphors.[127]

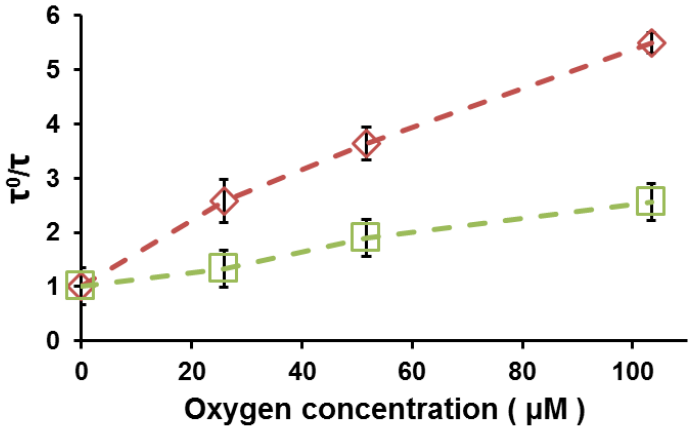

Figure 27. Lifetime (normalized to the lifetime at zero oxygen concentration) against varying oxygen concentrations for MPAC hydrogels containing both GOx/PdTCPP micro domains (red ◊) and HULK microdomains (green □). Error bars represent 95% confidence intervals for three separate MPAC hydrogels. The dashed lines are provided only as a guide to the eyes.

6.3.2. Cooperative effect

Microdomains that contain GOx and PdTCPP behave as optical glucose sensors. As glucose gradually diffuses into the interior of the microdomains, it reacts with GOx according to the reaction: Glucose + O_2 + glucose oxidase + H_2O → gluconic acid + H_2O_2. The enzyme-mediated reaction depletes oxygen in the process, and monitoring the amount of depleted oxygen allows indirect detection of the amount of glucose consumed. Depletion of oxygen facilitated by GOx present in one microdomain might also affect oxygen concentrations in the neighboring microdomains, resulting in a cooperative behavior. To assess this hypothesis, MPAC hydrogels containing both GOx/PdTCPP microdomains and HULK microdomains were exposed to different concentrations of glucose. Ideally, if microdomains in the MPAC hydrogel behave non-

cooperatively, the lifetime response of the HULK microdomains would remain unaffected, irrespective of the concentration of glucose.

Figure 28A represents a plot of lifetime (normalized to lifetime obtained at 400 mg/dl glucose concentration) against different glucose concentrations, for both non-cross-linked nanofilm bound glucose sensing microdomains and oxygen sensing microdomains entrapped in MPAC hydrogels. Lifetime response recorded from both the glucose and oxygen sensing microdomains increase, as the concentration of glucose increases, suggesting that the depletion of oxygen facilitated by GOx present in the GOx/PdTCPP microdomains affects the oxygen concentrations in the HULK microdomains. Thus, the microdomains behave cooperatively with an α value of 145.7 ± 22.0 %, where α (cooperativity coefficient) is defined as the percent increase in the normalized response of the HULK domains when glucose concentration is increased from 0 mg/dl to 400 mg/dl, as at 400 mg/ml maximum possible oxygen is depleted from the system. Finding a means to eliminate or reduce this cooperative effect amongst glucose and oxygen sensing domains would enable the construction of a hydrogel based sensing platform, where multiple enzymatic sensing domains can function independently.

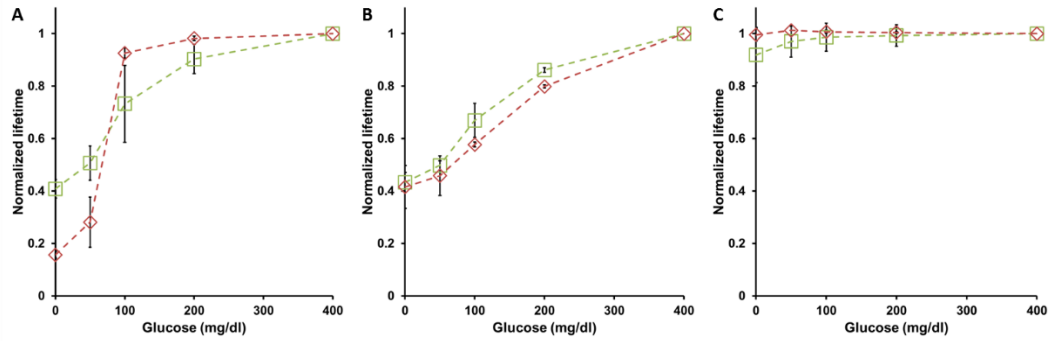

Figure 28. Lifetime (normalized to the lifetime at 400 mg/ml glucose concentration) against varying glucose concentrations for MPAC hydrogels containing (A) non-cross-linked nanofilm bound GOx/PdTCPP microdomains (red ◊) and HULK microdomains (green □), (B) cross-linked nanofilm bound GOx/PdTCPP microdomains (red ◊) and HULK microdomains (green □) and (C) cross-linked nanofilm bound GOx/PdTCPP microdomains (red ◊) and HULK microdomains (green □) with CAT cross-linked to the hydrogel matrix. Error bars represent 95% confidence intervals for three separate MPAC hydrogels. The dashed lines are provided only as a guide to the eyes.

In an attempt to decrease the amount of oxygen consumed by the glucose sensing microdomains, we increased the diffusion barrier around GOx/PdTCPP microdomains by cross-linking the nanofilm layers with glutaraldehyde. Prior studies have shown that restricting the amount of glucose diffusing into the GOx/PdTCPP microdomains would engender less oxygen consumption, which would consequently decrease cooperative oxygen depletion. [105, 122] Lifetime (normalized to lifetime obtained at 400mg/dl glucose concentration) of both glucose sensing microdomains bound by a high glucose diffusion barrier and oxygen sensing microdomains plotted against different glucose concentrations (Figure 28B), reveals that the response of the HULK microdomains mimics the response of the glucose sensing microdomains signifying that cooperative behavior still existed ($\alpha = 131.7 \pm 19.6$ %). Next, the concentration of the cross-linked

glucose sensing capsules contained within these hydrogels was decreased by ¼ times; although the concentration was reduced, no change in lifetime response from either the glucose or oxygen sensors was recorded. By lowering the concentration of glucose sensing capsules, the effective GOx concentration within the system was lowered to the extent that enough oxygen was not consumed to produce a discernible response to glucose by either types of microdomains; although a reduced concentration of glucose sensing microdomains eliminated cooperative effect completely, it rendered the glucose sensor inoperable.

Next, covalently cross-linked catalase (Cat) was introduced in the hydrogel matrix surrounding the cross-linked nanofilm bound glucose sensing microdomains to decrease the amount of oxygen consumed further. Cat reduces H_2O_2 ($2\ H_2O_2 \rightarrow 2\ H_2O + O_2$) which is produced by the GOx mediated oxidation of glucose, and generates oxygen in the process. Increasing the oxygen contents in the vicinity of the GOx/PdTCPP microdomains would theoretically reduce the cooperative depletion of oxygen. Figure 28C show the response curves of the cross-linked nanofilm bound glucose sensing microdomains and oxygen sensing microdomains, entrapped in alginate matrix, which has covalently immobilized Cat. The cooperative coefficient α drastically reduces to 4.2 ± 3.5 %, indicating that we successfully decreased the cooperative depletion of oxygen. However the decrease in α was achieved at the expense of losing sensor response of the glucose sensing microdomains, which leads us to believe that a certain degree of cooperativity is necessary among glucose sensing microdomains for effective analyte sensing. SV experiments run on hydrogels with or without immobilized Cat show no

significant difference in K_{SV} values (Figure 29A); verifying that the oxygen permeability characteristics were unaltered as Cat is introduced. Furthermore a control experiment (Figure 29B), where Cat was introduced in a hydrogel that contains oxygen sensing microdomains and non-cross-linked nanofilm bound glucose sensing microdomains revealed that cooperative effect ($\alpha = 191.4 \pm 6.5$ %) still existed.

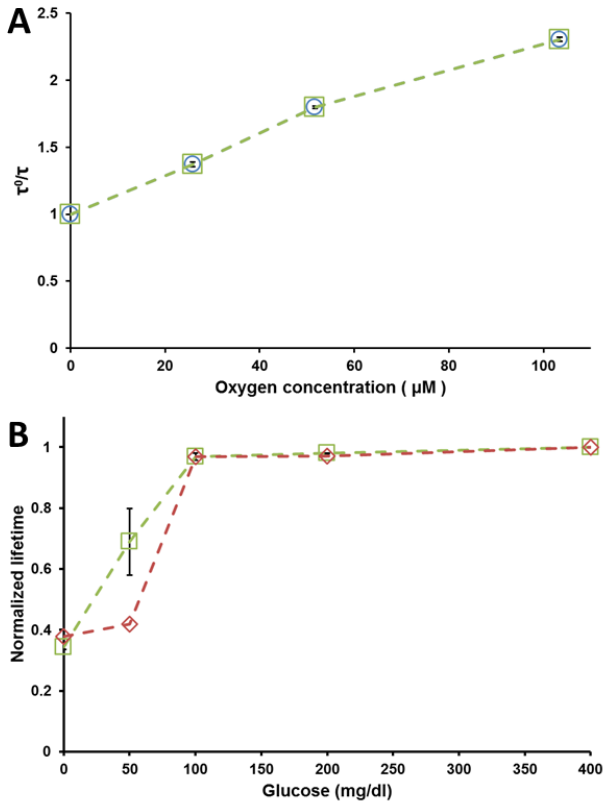

Figure 29. SV plot of hydrogels containing Cat (green □) and without Cat (blue ○), (B) non-cross-linked nanofilm bound GOx/PdTCPP microdomains (red ◊) and HULK microdomains (green □) with CAT cross-linked to the hydrogel matrix. Error bars represent 95% confidence intervals for three separate MPAC hydrogels. The dashed lines are provided only as a guide to the eyes.

6.3.3. GIG'em design

In a different approach to reduce cooperativity, we separated the glucose sensing and the oxygen sensing elements into discrete macrodomains and enclosed both the macrodomains within the same hydrogel (gel in gel enzymatic multiplexed sensors or GIG'em sensors). The glucose sensing and the oxygen sensing macrodomains consisted of circular MPAC punches containing glucose sensing microdomains lined by glutaraldehyde cross-linked $[PDAMAC/PSS]_5$-$[PAH/PSS]_9$ and oxygen sensing microdomains bound by $[PDAMAC/PSS]_5$-$[PAH/PSS]_5$ respectively. The circular design was chosen as studies conducted prior to this work (Chapter 3) have demonstrated circular nanocomposite hydrogels that operate at the physiological range; it should be noted that this study was performed to study co-operatively between sensors that actually work. A different form of sensor other than a circular form would require extensive optimization prior to performing other studies, which would digress from the objective of this work. Both the macrodomains were in turn entrapped within an outer alginate matrix, such that the glucose/oxygen sensing elements were in contact with each other at the edges. Figure 30A demonstrates the normalized lifetime response of the glucose sensing macrodomains at different glucose concentrations, when the size of the glucose sensing macrodomain is gradually increased.

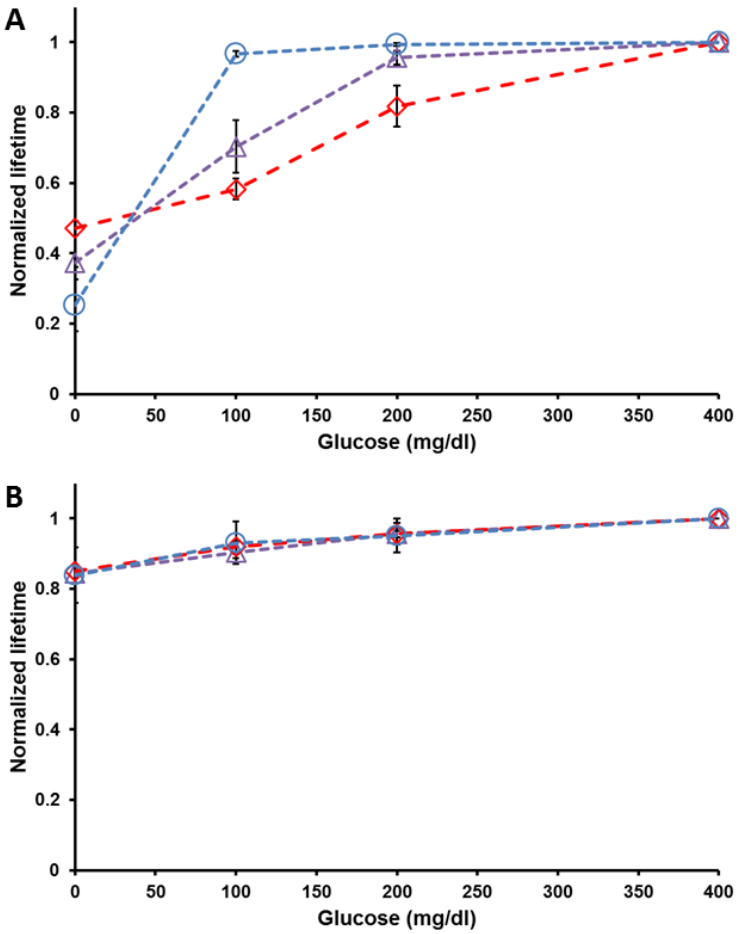

Figure 30. Lifetime (normalized to the lifetime at 400 mg/ml glucose concentration) against varying glucose concentrations for GIG'em hydrogels containing (A) glucose sensing macrodomains 4 mm (red ◊), 6 mm (purple Δ), 8 mm (blue ○) and (B) their corresponding oxygen sensing macrodomains 4 mm (red ◊), 6 mm (purple Δ), 8 mm (blue ○). Error bars represent 95% confidence intervals for three separate MPAC hydrogels. The dashed lines are provided only as a guide to the eyes.

The response parameters of the glucose sensors are listed in Table 3. As the diameter of the glucose sensing macrodomain increases from 4 mm to 8 mm the analytical range of the sensor gradually decreases from 232.0 mg/dl to 89.1 mg/dl. The decrease in analytical range is attributed to the increase in the total number of GOx

containing microdomains, which facilitates the rapid depletion of oxygen at a rate higher than the rate at which oxygen is replenished. The greater number of GOx containing microdomains provokes a greater degree of cooperativity within the glucose sensing macrodomain, which further augments the decrease of oxygen in individual glucose sensing microdomains. It should be noted that as we increased the size (4-8 mm) of the glucose sensing macrodomains the size of the adjacent oxygen sensing macrodomain was maintained at 4 mm. At this point, one might speculate that as the size of the glucose sensor is increased the cooperative effect the glucose sensor has on the adjacent oxygen sensor will also increase. However, examining the change in lifetime of the oxygen sensing macrodomain revealed that increasing glucose concentrations had negligible effect on it, irrespective of size of the glucose sensing macrodomain (Figure 30B) with an average cooperative coefficient of 18.9 ± 1.2 %. The meager cooperative effect between the macrodomains is ascribed to local changes in oxygen concentration at the point of contact of the glucose sensing and oxygen sensing macrodomains, or due to decreased oxygen levels inside the flow cell during the enzymatic reaction irrespective of the size of the enzymatic sensor. Thus in this gel-in-gel (GIG) design, the major depletion of oxygen takes place from within the glucose sensing macrodomain, containing the GOx/PdTCPP microdomains, allowing desirable sensor response over the physiological glucose range without drastically affecting oxygen concentrations in its adjacent oxygen sensing macrodomain.

Table 3. Calculated sensor parameters for MPACs containing cross-linked $[PAH/PSS]_9$ bound glucose sensing microdomains with increase in size

Diameter (mm)	***LOD (mg/dl)[a]***	***MDGC (mg/dl)[b]***	***Range (mg/dl)[c]***	***Sensitivity/range (% per mg/dl)***
4	40.6 ± 2.5	272.6 ± 37.8	232.0 ± 36.2	0.5 ± 0.1
6	8.5 ± 8.3	177.0 ± 9.5	168.5 ± 2.0	1.0 ± 0.1
8	3.7 ± 1.7	92.8 ± 2.8	89.1 ± 1.1	3.5 ± 1.2

[a]*LOD,* limit of detection; [b]*MDGC,* maximum differentiable glucose concentration; [c]Range*, MDGC-LOD*.

Table 4. Calculated sensor parameters for MPACs containing non-cross-linked and cross-linked $[PAH/PSS]_9$ bound glucose sensing microdomains contained in a GIG'em

Microdomain type	***LOD (mg/dl)[a]***	***MDGC (mg/dl)[b]***	***Range (mg/dl)[c]***	***Sensitivity/range (% per mg/dl)***
Non-cross-linked	9.0 ± 3.3	85.1 ± 18.4	76.0 ± 15.7	1.9 ± 0.7
Cross-linked	44.5 ± 18.0	262.6 ± 33.9	218.1 ± 43.7	0.7 ± 0.2

[a]*LOD,* limit of detection; [b]*MDGC,* maximum differentiable glucose concentration; [c]Range*, MDGC-LOD*.

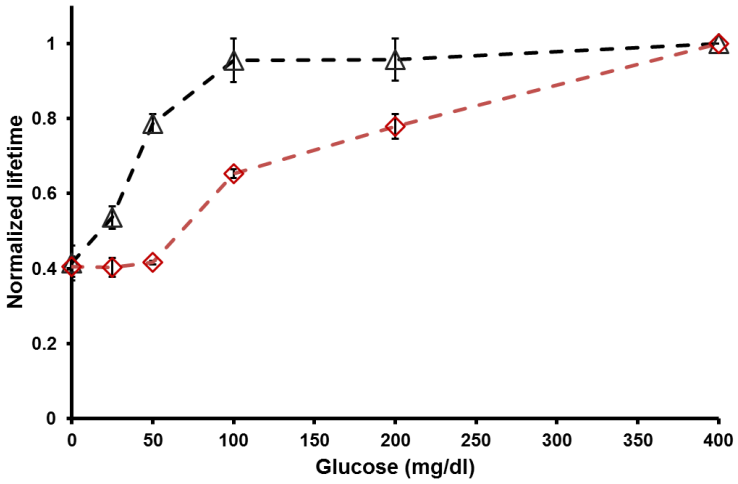

Figure 31. Lifetime (normalized to the lifetime at 400 mg/ml glucose concentration) against varying glucose concentrations for GIG'em hydrogels containing (red ◊) glucose sensing macrodomain comprised of cross-linked GOx/PdTCPP micro domains and (black Δ) glucose sensing macrodomain comprised of non-cross-linked GOx/HULK micro domains. Error bars represent 95% confidence intervals for three separate MPAC hydrogels. The dashed lines are provided only as a guide to the eyes.

6.3.4. Multiplexed enzymatic sensors

Having demonstrated that we can minimize the cooperativity between sensing elements when enclosed in a gel-in-gel (GIG) design, we used the GIG system to fabricate multiplexed enzymatic sensors encapsulated in a single hydrogel matrix. Enzymatic sensors are flux-based systems that have a characteristic inverse relationship between range and sensitivity.[107] Using glutaraldehyde cross-linked nanofilm bound microdomains the effective range of the glucose sensing element may be increased at the expense of losing considerable amount of sensor sensitivity, especially in the hypoglycemic region. [124] In order to achieve glucose sensor response over the physiological range (0-400 mg/dl) while maintaining high sensitivity in the

hypoglycemic region, we fabricated GIG'em (gel-in-gel enzymatic multiplexed) sensors with two macrodomains, one containing GOx/HULK microdomains bound by non-cross-linked $[PDADMAC/PSS]_5$-$[PAH-PSS]_9$ and the other containing GOx/PdTCPP microdomains bound by glutaraldehyde cross-linked $[PDADMAC/PSS]_5$-$[PAH-PSS]_9$. Figure 31 depicts the response of the GIG'em glucose sensors, at varying glucose concentrations. As expected the analytical range of the GOx/PdTCPP containing macrodomain was ~ 191% higher than the analytical range of the GOx/HULK containing macrodomain, whereas the sensitivity of the GOx/PdTCPP containing macrodomain was ~ 183% lower than the sensitivity of the GOx/HULK containing macrodomain. The response parameters of the glucose detecting GIG'em sensors are listed in Table 4. Using this system we were able achieve an extended analytical range ~ 218.1 mg/dl while having a high sensitivity of ~ 1.9% per mg/dl in the hypoglycemic region.

6.3.5. Multianalyte sensor

We extended the concept of a multiplexed enzymatic sensor, to fabricate a multianalyte GIG'em sensor capable of sensing glucose and lactate independently. The glucose sensing component comprised of a MPAC hydrogel containing encapsulated GOx/PdTCPP microdomains bound by cross-linked $[PDADMAC/PSS]_5$-$[PAH-PSS]_9$, whereas the lactate sensing component consisted of HEMA-co-AaM hydrogel punch containing covalently immobilized LOx, CAT and PdBP. Figure 32A shows the response of both the glucose sensing and the lactate sensing components when the

multianalyte sensor was exposed to different concentrations of glucose. The change in response of the lactate sensor was ~ 0.4% when we increased the glucose concentration from 0 mg/dl to 400 mg/dl. Similarly, we recorded the response of both the glucose and lactate sensors at different concentrations of lactate (Figure 32B). The change in response of the glucose sensor was ~ 6.3%, as lactate concentration was varied from 0 mg/dl to 40 mg/dl. In both cases, the characteristic response of the glucose sensor to changing glucose concentrations and the characteristic response of the lactate sensor to changing lactate concentrations was unaffected. The marginal difference in the non-cooperative behavior of the lactate and the glucose sensor is accredited to low oxygen diffusivity in the lactate sensor, which engenders less oxygen depletion within the lactate sensor when glucose is flowed over the multianalyte GIG'em sensor. To further, substantiate the independent response characteristics of the multianalyte sensor we tested sensor response at low glucose/high lactate and high glucose/low lactate analyte concentrations (Figure 32C). At low glucose/high lactate (100 mg/dl glucose, 20 mg/dl lactate) combination the normalized lifetime for the individual sensors (glucose = 0.64 ± 0.04; lactate = 0.72 ± 0.05) corresponds closely to the normalized lifetimes obtained (glucose = 0.62 ± 0.08; lactate = 0.60 ± 0.07) when only glucose or lactate is flowed. Similarly, the normalized lifetime for the individual sensors (glucose = 0.80 ± 0.07; lactate = 0.33 ± 0.03) at high glucose/low lactate concentration (200 mg/dl glucose, 10 mg/dl lactate) tallies with the response obtained (glucose = 0.84 ± 0.03; lactate = 0.24 ± 0.02) when only glucose or lactate is flowed separately.

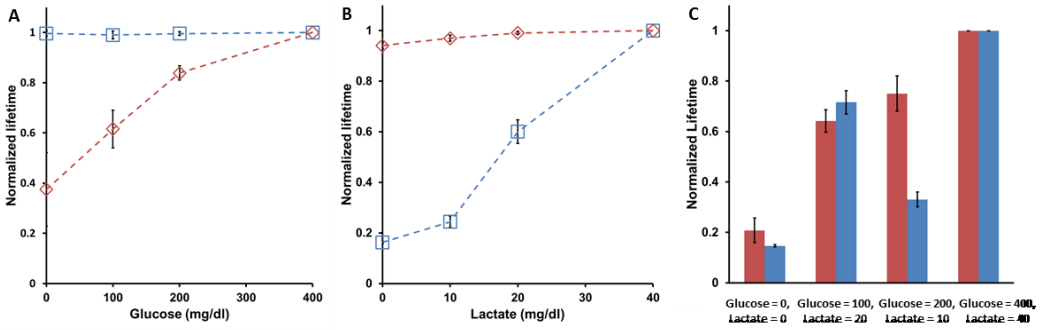

Figure 32. (A) Lifetime (normalized to the lifetime at 400 mg/ml glucose concentration) against varying glucose concentrations for GIG'em hydrogels containing (red ◊) glucose sensing macrodomain comprised of cross-linked GOx/PdTCPP micro domains and (blue □) lactate sensing macrodomain. (B) Lifetime (normalized to the lifetime at 40 mg/ml lactate concentration) against varying lactate concentrations for GIG'em hydrogels containing (red ◊) glucose sensing macrodomain comprised of cross-linked GOx/PdTCPP micro domains and (blue □) lactate sensing macrodomain. (C) Lifetime (normalized to the lifetime at 400 mg/ml glucose/40 mg/ml lactate concentration) against varying glucose/lactate concentrations for GIG'em hydrogels containing (red) glucose sensing macrodomain comprised of cross-linked GOx/PdTCPP micro domains and (blue) lactate sensing macrodomain. Error bars represent 95% confidence intervals for three separate MPAC hydrogels. The dashed lines are provided only as a guide to the eyes.

In our study, we found that in microdomain based enzymatic sensors, which indirectly detect analyte concentrations by measuring co-substrate (oxygen) depletion, a degree of cooperative oxygen depletion exists and is necessary for effective sensor response. Using the GIG'em design, we were successful in reducing the cooperative oxygen depletion between the glucose sensing component and the oxygen sensing component by spatially separating and confining glucose sensing and oxygen sensing microdomains into discrete macro sized domains. We effectively translated the GIG'em design to fabricated multiplexed glucose sensors, and multianalyte glucose-lactate sensors.

6.4. Conclusion

In this work, we have been able to demonstrate the existence of cooperative oxygen depletion between sensing domains contained within a hydrogel matrix for the first time. We have also showed that by decreasing the amount cooperative oxygen depletion between sensing domains, a multiplexed enzymatic sensor can be designed. By decreasing the amount of cooperative oxygen depletion amongst glucose sensing microdomains, we found that the sensing capability of the microdomains was greatly affected making them ineffective. Thus, micro-sized enzymatic sensors require a degree of cooperation to operate, which adversely interferes with potential multiplexed sensor design. To overcome this conundrum, we developed a GIG (gel-in-gel) design, which allows separate sensing domains to function independently without affecting each other. Using this design, the cooperative oxygen depletion within a sensing macrodomain remains unaffected, keeping sensor response characteristics unaltered, while having negligible cooperative oxygen depletion in its vicinity. Although not non-existent, the cooperative oxygen depletion amongst sensing macrodomains in the GIG design was ~ 84.4% less than cooperative oxygen depletion between oxygen and glucose sensing microdomains entrapped within the same hydrogel. Using the developed GIG scheme, we successfully constructed a multiplexed glucose sensor and a multianalyte glucose-lactate sensor. The next chapter describes the development of unique nanomaterial enabled microcapsule based polymeric optical sensors that may be used to detect enzymatic reactions as well.

7. GOLD NANOCLUSTER CONTAINING POLYMERIC MICROCAPSULES FOR RATIOMETRIC FLUORESCENCE BIOSENSING*

7.1. Introduction

Detection of hydrogen peroxide (H_2O_2) has received extensive attention due to its relevance in chemical, environmental, clinical, and biological applications. [170, 171] H_2O_2 is released as a by-product of several enzymatic reactions that enables the indirect detection of the reaction substrates and the tracking of enzymatic activity by monitoring fluctuations in H_2O_2 levels. [170, 172] Over the years H_2O_2 detection has enabled the development of numerous enzymatic biosensors[170, 172-175] and has also permitted advances in enzymatic activity assays.[176, 177] As stated and demonstrated in Chapter 3, enzyme deactivation poses to be a big problem for enzymatic sensors and H_2O_2 mediated deactivation plays a major role. All forms of enzymatic sensors are marred by enzyme deactivation over time that eventually leads to complete sensor failure; additionally all implantable devices trigger host immune response that is usually characterized by an increase in local H_2O_2 levels. Both, oxidoreductase enzyme catalyzed H_2O_2 release and macrophage mediated H_2O_2 have detrimental effects on the sensor's operational lifetime; thus having a means to monitor H_2O_2 in hydrogel based enzymatic sensors is necessary to facilitate better sensor design. For composite hydrogel based enzymatic sensors, it

* Reprinted with permission from "Gold Nanocluster Containing Polymeric Microcapsules for Intracellular Ratiometric Fluorescence Biosensing" by Biswas. A., Banerjee. S., Gart. E.V., Nagaraja. A.T., McShane. M.J. *ACS Omega* 2017, *2 (6), 2499-2506*. Copyright 2017 by American Chemical Society.

would be beneficial to be able optically detect levels of H_2O_2. There have been a number of optical methods to detect H_2O_2 concentrations using small-molecule fluorescent probes, [178-182] nanoparticles, [183-185] and recombinant fluorescent proteins. [186-188] However, these methods utilize custom made dyes or recombinant protein that are experimentally difficult to make and/or often require specialized techniques (two photon detection, short lifetime detection).

Gold nanoclusters (AuNCs) have emerged as a promising tool for biosensing and bioimaging applications owing to their high quantum yield, large stokes shift, photo and chemical stability, nano-size and low toxicity. [189-191] AuNCs are usually capped by a protein or chemical ligand in order to enhance structural stability and photo-luminescence characteristics. [192, 193] Bovine serum albumin (BSA) mediated biomineralization technique to fabricate luminescent AuNCs entrapped within BSA (BSA-AuNCs) has gained popularity due to its moderately high quantum yield, long wavelength emission, surface modification capabilities, and facile synthesis using mild reaction conditions. The BSA scaffold covalently interacts with the AuNCs and provides steric shielding, enhancing the structural stability of the AuNCs that in turn engenders highly stable luminescence over a broad range of pH and salt concentrations. [194] Prior studies have shown that the luminescence of BSA-AuNCs is sensitive to H_2O_2; potentially offering a cheaper and non-toxic alternative to commercially available H_2O_2 quantification systems (*e.g.* o-dianisidine, tetramethylbenzidine, and 2,2-azino-bis(3-ethylbenzothiazoline-6-sulphonicacid)). To further take advantage of H_2O_2 mediated quenching of BSA-AuNCs, a number of optical sensing assays for analytes including

glucose, cholesterol, and acetylcholine have been developed by combining BSA-AuNCs and substrate specific enzymes. [64, 195, 196] However, protease induced enzymatic degradation of the BSA scaffold can also affect the luminescence of BSA-AuNCs [197, 198] which poses a problem for the use of BSA-AuNC enabled sensors to detect small-molecule analytes (*e.g.* H_2O_2, glucose, lactate *etc*.) in complex biological samples.

In this work, microcapsules containing BSA-AuNCs and FluoSpheres are introduced as H_2O_2 sensors with two key features overcoming limitations of non-encapsulated BSA-AuNCs: (1) the capsules protect the BSA-AuNCs from detrimental interactions with the external environment and (2) the incorporation of FluoSpheres with complementary emission spectra facilitates ratiometric luminescence intensity measurements. Micro- and nano- sized polymeric capsules fabricated with the layer-by-layer (LbL) method have been shown as effective carriers for optical indicators in biosensing applications [12, 93, 96] due to the semipermeable nature of the polyelectrolyte multilayer (PEM) films. These LbL nanofilms physically confine the sensing reagents, allowing selective permeability of small molecules while excluding larger macromolecules and proteins [89, 199]. In this case, the capsules shield the BSA-AuNCs from damaging proteases while permitting the free entry of analyte (H_2O_2).

The photostable fluospheres are unaffected by changes in pH [200] and therefore serve as a highly effective reference material when it is used in combination with BSA-AuNCs to monitor changes in H_2O_2. Such an intensity reference enables ratiometric measurements by reducing the influence of nonspecific effects on sensor response such as excitation source intensity fluctuations, variations in sensor concentration, and sample

scattering; this is imperative for intensity based *in vivo* and intracellular measurements where there are numerous interfering factors. There are a few prior examples of BSA-AuNC based ratiometric pH assays, forged by covalently tagging pH responsive fluorescein-isothiocyanate (FITC) to the amine groups of BSA-AuNCs. [201-203] These single-molecule sensors exhibit strong pH sensitivity, potentially making them susceptible to errors in tracking H_2O_2 fluctuations. Herein the response of the FluoSpheres and BSA-AuNCs containing microcapsule sensors to changes in H_2O_2 was evaluated and for the first time the use of these ratiometric microcapsule based sensors to sense H_2O_2 *in vitro* and *in vivo* (murine RAW 264.7) was demonstrated (Appendix A). Furthermore, the ability of these capsules to monitor glucose oxidase mediated reaction in order to track analyte and enzyme activity was also demonstrated.

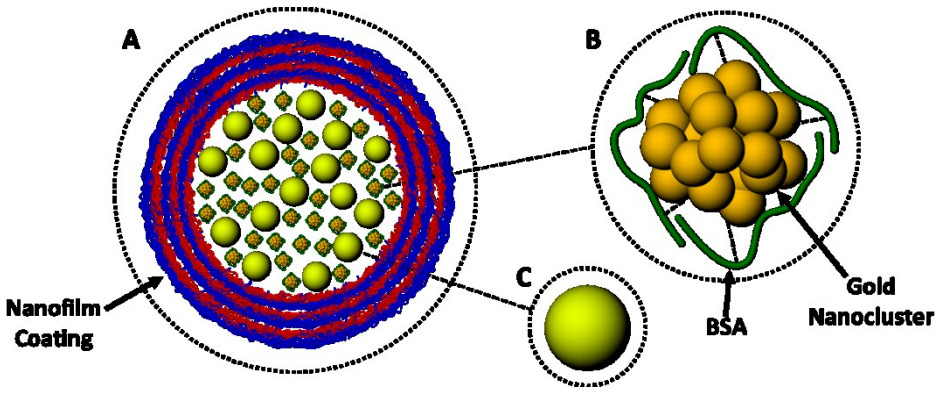

Figure 33. (A) Microcapsule based hydrogen peroxide sensor, (B) BSA-AuNC, (C) FluoSphere.

7.2. Experimental section

7.2.1. Chemicals

Sodium carbonate (Na_2CO_3), calcium chloride ($CaCl_2$), bovine serum albumin (BSA), α -chymotrypsin from bovine pancreas, trypsin from bovine pancreas, papain from papaya latex, proteinase K from *Tritirachium album*, gold (III) chloride trihydrate ($HAuCl_4.3H_2O$), hydrogen peroxide (H_2O_2), poly (sodium 4-styrenesulfonate) (PSS, average Mw 70000 Da), poly (diallyldimethylammonium chloride) (PDADMAC, average Mw 100000-200000 Da), phorbol 12-myristate 13-acetate (PMA), poly (vinylsulfonic acid) (PVSA), Dulbecco's modified Eagle's medium (DMEM), fetal bovine serum (FBS), sodium hydroxide (NaOH), phosphate buffered saline (PBS), buffer salts ($NaHCO_3$, HEPES, CHES, CH_3COONa), and ethylenediaminetetraacetic acid (EDTA) were purchased from Sigma-Aldrich and used without further purification. Carboxylate modified, 0.02 μm, yellow-green (505/515) FluoSpheres were obtained from Thermo Fisher Scientific. Glucose oxidase (GOx) from *Aspergillus niger* was purchased from BBI solutions.

7.2.2. Fabrication of H_2O_2 sensing microcapsules

BSA gold nanoclusters (BSA-AuNCs) were fabricated using the green-one-pot synthesis method described elsewhere. [194] Briefly, 1 mL of aqueous BSA (50 mg/mL), 1 mL of $HAuCl_4$ (10 mM), and 100 μL of NaOH (1 M) were mixed and stirred moderately for 12 h at 37 ^{O}C. The resulting AuNC solution was mixed with FluoSpheres (0.78 nM) and 0.2 M Na_2CO_3 to obtain a final volume of 9 mL while maintaining the volume ratio

66:3:95. To the mixture 9 mL of 0.16 M $CaCl_2$ was added and allowed to react for 10 min at 25 °C while being stirred rapidly (800 RPM). PVSA (225 µL, 25 wt. % in H_2O) was also added to the mixture, 2 min after the start of the reaction. PEMs were coated onto the BSA-AuNC/FluoSpheres loaded $CaCO_3$ microparticles by alternately exposing the particles to oppositely charged PDADMAC (20 mg/mL, pH 8) and PSS (20 mg/mL, pH 8) until 10 bilayers were deposited. After each polyelectrolyte deposition step the particles were washed with $NaHCO_3$ (5 mM, pH 8) to get rid of excess polyelectrolytes. To quantify encapsulation efficiency, a fraction of the cargo-loaded microparticles was exposed to EDTA (0.2 M, pH 7.2) to release encapsulated materials [12, 204] The relative amount of BSA-AuNCs and FluoSpheres released was calculated by measuring fluorescence intensity at 682 nm and 516 nm, respectively, when excited at 445 nm and by using calibration curves obtained from known concentrations of BSA-AuNCs and FluoSpheres. Finally, hollow microcapsules were made by suspending the PEM coated $CaCO_3$ microparticles containing BSA-AuNCs / FluoSpheres in EDTA solution (0.2 M, pH 7.2) for 1 h followed by washing with $NaHCO_3$ (5 mM, pH 8). Zeta potential was measured using a Malvern ZetaSizer Nano Series ZEN 3600 spectrometer.

7.2.3. Sensitivity of sensors to proteases and to pH variation

Non-encapsulated BSA-AuNCs (10 µL from the prepared stock) or encapsulated BSA-AuNCs / FluoSpheres ratiometric sensors (made from 0.67 mg of LbL coated microparticles) was added to proteases solution (1mg/mL in PBS) and incubated at 37 ^{O}C for 4 h. The control experiments were similarly conducted in the absence of

proteases. The relative sensor response R/R^0 was calculated where R and R^0 represent BSA-AuNC luminescence intensities in the presence and absence of proteases respectively. To evaluate the sensitivity of the ratiometric sensors to pH, microcapsules were suspended in CH_3COONa (5mM, pH 5), HEPES (5mM, pH 7), and CHES (5mM, pH 9) for 2 h at 37 ^{O}C. Photoluminescence measurements were made using Tecan Infinite M200 PRO with i-Control 1.8 software. Samples contained in black 96 well plates were excited at 445 nm to collect emission spectra from 500 to 800 nm.

7.2.4. Sensor response measurements

Microcapsule sensors fabricated by dissolving 0.67 mg of PEM coated microparticles were incubated for 30 min at 37 °C in different concentrations of H_2O_2 (0 – 1000 μM, 100 μL). H_2O_2 solutions were prepared using PBS and the photoluminescence response of the sensors at each H_2O_2 concentration was measured. For glucose sensing experiments, 0.67 mg of PEM coated microparticles suspended in 50 μL GOx (0.6 mg/mL) were incubated for 30 min at 37 °C with different concentrations of glucose (0-3.2 mM) prepared in PBS. The microcapsule responses were measured using a Tecan Infinite M200 PRO plate reader with i-Control 1.8 software. The luminescence intensity of composite hydrogels containing H_2O_2 sensing microcapsules was measured using an ISS PC1 spectrofluorometer connected to a bifurcated fiber optic bundle. Response time of the sensors when exposed to H_2O_2 was computed by evaluating the time required for the response ratio to drop by 63.2% from the initial ratio. [205] The limit of detection (*LOD*) and maximum observable peroxide

concentration (*MOPC*) was calculated by determining the H_2O_2 concentrations at $R_{516/682(min)} + 3\sigma$ and $R_{516/682(max)} - 3\sigma$ respectively, where $R_{516/682(min)}$ is the sensor response at 0 μM H_2O_2, $R_{516/682(max)}$ is the sensor response at 1000 μM H_2O_2, and σ is the standard error of the response across three separate sensor batches. The analytical range was calculated as *Range* = *MOPC-LOD* and sensor sensitivity was computed using $S = [R_{516/682\,(max)} - R_{516/682\,(min)}] / R_{516/682\,(min)} \cdot 100 / Range$.

7.2.5. Confocal imaging

All confocal and differential interference contrast (DIC) images of samples were obtained using an inverted microscope (Olympus IX81) having a spinning disk confocal unit (Yokogawa CSU-X1) and attached to an iXon897 EMCCD camera (Andor Technology). For confocal imaging, samples were viewed with a 40X oil immersion objective (1.3 NA), and excited using a 445 nm laser. Fluorescence images of FluoSpheres and BSA-AuNCs were captured using 525/15 nm band pass and 633 long pass emission filters, respectively. To image response of microcapsule sensors to varying concentrations of H_2O_2, 10 μL of microcapsule suspension was dropped on a cover slip for imaging. Confocal images of macrophages were obtained directly in glass bottom dishes. Mean luminescence intensity values were calculated from images in FluoSpheres and BSA-AuNC emission channels; sensor response ratios were generated by dividing FluoSphere mean intensity by BSA-AuNC average intensity values. Pseudocolored images were obtained by dividing the FluoSpheres pixel intensities by the BSA-AuNCs

pixel intensities. All images were analyzed using ImageJ software. Sensor parameters were calculated from mean sensor intensity ratios.

7.3. Results and discussion

7.3.1. Characterization of microcapsule sensors

Microcapsule based ratiometric hydrogen peroxide sensors (Figure 33A) were fabricated by co-encapsulating H_2O_2 sensitive BSA-AuNCs (Figure 33B) and H_2O_2-insensitive FluoSpheres (Figure 33C). These materials have spectrally separate emission spectra but overlapping excitation spectra, [194, 200] which enables the use of a single excitation source to simultaneously excite both materials and generate dual-emission. Figure 34A depicts the individual emission spectra of the FluoSpheres and the BSA-AuNCs along with the emission spectra of the microcapsule sensors containing both the FluoSpheres and the BSA-AuNCs. When excited at 445 nm the microcapsule sensors exhibited dual emission with peaks centered at 516 and 682 nm, which are similar to those observed when illuminating FluoSpheres and AuNCs separately. The loading efficiency of BSA-AuNCs and FluoSpheres was estimated to be ~ 53% and ~ 20%, respectively; proteins (BSA) act as additives during the nucleation process and are more readily adsorbed onto the surface of the primary nanocrystallites that ultimately combine to form the highly porous $CaCO_3$ microstructure, resulting in higher encapsulation.[167] As estimated from analysis of confocal images, the mean diameter of the microcapsule sensors was ~ 7 μm. When suspended in buffer solution (0.01 M $NaHCO_3$, pH 8) the microcapsule sensors were well dispersed and showed no visible signs of aggregation;

zeta potential measurement revealed that the PEM-coated microcapsules had a high surface charge (-70.3 ± 1.4 mV) corroborating their colloidal stability.

Prior studies have demonstrated that degradation of the BSA shell *via* protease-catalyzed hydrolysis of peptide bonds decreases BSA-AuNC luminescence intensity, [197, 198] thereby rendering the sensors ineffective in reporting peroxide changes in the presence of proteases found in many biological systems. We hypothesized that protecting the BSA-AuNCs within LbL microcapsules would protect against this degradation and preserve function of the BSA-AuNC in peroxide response. The ability of PEMs to exclude damaging proteases and prevent quenching of the BSA-AuNCs was assessed by exposing the sensors to common proteases (chymotrypsin, trypsin, papain, and proteinase K). Non-encapsulated BSA-AuNCs showed ~ 55%, ~ 44%, ~ 37%, and ~ 64% loss in luminescence when exposed to chymotrypsin, trypsin, papain, and proteinase K respectively (Figure 34B). In contrast, BSA-AuNCs encapsulated in PEM-lined microcapsules retained their luminescence intensities (~ 100%) when exposed to the same proteases, (Figure 34B) indicating that PEMs exclude proteases and protect the luminescent reporters. Furthermore, we found no significant difference ($p > 0.05$) in luminescence of co-encapsulated FluoSpheres and BSA-AuNCs when incubated in different pH (5, 7, 9) solutions (Figure 35); confirming that the co-encapsulated FluoSpheres serve as a more robust reference material than pH-sensitive organic dyes such as FITC.

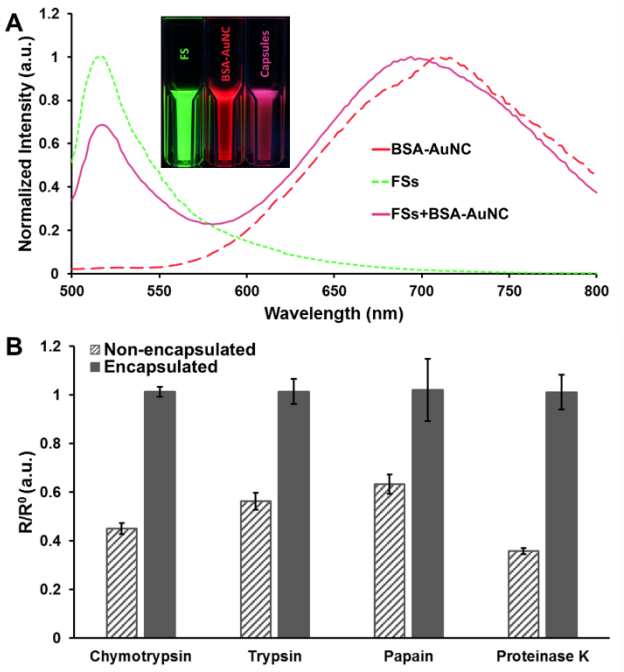

Figure 34. (A) Normalized emission spectra of FluoSpheres (green - - -), BSA-AuNC (red — —), and microcapsules containing both FluoSpheres and BSA-AuNC (pink —), (Inset) photographs of luminescent FluoSpheres, BSA-AuNC, and microcapsules containing both FluoSpheres and BSA-AuNC suspended in solution under UV illumination, (B) plots of R/R^0 of non-encapsulated BSA-AuNC (dark grey stripe) and encapsulated BSA-AuNC (dark grey solid) in the presence of proteases. Here R and R^0 represent BSA-AuNC luminescence intensities in the presence and absence of proteases respectively. Error bars represent 95% confidence intervals for three separate batches of sensors.

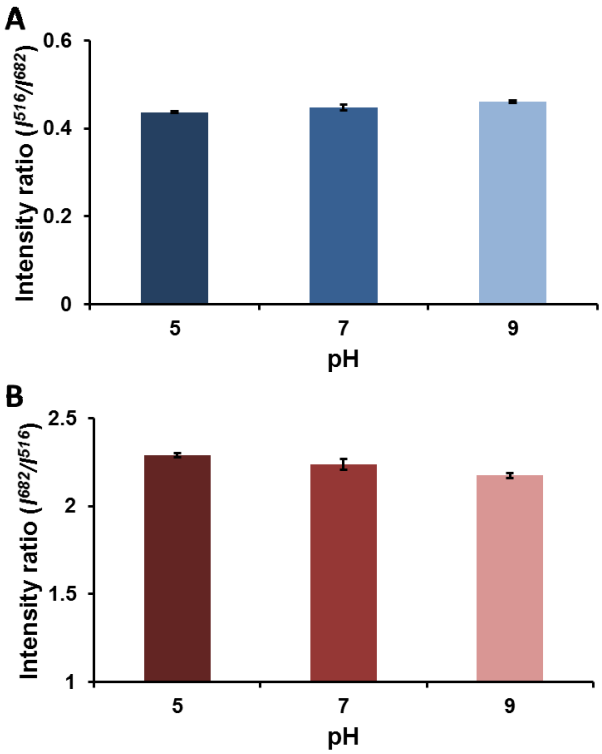

Figure 35. Ratiometric response of microcapsule sensors at different pH, normalized to (A) BSA-AuNC peak (682 nm) and (B) FSs peak (516 nm). Error bars represent 95% confidence intervals for three separate batches of microcapsule sensors.

7.3.2. Response of microcapsule sensors to H_2O_2

The microcapsule sensors responded rapidly to the exposure of H_2O_2, with a mean response time of ~ 9 min. The change in response of the microcapsule sensors at varying concentrations of H_2O_2 was evaluated; as seen in Figure 36A an increase in H_2O_2 concentration decreased the emission of the BSA-AuNCs progressively, while the emission of the FluoSpheres remained relatively constant. By plotting the intensity ratios (I_{516} / I_{682}) against H_2O_2 concentrations (Figure 36B) two distinct linear regions in the

range 0-200 μM (R^2=0.98) and 200-1000 μM (R^2=0.98) were observed. These findings are similar to the quenching profiles reported previously for BSA-AuNCs. [64, 201] The average *LOD*, *MOPC*, analytical range and sensitivity per unit range were ~ 26.20 μM, ~ 858.5 μM, ~ 832.7 μM, and ~ 0.2% / μM, respectively. Subsequently, these sensors were imaged using confocal microscopy at various H_2O_2 concentrations. Microcapsules were incubated in different H_2O_2 concentrations and were imaged to obtain average luminescence intensity ratios. Figure 36 D-F contain representative pseudocolored images of microcapsules at 0 μM, 400 μM, and 1000 μM H_2O_2 respectively. Figure 36D is predominantly blue, characteristic to a low mean intensity ratio (0.56 ± 0.04) whereas Figure 36F has a mixture of yellow-red microcapsules representing a higher mean ratio (1.58 ± 0.06) and Figure 36E has a green microcapsule population with an intermediate mean ratio (1.25 ± 0.03). By plotting the mean intensity ratios acquired from confocal imaging against H_2O_2 concentrations, a response curve (Figure 36C) analogous to that obtained using the plate reader was obtained. Similar to Figure 36B, Figure 36C reveals a ratiometric response with two separate linear regions spanning 0-200 μM (R^2=0.99) and 200-1000 μM (R^2=0.97). The average *LOD*, *MOPC*, analytical range and sensitivity per unit range were found to be ~ 34.90 μM, ~ 619.8 μM, ~ 584.9 μM, and ~ 0.3% / μM respectively; the differences in calculated sensor parameters between the data acquired using spectrophotometry and confocal microscopy, is ascribed to the differences in the optical set-ups used to collect data.

If these microcapsules are immobilized in a glucose sensing hydrogels containing GOx and Cat, the capsules could potentially monitor the gradual release of H_2O_2 over

time as micromolar levels of H_2O_2 can drastically reduce sensor performance. It is known that in two enzyme sensor systems, Cat scavenges H_2O_2 produced *via* enzymatic reactions that drive the sensor; this enhances the longevity of the analyte specific enzyme (GOx in this case) and Cat as well. It should also be noted that Cat is more susceptible to H_2O_2 mediated deactivation than GOx, as such the concentration of Cat in enzymatic sensors has traditionally been greater than GOx concentration.[51, 206] Having a method to optically detect low levels of H_2O_2 release would be extremely useful in better sensor design.

7.3.3. Use of microcapsule sensors to monitor enzymatic reactions

Before incorporating the microcapsules in hydrogels the response of these sensors to enzymatic reactions that generate H_2O_2 was evaluated, while the capsules were suspended in solution. Although, this dissertation is focused on using these microcapsules to monitor enzymatic activity and H_2O_2 release in hydrogels, these microcapsules may also be used to detect physiologically relevant analytes *in vitro,* when coupled with an appropriate enzyme. We evaluated the response of these microcapsules at constant GOx concentration while increasing glucose concentration; with increase in glucose concentration the fluorescence intensity (Figure 37A) decreases progressively at 682 nm while intensity at 516 nm remains constant. A plot of the intensity ratio I_{516} / I_{682} (Figure 37B) reveals that the ratio increases with increasing glucose, having high linearity (R^2=0.99) between 0.08-0.8 mM glucose; the average *LOD*, *MOPC*, analytical range and were found to be ~ 0.06 mM, ~ 1.23 μM, and ~ 1.17 μM respectively. These

experiments not only underscore the use of the microcapsules to monitor enzymatic reactions but it also demonstrates that the microcapsules can be used to *in vitro* detection of glucose, especially in biological samples as the sensing chemistry is protected by the capsule walls.

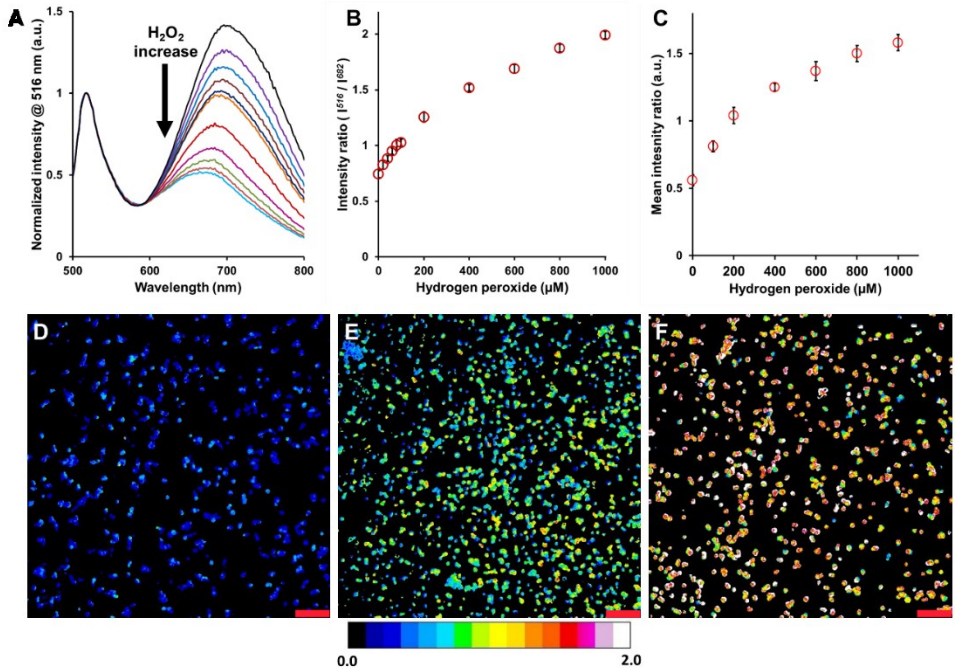

Figure 36. (A) Emission spectra of microcapsules containing both FluoSpheres and BSA-AuNC to 0 μM (black), 20 μM (purple), 40 μM (blue), 60 μM (maroon), 80 μM (navy blue), 100 μM (orange), 200 μM (bright red), 400 μM (pink), 600 μM (green), 800 μM (red), and 1000 μM hydrogen peroxide (light blue), mean ratiometric response of microcapsules containing both FluoSpheres and BSA-AuNC to varying concentrations of hydrogen peroxide obtained using microplate spectrophotometer (B) and obtained using ratiometric images (C) of microcapsules. Confocal, ratiometric fluorescence images of microcapsules containing both FluoSpheres and BSA-AuNC at (D) 0 μM, (E) 400 μM, and (F) 1000 μM hydrogen peroxide. Pseudocolored images represent the ratio of emission intensities collected using 510-540 nm band pass filter and 633 long pass filter, when excited at 445 nm. Scale bars correspond to 20 μm. Error bars represent 95% confidence intervals for at least three separate samples of microcapsule sensors.

7.3.4. Incorporation of microcapsules into hydrogels

The microcapsule sensors were designed to potentially monitor the release of H_2O_2 over time, when hydrogel based glucose or lactate sensors were subjected to extreme glucose or lactate levels. Just like other optical H_2O_2 reporters, BSA-AuNCs are quenched cumulatively and non-reversibly by H_2O_2, thus they cannot measure the instantaneous level of H_2O_2 within a dynamic system (*e.g.* within an enzymatic hydrogel sensor). However, this is a step forward in the right direction as measuring H_2O_2 liberation within hydrogel based sensors would provide insights to design more stable enzymatic sensors. That being said, due to instrumentation constraints it was not possible to obtain discernible signal from capsules entrapped inside hydrogels. Before even moving on to hydrogel based sensors, the capsules were immobilized in hydrogels that do not contain any sensing chemistry. First, capsules fabricated from 0.67 mg, 6.7 mg, and 13.4 mg of calcium carbonate particles were disperse in an alginate precursor-mix to fabricate composite alginate hydrogels (for details refer to section 3.2.5). Even with a really high concentration of microcapsules no distinct emission peaks were observed when excited appropriately (300-450 nm); we speculate that a high degree of scattering from the hydrogel and the capsules produces a low signal-to-noise ratio, prohibiting any emission intensity measurements. A different hydrogel, HEMA-co-Aam was also used for microcapsule immobilization; this hydrogel allows more transmission of light and thus is a better candidate to immobilize the capsule based optical sensors. However, even with HEMA-co-Aam we could not obtain any emission signal from immobilized capsules fabricated from 0.67 mg, 6.7 mg, and 13.4 mg of calcium carbonate particles. It seems that at such short excitation wavelengths that inherently engender a high degree of scattering, it would be

logical to use an excitation source with a higher intensity or to use a two photon system. A two photon system would enable the use of longer wavelengths to excite the microcapsules; longer excitation wavelengths would mitigate excessive scattering which might lead to a better signal-to-noise ratio. However, due to unavailability of such instruments these experiments were not further pursued.

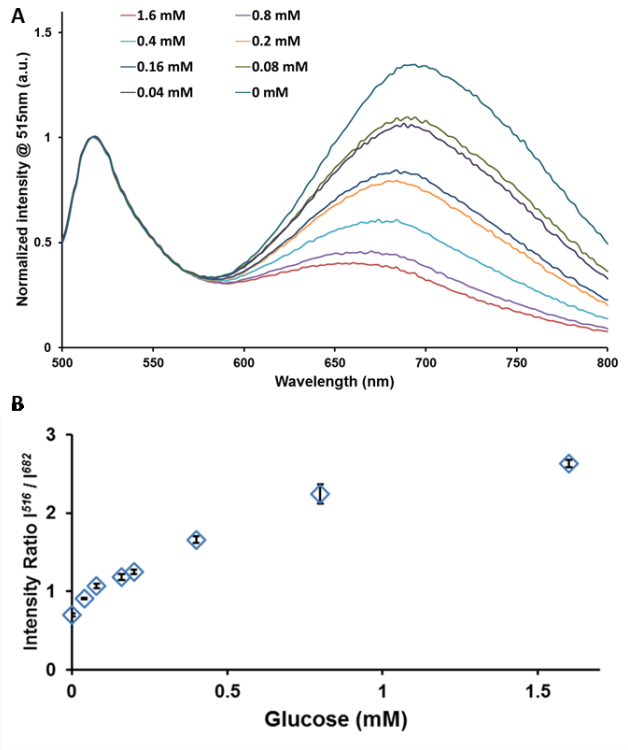

Figure 37. (A) Emission spectra of microcapsules containing both FluoSpheres and BSA-AuNC to increasing glucose, (B) mean ratiometric response of microcapsules containing both FluoSpheres and BSA-AuNC to varying concentrations of glucose obtained using microplate spectrophotometer. Error bars represent 95% confidence intervals for at least three separate samples of microcapsule sensors.

7.4. Conclusion

A method to fabricate polymeric microcapsule-based ratiometric H_2O_2 sensors was demonstrated using a combination of BSA-AuNC and a reference fluorescent nanoparticle. The microcapsules are beneficial for direct detection of H_2O_2, in applications that involve complex biological samples. Additionally, it is noteworthy that BSA-AuNCs have also been used for environmental monitoring of hazardous materials (*e.g.* Hg^{2+}, cyanide)[207, 208]; thus, the ratiometric microcapsule-based platform may also be advantageous for use in similar applications. Ratiometric sensing facilitates reliable measurements and the semi-permeable nature of the LbL microcapsule walls protects the BSA-AuNCs from catalytic enzymes and non-specifically binding macromolecules. The microcapsule sensors were also used to monitor glucose oxidation by GOx in order to determine glucose concentration changes. Potentially these H_2O_2 sensors could be coimmobilized in enzymatic hydrogels to track release of H_2O_2 over time; however, neither FluoSphere nor BSA-AuNC emission signal could be detected.

8. CONCLUSIONS AND FUTURE DIRECTIONS

This work has shown the ability to use PEMs as the lining to microdomains containing encapsulated sensing chemistry, and particularly that these PEMs significantly affect the overriding response characteristics of nanocomposite enzymatic sensors. It was possible to tune the diffusion of a model analyte (glucose) over a rather wide range by changing the multilayer composition and also by chemical cross-linking. This capability to adjust response is critical to engineering devices that function well in different environments (*e.g.* in vivo, interstitial fluid, inflamed tissue), where substrate delivery may be altered from normal. The substrate permeation rate may be precisely regulated by changing the layer composition or number of spacer bilayers, as these factors determine the extent of intralayer and interlayer crosslinking. On average, the cross-linked films showed ~86 % decrease in glucose diffusion compared to non-cross-linked films, without affecting corresponding oxygen permeation. The cross-linked microcapsule sensors embedded in an MPAC hydrogel demonstrate the potential for complete control over relevant analytical range and sensitivity between 3 and 9 cross-linked layers. It is expected that use of other materials with alternative reactive side groups as well as deposition under different conditions to alter film structure (*e.g.* pH, salt control over polyelectrolyte conformation) will enable additional adjustment of diffusion. This provides a powerful tool to tune the dynamics of any flux-based system, which includes sensors such as the model glucose system explored here as well as controlled-release systems for medicines, fertilizers, self-healing materials, *etc*.

Although these nanocomposite glucose sensors showed promise for use as implantable sensors, sensor stability studies revealed that these hydrogel sensors, which were fabricated by using $CaCO_3$ templates were highly unstable for long term. The lifetime response of these sensors progressively deteriorated > 50% within 3 days of continuous glucose exposure. The loss in sensor response was attributed to GOx deactivation overtime, prompting the search for alternative GOx encapsulation templates to enhance GOx stability.

GOx is highly susceptible to deactivation by spontaneous enzyme denaturation and *via* H_2O_2 mediated inactivation.[110] In case of enzymatic glucose sensors, deactivated GOx leads to drifting sensor response over time requiring frequent recalibrations eventually leading to complete sensor failure. Researchers have investigated various techniques to alleviate GOx deactivation in order to prolong a sensor's operational lifetime. To reduce enzyme deactivation in the nanocomposite glucose sensors prepared by GOx encapsulation in $CaCO_3$ microparticles, two strategies were employed: (1) introduction of Cat and (2) immobilization of GOx in a polymeric matrix. H_2O_2 irreversibly causes enzyme deactivation especially under low oxygen conditions; this is particularly important as the hydrogels sensors are designed for tissue implantation where oxygen levels are significantly lower than ambient oxygen.[110] Furthermore, in continuously operating sensors H_2O_2 mediated GOx inactivation contributes to the majority of enzyme activity loss. The released H_2O_2 can be easily counteracted by Cat facilitated catalysis of H_2O_2 that produces H_2O and O_2. Thus, we introduced a second enzyme Cat in our sensors to assuage H_2O_2 mediated GOx inactivation. Additionally, it

has also been proven that enzyme stability is enhanced when enzymes are immobilized in polymer matrices. This is due to stabilization of the enzyme's tertiary structure *via* interactions with the surrounding polymer matrix.[150] Therefore, we replaced the hollow microcontainers with alginate hydrogel microspheres that contain sensing chemistry. Oxidoreductase based enzymatic sensors usually contain excess Cat in order to reduce the rate of GOx inactivation.[209] Ideally, it would be advantageous to have a higher concentration of Cat in the hydrogel microspheres; however, it should be remembered that an increased Cat concentration would reduce sensor sensitivity drastically.

An updated and a newer generation of nanocomposite hydrogels was developed using AMPs containing PdTCPP, GOx, and Cat. The versatility of the LbL process allows the deposition of LbL coatings on a variety of micro- and nano- sized colloidal templates; thus the cross-linked PAH/PSS diffusion barrier was easily translated onto bioactive AMPs that were used to make AnA sensors. These sensors outperformed all other generations of optical hydrogel based glucose sensors by having: (1) a wide analytical range while operating at physiologically low oxygen levels and (2) a high degree of sensor signal retention under continuous operation. The AnA sensors exhibited an analytical range of 2.6 – 350 mg/dL glucose at low oxygen, and it was estimated that the sensor response would drop by 50% if exposed to ~173 intermittent bursts of high glucose over 2 weeks. Furthermore, to establish the versatility of this sensor design lactate sensors were developed; for the first time nanocomposite hydrogel based optical lactate sensors that operate at physiologically low oxygen was demonstrated. These

sensors revealed exceptional sensitivity in the range 4.5 – 13.5 mg/dL of lactate at low oxygen and were extremely stable under continuous operation.

Although both the glucose and the lactate sensors perform extraordinary well at low oxygen and similar nanocomposite hydrogels have shown good tissue integration with minimal host response in animal studies (data not shown), there are certain limitations. The major drawback is the use of green excitable phosphor PdTCPP for *in vivo* applications. The complex nature of skin causes absorption and scattering of photons when light is either incident (excitation) on skin or emanating (emission) from skin; thus, hindering unaltered propagation of light leading to reduced signal-to-noise ratio. Early research pertaining to tissue optics identified 600 - 1300 nm as the optical window where there is minimal scattering and absorption of light from tissue.[17] Although PdTCPP emits around 700 nm, its 530 nm (green) excitation wavelength causes low signal-to-noise ratio when collecting data from implanted hydrogel sensors. Substituting PdTCPP with another phosphorescent metalloporphyrin dye that has longer excitation and emission wavelengths would allow greater light penetration into tissue and solve the low signal-to-noise ratio problem. Both commercially available and custom made metallo-benzo-porphyrins that are red excitable (~700 nm) and emit in the near infrared region (~830 nm) may be used as alternative optical indicators. However, metallo-benzo-porphyrins are usually less sensitive to oxygen (low lifetime when unquenched), which would mandate careful sensor response optimization. Another aspect that may be altered is the alginate matrix that houses the nanofilm bound microspheres; the outer hydrogel matrix interacts with the body physiology when

implanted and plays a huge role in biocompatibility. The alginate hydrogel matrix can potentially be replaced by other antifouling hydrogels (*e.g.* poly(ethylene glycol) diacrylate,[210] poly (hydroxyethyl methacrylate),[211] poly-L-lactic acid,[212] poly (vinyl alcohol)[213]) or foul releasing hydrogels (*e.g.* poly(N -isopropylacrylamide) based copolymers[214, 215]). However, depending on the matrix used the permeability of analyte (glucose or lactate) would change and mandate reoptimization of the nanofilms that coat the microspheres. It should also be noted that the glucose and lactate sensors discussed in this dissertation are in the form of hydrogel discs, which cannot be implanted easily; ideally the sensors should be small enough to fit a ~18 gauge needle in order to be subcutaneously implanted. Nevertheless, any changes in sensor size would require further sensor response optimization as well. For a particular optical reporter and sensor size-shape combination, several parameters may be altered to modulate sensor response; these parameters include relative amounts of encapsulated enzyme (GOx, LOx, and Cat) in each microdomain, number of microdomains per unit volume of the hydrogel sensors, and the rate of permeation of analyte into the microdomains.

Cooperative effect, a phenomenon characteristic to any enzyme based nanocomposite hydrogel sensor was also demonstrated. Understanding cooperative effect is imperative to design a future generation of multiplexed, multimodal, or multianalyte enzymatic sensors. Using glucose sensing and oxygen sensing microdomains it was found that enzyme-based microdomain sensors embedded within a hydrogel matrix affect local oxygen concentrations in a cooperative fashion; oxygen levels and hence optical response of a particular enzymatic microdomain was influenced

by other surrounding microdomains. Hypothetically it might seem possible to elicit independent sensor response by entrapping different types of bioactive microdomains within the same matrix; however experiments revealed that it was near impossible to achieve independent response without losing individual sensor response. In order to achieve independent multianalyte and multi-functional sensing we developed the GIG'em design for hydrogel based sensors; this design lays the groundwork to develop implantable multiplexed sensors. Once enzymatic sensors that operate at physiological conditions are miniaturized sufficiently to allow direct implantation the GIG'em design may be used to fabricate dual- or multi- analyte sensors. This design would also allow the introduction of reference oxygen sensors to correct for internal oxygen fluctuations when using enzymatic glucose and lactate sensors.

Finally, a new microcapsule based ratiometric H_2O_2 sensor is introduced for potentially monitoring enzymatic reactions in hydrogel based enzymatic sensors (*e.g.* glucose sensor, lactate sensor). Although preliminary results using a plate reader were promising, it was not possible to obtain any emission signal from such microcapsules immobilized in hydrogel matrices. This could possibly be due to intense scattering of lower wavelength excitation light incident on hydrogels; this limitation can probably be circumvented by using a higher power excitation source or a two photon excitation system. The current generation of AlgMP based glucose and lactate sensors have been shown to be highly stable under near physiological conditions, as such there is no urgent need to develop a system to monitor H_2O_2 release inside hydrogel sensors. However, with proper instrumentation and by using other H_2O_2 probes, preferably with long

wavelength excitation and emission characteristics, enzymatic activity inside hydrogel sensors might be easily tracked.

REFERENCES

1. B. W. Ward, *Preventing chronic disease*, 2014, **11**.
2. D. L. Hoyert and J. Xu, *Natl Vital Stat Rep*, 2012, **61**, 1-51.
3. J. Gerteis, D. Izrael, D. Deitz, L. LeRoy, R. Ricciardi, T. Miller and J. Basu, *Rockville, MD: Agency for Healthcare Research and Quality (AHRQ) Publications*, 2014.
4. A. M. Miniño and S. L. Murphy, *NCHS data brief*, 2012, **99**, 1-8.
5. U. E. Bauer, P. A. Briss, R. A. Goodman and B. A. Bowman, *The Lancet*, 2014, **384**, 45-52.
6. L. C. Clark and C. Lyons, *Annals of the New York Academy of sciences*, 1962, **102**, 29-45.
7. J. D. Newman and A. P. F. Turner, *Biosensors and Bioelectronics*, 2005, **20**, 2435-2453.
8. J. Wang, *Electroanalysis*, 2001, **13**, 983.
9. D. C. Klonoff, *Diabetes care*, 2005, **28**, 1231-1239.
10. M. J. McShane, R. J. Russell, M. V. Pishko and G. L. Cote, *IEEE Engineering in Medicine and Biology Magazine*, 2000, **19**, 36-45.
11. J. Roberts, B. B. Collier and M. J. McShane, 2011.
12. A. Biswas, A. T. Nagaraja and M. J. McShane, *ACS applied materials & interfaces*, 2014, **6**, 21193-21201.

13. C. f. D. Control and Prevention, *Atlanta, GA: US Department of Health and Human Services*, 2014, **2014**.

14. W. H. Organization, *Journal*, 2016.

15. M. J. Sheetz and G. L. King, *Jama*, 2002, **288**, 2579-2588.

16. G. Freckmann, C. Schmid, A. Baumstark, S. Pleus, M. Link and C. Haug, *Journal of diabetes science and technology*, 2012, **6**, 1060-1075.

17. D. D. Cunningham and J. A. Stenken, *In vivo glucose sensing*, John Wiley & Sons, 2009.

18. K. Nakamura and A. Balo, *Journal of diabetes science and technology*, 2015, 1932296815577812.

19. R. R. Gehlaut, G. Y. Dogbey, F. L. Schwartz, C. R. Marling and J. H. Shubrook, *Journal of diabetes science and technology*, 2015, 1932296815581052.

20. S. Garg and L. Jovanovic, *Diabetes Care*, 2006, **29**, 2644-2649.

21. E. Toschi and H. Wolpert, *Endocrinology and Metabolism Clinics of North America*, 2016, **45**, 895-904.

22. S. K. Vashist, *Diagnostics*, 2013, **3**, 385-412.

23. N. Wisniewski and M. Reichert, *Colloids and Surfaces B: Biointerfaces*, 2000, **18**, 197-219.

24. M. T. Novak, F. Yuan and W. M. Reichert, *Analytical and bioanalytical chemistry*, 2010, **398**, 1695-1705.

25. S. P. Nichols, A. Koh, W. L. Storm, J. H. Shin and M. H. Schoenfisch, *Chemical Reviews*, 2013, **113**, 2528-2549.

26. L. Zhang, Z. Cao, T. Bai, L. Carr, J.-R. Ella-Menye, C. Irvin, B. D. Ratner and S. Jiang, *Nature biotechnology*, 2013, **31**, 553-556.

27. H. Shibata, Y. J. Heo, T. Okitsu, Y. Matsunaga, T. Kawanishi and S. Takeuchi, *Proceedings of the National Academy of Sciences*, 2010, **107**, 17894-17898.

28. Y. J. Heo, H. Shibata, T. Okitsu, T. Kawanishi and S. Takeuchi, *Proceedings of the National Academy of Sciences*, 2011, **108**, 13399-13403.

29. J. Roberts, B. B. Collier and M. J. McShane, 2011.

30. O. S. Wolfbeis, *Fresenius' Zeitschrift für analytische Chemie*, 1986, **325**, 387-392.

31. K. Kajiwara, T. Uemura, H. Kishikawa, K. Nishida, Y. Hashiguchi, M. Uehara, M. Sakakida, K. Ichinose and M. Shichiri, *Medical & biological engineering & computing*, 1993, **31**, S17-S22.

32. C. D. Malchoff, K. Shoukri, J. I. Landau and J. M. Buchert, *diabetes care*, 2002, **25**, 2268-2275.

33. J. L. Lambert, J. M. Morookian, S. J. Sirk and M. S. Borchert, *Journal of Raman Spectroscopy*, 2002, **33**, 524-529.

34. B. D. Cameron, J. S. Baba and G. L. Coté, *Diabetes technology & therapeutics*, 2001, **3**, 201-207.

35. K. V. Larin, M. S. Eledrisi, M. Motamedi and R. O. Esenaliev, *Diabetes care*, 2002, **25**, 2263-2267.

36. M.-S. Steiner, A. Duerkop and O. S. Wolfbeis, *Chemical Society Reviews*, 2011, **40**, 4805-4839.

37. M. A. Arugula and A. Simonian, *Measurement Science and Technology*, 2014, **25**, 032001.

38. S. Chinnayelka and M. J. McShane, *Biomacromolecules*, 2004, **5**, 1657-1661.

39. F. Khan, T. E. Saxl and J. C. Pickup, *Analytical biochemistry*, 2010, **399**, 39-43.

40. T. D. James, in *Creative Chemical Sensor Systems*, Springer, 2007, pp. 107-152.

41. V. V. Karnati, X. Gao, S. Gao, W. Yang, W. Ni, S. Sankar and B. Wang, *Bioorganic & medicinal chemistry letters*, 2002, **12**, 3373-3377.

42. A. Sensor, *Schultz, Sohrab Mansouri, Irwin J. Goldstein--Diabetes Care*, 1982, **5**.

43. M. Mortellaro and A. DeHennis, *Biosensors and Bioelectronics*, 2014, **61**, 227-231.

44. F. Hussain, D. J. S. Birch and J. C. Pickup, *Analytical Biochemistry*, 2005, **339**, 137-143.

45. A. M. Hartnett, C. M. Ingersoll, G. A. Baker and F. V. Bright, *Analytical chemistry*, 1999, **71**, 1215-1224.

46. R. Esposito, B. Della Ventura, S. De Nicola, C. Altucci, R. Velotta, D. G. Mita and M. Lepore, *Sensors*, 2011, **11**, 3483-3497.

47. R. Narayanaswamy and F. Sevilla III, *Analytical letters*, 1988, **21**, 1165-1175.

48. J. F. Sierra, J. Galban, S. de Marcos and J. R. Castillo, *Analytica Chimica Acta*, 1998, **368**, 97-104.

49. S. De Marcos, J. Galindo, J. Sierra, J. Galban and J. Castillo, *Sensors and Actuators B: Chemical*, 1999, **57**, 227-232.

50. J. F. Sierra, J. Galban and J. R. Castillo, *Analytical Chemistry*, 1997, **69**, 1471-1476.

51. R. Wilson and A. Turner, *Biosensors and Bioelectronics*, 1992, **7**, 165-185.

52. W. Trettnak, M. J. Leiner and O. S. Wolfbeis, *Biosensors*, 1989, **4**, 15-26.

53. S. R. Nayak and M. J. McShane, *Sensor Letters*, 2006, **4**, 433-439.

54. J. W. Attridge and G. A. Robinson, *Journal*, 1993.

55. Y.-H. You, A. Nagaraja, A. Biswas, H. Marks, G. L. Coté and M. J. McShane, 2015.

56. M. McCurley, *Biosensors and Bioelectronics*, 1994, **9**, 527-533.

57. A. C. Mack, M. Jinshu and M. J. McShane, 2005.

58. O. S. Wolfbeis, A. Dürkop, M. Wu and Z. Lin, *Angewandte Chemie International Edition*, 2002, **41**, 4495-4498.

59. T. Chih, H.-J. Jao and C. M. Wang, *Journal of Electroanalytical Chemistry*, 2005, **581**, 159-166.

60. P. Wu, Y. He, H.-F. Wang and X.-P. Yan, *Analytical chemistry*, 2010, **82**, 1427-1433.

61. L. Cao, J. Ye, L. Tong and B. Tang, *Chemistry–A European Journal*, 2008, **14**, 9633-9640.

62. L.-L. Wang, J. Qiao, L. Qi, X.-Z. Xu and D. Li, *Science China Chemistry*, 2015, **58**, 1508-1514.

63. L.-L. Wang, J. Qiao, H.-H. Liu, J. Hao, L. Qi, X.-P. Zhou, D. Li, Z.-X. Nie and L.-Q. Mao, *Analytical Chemistry*, 2014, **86**, 9758-9764.

64. L. Jin, L. Shang, S. Guo, Y. Fang, D. Wen, L. Wang, J. Yin and S. Dong, *Biosensors and Bioelectronics*, 2011, **26**, 1965-1969.

65. M. Wu, Z. Lin, A. Dürkop and O. S. Wolfbeis, *Analytical and bioanalytical chemistry*, 2004, **380**, 619-626.

66. W. Trettnak, M. J. Leiner and O. S. Wolfbeis, *Analyst*, 1988, **113**, 1519-1523.

67. B. P. Schaffar and O. S. Wolfbeif, *Biosensors and Bioelectronics*, 1990, **5**, 137-148.

68. B. Dremel, S.-Y. Li and R. Schmid, *Biosensors and Bioelectronics*, 1992, **7**, 133-139.

69. M. C. Moreno-Bondi, O. S. Wolfbeis, M. J. Leiner and B. P. Schaffar, *Analytical chemistry*, 1990, **62**, 2377-2380.

70. Z. Rosenzweig and R. Kopelman, *Analytical chemistry*, 1996, **68**, 1408-1413.

71. X.-D. Wang, T.-Y. Zhou, X. Chen, K.-Y. Wong and X.-R. Wang, *Sensors and Actuators B: Chemical*, 2008, **129**, 866-873.

72. A. Neubauer, D. Pum, U. B. Sleytr, I. Klimant and O. S. Wolfbeis, *Biosensors and Bioelectronics*, 1996, **11**, 317-325.

73. A. Pasic, H. Koehler, L. Schaupp, T. R. Pieber and I. Klimant, *Analytical and bioanalytical chemistry*, 2006, **386**, 1293-1302.

74. A. Pasic, H. Koehler, I. Klimant and L. Schaupp, *Sensors and Actuators B: Chemical*, 2007, **122**, 60-68.

75. J. B. Slate and P. C. Lord, *Journal*, 1996.

76. K. M. Curry, *Journal*, 1989.

77. G. H. Thomas, R. M. Watson and J. O. Noell, *Journal*, 1992.

78. D. B. Papkovsky, *Sensors and Actuators B: Chemical*, 1993, **11**, 293-300.

79. R. W. Mason, R. E. Slovacek and K. J. Sullivan, *Journal*, 2002.

80. J. R. Lakowicz, *Principles of fluorescence spectroscopy*, Springer Science & Business Media, 2013.

81. Y. Amao, *Microchimica Acta*, 2003, **143**, 1-12.

82. D. B. Papkovsky and T. C. O'Riordan, *Journal of fluorescence*, 2005, **15**, 569-584.

83. G. S. Wilson and Y. Hu, *Chemical Reviews*, 2000, **100**, 2693-2704.

84. J. Lu, I. Do, L. T. Drzal, R. M. Worden and I. Lee, *ACS Nano*, 2008, **2**, 1825-1832.

85. R. Rego, N. Caetano, R. Vale and A. Mendes, *Journal of Membrane Science*, 2004, **244**, 35-44.

86. J. Q. Brown, R. Srivastava and M. J. McShane, *Biosensors and Bioelectronics*, 2005, **21**, 212-216.

87. R. Srivastava, J. Q. Brown, H. Zhu and M. J. McShane, *Macromolecular Bioscience*, 2005, **5**, 717-727.

88. E. W. Stein, D. V. Volodkin, M. J. McShane and G. B. Sukhorukov, *Biomacromolecules*, 2006, **7**, 710-719.

89. M. McShane and D. Ritter, *Journal of Materials Chemistry*, 2010, **20**, 8189-8193.

90. J. Park and M. J. McShane, *ACS applied materials & interfaces*, 2010, **2**, 991-997.

91. G. Decher, *science*, 1997, **277**, 1232-1237.

92. G. B. Sukhorukov, E. Donath, H. Lichtenfeld, E. Knippel, M. Knippel, A. Budde and H. Möhwald, *Colloids and Surfaces A: physicochemical and engineering aspects*, 1998, **137**, 253-266.

93. W. Tong, X. Song and C. Gao, *Chemical Society Reviews*, 2012, **41**, 6103-6124.

94. M.-L. De Temmerman, J. Demeester, S. C. De Smedt and J. Rejman, *Nanomedicine*, 2012, **7**, 771-788.

95. T. A. Duchesne, J. Brown, K. B. Guice, Y. M. Lvov and M. J. McShane, *Sensors and materials*, 2002, **14**, 293-308.

96. M. J. McShane, J. Brown, K. B. Guice and Y. M. Lvov, *Journal of nanoscience and nanotechnology*, 2002, **2**, 411-416.

97. X. Liu and M. L. Bruening, *Chemistry of Materials*, 2004, **16**, 351-357.

98. M. D. Miller and M. L. Bruening, *Langmuir*, 2004, **20**, 11545-11551.

99. R. Malaisamy and M. L. Bruening, *Langmuir*, 2005, **21**, 10587-10592.

100. J. R. Roberts, J. Park, K. Helton, N. Wisniewski and M. J. McShane, *Journal*, 2012.

101. R. M. Unruh, J. R. Roberts, S. P. Nichols, S. Gamsey, N. A. Wisniewski and M. J. McShane, *Journal of diabetes science and technology*, 2015, **9**, 985-992.

102. L. P. Andrus, R. Unruh, N. A. Wisniewski and M. J. McShane, *Biosensors*, 2015, **5**, 398-416.

103. J. R. Roberts, D. W. Ritter and M. J. McShane, *Journal of Materials Chemistry B*, 2013, **1**, 3195-3201.

104. J. R. Roberts, Texas A&M University, 2014.

105. S. Singh and M. McShane, *Biosensors and Bioelectronics*, 2010, **25**, 1075-1081.

106. S. Singh, Texas A&M University, 2010.

107. D. A. Gough, J. Y. Lucisano and P. H. S. Tse, *Analytical Chemistry*, 1985, **57**, 2351-2357.

108. J. Parker and C. Schwartz, *Biotechnology and bioengineering*, 1987, **30**, 724-735.

109. D. A. Gough, L. S. Kumosa, T. L. Routh, J. T. Lin and J. Y. Lucisano, *Science Translational Medicine*, 2010, **2**, 42ra53-42ra53.

110. P. H. Tse and D. A. Gough, *Biotechnology and bioengineering*, 1987, **29**, 705-713.

111. J. K. Leypoldt and D. A. Gough, *Analytical Chemistry*, 1984, **56**, 2896-2904.

112. B. B. COLLIER, Texas A&M University, 2013.

113. G. Jobst, I. Moser, M. Varahram, P. Svasek, E. Aschauer, Z. Trajanoski, P. Wach, P. Kotanko, F. Skrabal and G. Urban, *Analytical Chemistry*, 1996, **68**, 3173-3179.

114. G. S. Wilson and R. Gifford, *Biosensors and Bioelectronics*, 2005, **20**, 2388-2403.

115. Y. You, A. Nagaraja, A. Biswas, J. Hwang, G. Cote and M. McShane, *IEEE Sensors Journal*, 2016, **PP**, 1-1.

116. J. M. Morais, F. Papadimitrakopoulos and D. J. Burgess, *The AAPS journal*, 2010, **12**, 188-196.

117. M. C. Frost and M. E. Meyerhoff, *Current Opinion in Chemical Biology*, 2002, **6**, 633-641.

118. S. Carrara, S. Ghoreishizadeh, J. Olivo, I. Taurino, C. Baj-Rossi, A. Cavallini, M. Op de Beeck, C. Dehollain, W. Burleson and F. G. Moussy, *Sensors*, 2012, **12**, 11013-11060.

119. D. M. Budgett, A. P. Hu, P. Si, W. T. Pallas, M. G. Donnelly, J. W. Broad, C. J. Barrett, S.-J. Guild and S. C. Malpas, *Journal of Applied Physiology*, 2007, **102**, 1658-1663.

120. L. S. Kumosa, T. L. Routh, J. T. Lin, J. Y. Lucisano and D. A. Gough, *Biomaterials*, 2014, **35**, 8287-8296.

121. E. W. Stein, P. S. Grant, H. Zhu and M. J. McShane, *Analytical chemistry*, 2007, **79**, 1339-1348.

122. J. Q. Brown and M. J. McShane, *Biosensors and Bioelectronics*, 2006, **21**, 1760-1769.

123. D. A. Gough, *Introduction to Bioengineering*, 2001, **44**, 57-66.

124. A. Biswas, A. T. Nagaraja, Y.-H. You, J. R. Roberts and M. J. McShane, *RSC Advances*, 2016, **6**, 71781-71790.

125. R. Srivastava, J. Brown, H. Zhu and M. J. McShane, *Biotechnology and bioengineering*, 2005, **91**, 124-131.

126. A. Vikartovská, M. Bučko, D. Mislovičová, V. Pätoprstý, I. Lacík and P. Gemeiner, *Enzyme and Microbial Technology*, 2007, **41**, 748-755.

127. D. B. Papkovsky, G. V. Ponomarev, W. Trettnak and P. O'Leary, *Analytical Chemistry*, 1995, **67**, 4112-4117.

128. M. F. Montero-Baker, K. Y. Au-Yeung, N. A. Wisniewski, S. Gamsey, L. Morelli-Alvarez, J. L. Mills, M. Campos and K. L. Helton, *Journal of vascular surgery*, 2015, **61**, 1501-1510.

129. G. Rocchitta, A. Spanu, S. Babudieri, G. Latte, G. Madeddu, G. Galleri, S. Nuvoli, P. Bagella, M. I. Demartis and V. Fiore, *Sensors (Basel, Switzerland)*, 2016, **16**, 780.

130. K. Kleppe, *Biochemistry*, 1966, **5**, 139-143.

131. T. Santoni, D. Santianni, A. Manzoni, S. Zanardi and M. Mascini, *Talanta*, 1997, **44**, 1573-1580.

132. D. A. Baker and D. A. Gough, *Biosensors and Bioelectronics*, 1993, **8**, 433-441.

133. D. A. Gough and T. Bremer, *Diabetes Technology and Therapeutics*, 2000, **2**, 377-380.

134. P. H. S. Tse and D. A. Gough, *Biotechnology and Bioengineering*, 1987, **29**, 705-713.

135. M. M. Choi, *Microchimica Acta*, 2004, **148**, 107-132.

136. V. P. Zanini, B. L. de Mishima and V. Solís, *Sensors and Actuators B: Chemical*, 2011, **155**, 75-80.

137. G. Palleschi, M. Mascini, L. Bernardi and P. Zeppilli, *Medical and biological Engineering and Computing*, 1990, **28**, B25-B28.

138. T. C. Jansen, J. van Bommel and J. Bakker, *Critical care medicine*, 2009, **37**, 2827-2839.

139. J. B. Claver, M. V. Mirón and L. Capitán-Vallvey, *Analyst*, 2009, **134**, 1423-1432.

140. N. J. White, *Science Translational Medicine*, 2015, **7**, 278ec243-278ec243.

141. K. Rathee, V. Dhull, R. Dhull and S. Singh, *Biochemistry and Biophysics Reports*, 2016, **5**, 35-54.

142. M. R. Romero, F. Ahumada, F. Garay and A. M. Baruzzi, *Analytical chemistry*, 2010, **82**, 5568-5572.

143. T. Shimomura, T. Sumiya, M. Ono, T. Itoh and T.-a. Hanaoka, *Procedia Chemistry*, 2012, **6**, 46-51.

144. S. Pérez and E. Fàbregas, *Analyst*, 2012, **137**, 3854-3861.

145. R. Jayant, M. McShane and R. Srivastava, *Drug delivery*, 2009, **16**, 331-340.

146. D. V. Volodkin, A. I. Petrov, M. Prevot and G. B. Sukhorukov, *Langmuir*, 2004, **20**, 3398-3406.

147. L. Bornhoeft, A. Biswas and M. McShane, *Biosensors*, 2017, **7**, 8.

148. A. Mills, *Sensors and Actuators B: Chemical*, 1998, **51**, 60-68.

149. G. J. Kost and M. McQueen, *Critical reviews in clinical laboratory sciences*, 1993, **30**, 153-202.

150. D. Dinelli, W. Marconi and F. Morisi, *Methods in enzymology*, 1976, **44**, 227-243.

151. I. Moser, G. Jobst and G. A. Urban, *Biosensors and Bioelectronics*, 2002, **17**, 297-302.

152. C. Cordeiro, M. de Vries, W. Ngabi, P. Oomen, T. Cremers and B. Westerink, *Biosensors and Bioelectronics*, 2015, **67**, 677-686.

153. G. Jobst, I. Moser, M. Varahram, P. Svasek, E. Aschauer, Z. Trajanoski, P. Wach, P. Kotanko, F. Skrabal and G. Urban, *Analytical Chemistry*, 1996, **68**, 3173-3179.

154. J. Yan, V. A. Pedrosa, A. L. Simonian and A. Revzin, *ACS applied materials & interfaces*, 2010, **2**, 748-755.

155. M. P. Massafera and S. I. C. de Torresi, *Electroanalysis*, 2011, **23**, 2534-2540.

156. H. Huang, W. Song, G. Chen, J. M. Reynard, T. Y. Ohulchanskyy, P. N. Prasad, F. V. Bright and J. F. Lovell, *Advanced healthcare materials*, 2014, **3**, 890-890.

157. M. Montero-Baker, L. Morelli-Alvarez, K. Helton and K. Y. Au-Yeung, *Journal of Vascular Surgery*, 2014, **2**, 548-549.

158. P. J. Brothers and J. P. Collman, *Accounts of Chemical Research*, 1986, **19**, 209-215.

159. D. Papkovsky and T. O'Riordan, *Journal of Fluorescence*, 2005, **15**, 569-584.

160. H. Huang, W. Song, J. Rieffel and J. F. Lovell, *Frontiers in Physics*, 2015, **3**.

161. S. Nagl and O. S. Wolfbeis, *Analyst*, 2007, **132**, 507-511.

162. B. Zelelow, G. E. Khalil, G. Phelan, B. Carlson, M. Gouterman, J. B. Callis and L. R. Dalton, *Sensors and Actuators B: Chemical*, 2003, **96**, 304-314.

163. M. E. Köse, A. Omar, C. A. Virgin, B. F. Carroll and K. S. Schanze, *Langmuir*, 2005, **21**, 9110-9120.

164. C. R. Schroeder, G. Neurauter and I. Klimant, *Microchimica Acta*, 2007, **158**, 205-218.

165. Y. Tian, B. R. Shumway, A. C. Youngbull, Y. Li, A. K.-Y. Jen, R. H. Johnson and D. R. Meldrum, *Sensors and Actuators B: Chemical*, 2010, **147**, 714-722.

166. B. B. Collier and M. J. McShane, 2011.

167. A. I. Petrov, D. V. Volodkin and G. B. Sukhorukov, *Biotechnology progress*, 2005, **21**, 918-925.

168. J. Jeon, V. Panchagnula, J. Pan and A. V. Dobrynin, *Langmuir*, 2006, **22**, 4629-4637.

169. B. B. Collier and M. J. McShane, *Analytical Chemistry*, 2012, **84**, 4725-4731.

170. W. Chen, S. Cai, Q.-Q. Ren, W. Wen and Y.-D. Zhao, *Analyst*, 2012, **137**, 49-58.

171. M. B. Grisham, *Comparative Biochemistry and Physiology Part A: Molecular & Integrative Physiology*, 2013, **165**, 429-438.

172. S. Chen, R. Yuan, Y. Chai and F. Hu, *Microchimica Acta*, 2013, **180**, 15-32.

173. S. A. Evans, J. M. Elliott, L. M. Andrews, P. N. Bartlett, P. J. Doyle and G. Denuault, *Analytical Chemistry*, 2002, **74**, 1322-1326.

174. J. Wang, *Journal of pharmaceutical and biomedical analysis*, 1999, **19**, 47-53.

175. S. P. Mohanty and E. Kougianos, *Ieee Potentials*, 2006, **25**, 35-40.

176. H. Bisswanger, *Perspectives in Science*, 2014, **1**, 41-55.

177. R. K. Scopes, *eLS*, 2002.

178. D. Srikun, E. W. Miller, D. W. Domaille and C. J. Chang, *Journal of the A merican Chemical Society*, 2008, **130**, 4596-4597.

179. E. W. Miller, O. Tulyathan, E. Y. Isacoff and C. J. Chang, *Nat Chem Biol*, 2007, **3**, 263-267.

180. E. W. Miller, A. E. Albers, A. Pralle, E. Y. Isacoff and C. J. Chang, *Journal of the American Chemical Society*, 2005, **127**, 16652-16659.

181. M. C. Y. Chang, A. Pralle, E. Y. Isacoff and C. J. Chang, *Journal of the American Chemical Society*, 2004, **126**, 15392-15393.

182. E. A. K. Warren, T. S. Netterfield, S. Sarkar, M. L. Kemp and C. K. Payne, *Scientific Reports*, 2015, **5**, 16929.

183. H. Jin, D. A. Heller, M. Kalbacova, J.-H. Kim, J. Zhang, A. A. Boghossian, N. Maheshri and M. S. Strano, *Nature Nanotechnology*, 2010, **5**, 302-309.

184. J.-H. Kim, C. R. Patra, J. R. Arkalgud, A. A. Boghossian, J. Zhang, J.-H. Han, N. F. Reuel, J.-H. Ahn, D. Mukhopadhyay and M. S. Strano, *Acs Nano*, 2011, **5**, 7848-7857.

185. D. A. Heller, H. Jin, B. M. Martinez, D. Patel, B. M. Miller, T.-K. Yeung, P. V. Jena, C. Höbartner, T. Ha and S. K. Silverman, *Nature nanotechnology*, 2009, **4**, 114-120.

186. M. Malinouski, Y. Zhou, V. V. Belousov, D. L. Hatfield and V. N. Gladyshev, *PloS one*, 2011, **6**, e14564.

187. V. V. Belousov, A. F. Fradkov, K. A. Lukyanov, D. B. Staroverov, K. S. Shakhbazov, A. V. Terskikh and S. Lukyanov, *Nature methods*, 2006, **3**, 281-286.

188. C. T. Dooley, T. M. Dore, G. T. Hanson, W. C. Jackson, S. J. Remington and R. Y. Tsien, *Journal of Biological Chemistry*, 2004, **279**, 22284-22293.

189. M. Abrams and B. Murrer, *Science*, 1993, **261**, 725-730.

190. X.-D. Zhang, Z. Luo, J. Chen, S. Song, X. Yuan, X. Shen, H. Wang, Y. Sun, K. Gao, L. Zhang, S. Fan, D. T. Leong, M. Guo and J. Xie, *Scientific Reports*, 2015, **5**, 8669.

191. L.-Y. Chen, C.-W. Wang, Z. Yuan and H.-T. Chang, *Analytical chemistry*, 2014, **87**, 216-229.

192. G. Wang, T. Huang, R. W. Murray, L. Menard and R. G. Nuzzo, *Journal of the American Chemical Society*, 2005, **127**, 812-813.

193. Z. Wu and R. Jin, *Nano Letters*, 2010, **10**, 2568-2573.

194. J. Xie, Y. Zheng and J. Y. Ying, *Journal of the American Chemical Society*, 2009, **131**, 888-889.

195. X. Chen and G. A. Baker, *Analyst*, 2013, **138**, 7299-7302.

196. H. Li, Y. Guo, L. Xiao and B. Chen, *Biosensors and Bioelectronics*, 2014, **59**, 289-292.

197. L. Hu, S. Han, S. Parveen, Y. Yuan, L. Zhang and G. Xu, *Biosensors and Bioelectronics*, 2012, **32**, 297-299.

198. Y. Wang, Y. Wang, F. Zhou, P. Kim and Y. Xia, *Small*, 2012, **8**, 3769-3773.

199. A. Biswas, A. Nagaraja, Y. You, J. Roberts and M. J. McShane, *RSC Advances*, 2016, DOI: 10.1039/C6RA13507B.

200. M. T. Spence and I. D. Johnson, *The molecular probes handbook: a guide to fluorescent probes and labeling technologies*, Live Technologies Corporation, 2010.

201. C.-Y. Ke, Y.-T. Wu and W.-L. Tseng, *Biosensors and Bioelectronics*, 2015, **69**, 46-53.

202. C. Ding and Y. Tian, *Biosensors and Bioelectronics*, 2015, **65**, 183-190.

203. Y.-T. Wu, C. Shanmugam, W.-B. Tseng, M.-M. Hiseh and W.-L. Tseng, *Nanoscale*, 2016, **8**, 11210-11216.

204. A. Fernández and M. Vendrell, *Chemical Society Reviews*, 2016, **45**, 1182-1196.

205. K. Fu, S. Chen, J. Zhao and B. G. Willis, *ACS Sensors*, 2016, **1**, 444-450.

206. P. F. Greenfield, J. R. Kittrell and R. L. Laurence, *Analytical Biochemistry*, 1975, **65**, 109-124.

207. B. C. Dickinson, C. Huynh and C. J. Chang, *Journal of the American Chemical Society*, 2010, **132**, 5906-5915.

208. Y. Liu, K. Ai, X. Cheng, L. Huo and L. Lu, *Advanced Functional Materials*, 2010, **20**, 951-956.

209. J. Prenosil, *Biotechnology and bioengineering*, 1979, **21**, 89-109.

210. C. A. Quinn, R. E. Connor and A. Heller, *Biomaterials*, 1997, **18**, 1665-1670.

211. A. Marshall and B. D. Ratner, *AIChE Journal*, 2005, **51**, 1221-1232.

212. H. Koschwanez, F. Yap, B. Klitzman and W. Reichert, *Journal of Biomedical Materials Research Part A*, 2008, **87**, 792-807.

213. A. A. Sharkawy, B. Klitzman, G. A. Truskey and W. M. Reichert, *Journal of Biomedical Materials Research Part A*, 1998, **40**, 586-597.

214. A. A. Abraham, R. Fei, G. L. Coté and M. A. Grunlan, *ACS applied materials & interfaces*, 2013, **5**, 12832.

215. R. Fei, A. K. Means, A. A. Abraham, A. K. Locke, G. L. Coté and M. A. Grunlan, *Macromolecular Materials and Engineering*, 2016, **301**, 935-943.

216. T. Finkel and N. J. Holbrook, *Nature*, 2000, **408**, 239-247.

217. A. R. Lippert, G. C. Van de Bittner and C. J. Chang, *Accounts of Chemical Research*, 2011, **44**, 793-804.

218. E. A. Veal, A. M. Day and B. A. Morgan, *Molecular Cell*, 2007, **26**, 1-14.

219. S. G. Rhee, *Science*, 2006, **312**, 1882-1883.

220. M. Geiszt and T. L. Leto, *Journal of Biological Chemistry*, 2004, **279**, 51715-5 1718.

221. Y. Luo, H. Liu, Q. Rui and Y. Tian, *Analytical chemistry*, 2009, **81**, 3035-3041.

APPENDIX A

INTRACELLULAR RESPONSE OF GOLD NANOCLUSTER CONTAINING MICROCAPSULE BASED H2O2 SENSORS*

H_2O_2 is a reactive oxygen species and an important metabolite in living systems acting as a biomarker for oxidative stress and an indicator of cell damage. [216, 217] Over the years it has also been established that H_2O_2 is of paramount importance for cellular signal transduction pathways. [218, 219] In mammals, H_2O_2 has been associated with triggering immune cell response cascades and remodeling injured vasculature. [220] Physiological levels of H_2O_2 fluctuate in the micromolar range and under pathological conditions H_2O_2 concentrations may rise to millimolar levels. [181, 221]The multifaceted role of H_2O_2 in biochemical processes has motivated research to quantify and image cellular H_2O_2 concentrations using different methods (small-molecule fluorescent probes, [178-182] nanoparticles, [183-185] and recombinant fluorescent proteins [186-188]) After evaluating the response of the FluoSpheres and BSA-AuNCs containing microcapsule sensors to changes in H_2O_2 (Chapter 7), herein the use of these ratiometric microcapsule based sensors to image H_2O_2 in murine RAW 264.7 macrophage cells was demonstrated for the first time.

---

* Reprinted with permission from "Gold Nanocluster Containing Polymeric Microcapsules for Intracellular Ratiometric Fluorescence Biosensing" by Biswas. A., Banerjee. S., Gart. E.V., Nagaraja. A.T., McShane. M.J. *ACS Omega* 2017, *2 (6), 2499-2506*. Copyright 2017 by American Chemical Society.

A.1 Cell culture

For methods to fabricate the microcapsule sensors and confocal imaging techniques please refer to Section 7.2. Murine macrophage cells (RAW 264.7) were cultured in DMEM, containing high glucose and 10% FBS. The cell cultures were split (1/6) twice a week. A day before incubating the cells with the microcapsule sensors, the cells were passaged and seeded at a density of 3 X 10^4 cells/dish in 35 mm glass bottom dishes (Cellvis). For all sensor-response experiments, cells were incubated at 37 ^{O}C and 5% CO_2 with microcapsule sensors (fabricated from 6.7 mg of PEM coated microparticles) for 1 h. However, cells were incubated with the sensors for 24 h for the cell vitality assay analysis. Before imaging, all cells were moderately washed with PBS to remove unbound cells and excess microcapsule sensors. PMA (1 mg/mL stock) and H_2O_2 (10 mM stock) were directly added to cell culture media and incubated for 30 min before imaging. For cell vitality assay experiments, cells were incubated with 3 mL PBS containing calcein AM (2 μM) and ethidium homodimer (1 μM) for 15 min.

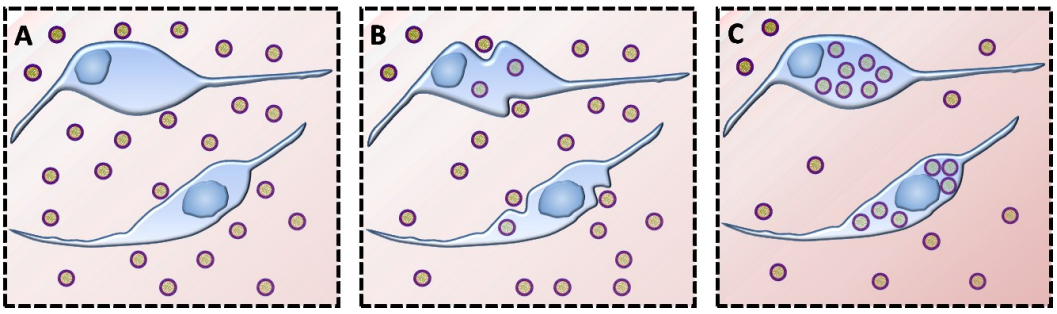

Figure A 1. (A) Microcapsule sensors incubated with macrophages, (B) microcapsule sensors being engulfed by macrophages, (C) microcapsule sensors ingested by macrophages.

A.2 Intracellular response of microcapsule sensors

Confocal and DIC images of RAW 264.7 macrophages incubated with microcapsule sensors for one hour indicated that the microcapsules were rapidly and effectively ingested by the cells (Figure A3 A-F). In comparison to macrophages that had not been incubated with microcapsules (Figure A3 F inset), the microcapsule-containing macrophages appear to be granular when viewed using DIC; this is ascribed to local optical-path gradients introduced by the internalized microcapsules. Using standard cell vitality assays, it was confirmed that the viability of the cells was unaltered after microcapsule ingestion (Figure A2). The mean intensity ratio (Figure A3 G) of the microcapsules ingested by the cells (Figure A3 A) was estimated to be 125% more than the ratio of the microcapsules that were not ingested (Figure A4 B) but present in the vicinity of the macrophages. The increase in ratio is attributed to the inherent H_2O_2 release by the macrophages to degrade the phagocytosed foreign materials. Treatment of the microcapsule-loaded cells with 500 μM H_2O_2 (Figure A3 B) served as a positive control and triggered an increase in ratio (Figure A3 G) of both the microcapsules inside the cells as well as the microcapsules present outside (Figure A4 D). The response of the extracellular microcapsules increased by 123% whereas the sensor response of the phagocytosed microcapsules increased by 35%. To further demonstrate the feasibility of the microcapsule based sensors to detect endogenous release of H_2O_2 in response to stimulants, the sensor-loaded cells were imaged after the cells were stimulated with PMA (Figure A3 C). The response (Figure A3 G) of the microcapsules outside the cells (Figure A4 F) was almost unaltered while the response of the sensors inside the cells

increased by 21%. This provides strong evidence that the macrophages release endogenous H_2O_2 in response to PMA stimulus, as reported by the internalized sensors, while the external sensors did not respond. These results demonstrate the benefit of BSA-AuNC microcapsule ratiometric sensors for imaging physiological H_2O_2 and detecting endogenous bursts of H_2O_2.

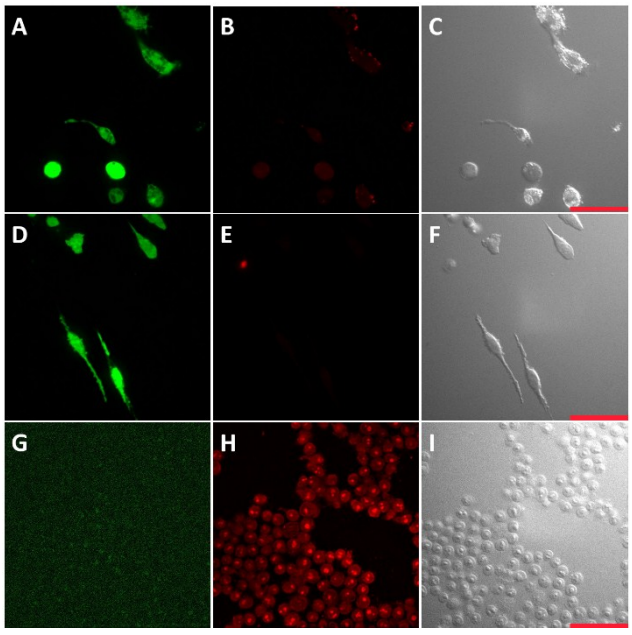

Figure A 2. Vitality assay of RAW 264.7 macrophages. CAM emission channel of (A) macrophages loaded with microcapsule sensors, (D) macrophages not incubated with microcapsule sensors [positive control], (G) macrophages treated with bug buster detergent (1X) [negative control]. Ethidium homodimer emission channel of (A) macrophages loaded with microcapsule sensors, (D) macrophages not incubated with microcapsule sensors [positive control], (G) macrophages treated with bug buster detergent (1X) [negative control]. (C), (F), and (I) DIC images of cells in panel (A, B), (D, E), and (G, H) respectively. Scale bars correspond to 50 µm.

To summarize, intracellular H_2O_2 fluctuations in response to external stimuli were detected. Given the excellent sensitivity and wide range of the response, these sensors may be potentially used to study cellular signaling pathways that involve low levels of H_2O_2 generation. Compared to other commercially available H_2O_2 detection assays, this microcapsule based system presents as an inexpensive and a non-toxic substitute. However, it is important to appreciate that internalization of microcapsules will depend, to a degree, on the external surface charge they present as well as the specific cells involved. It is therefore worth noting that these microcapsules are highly tailorable; the types of polyelectrolytes used and the conditions (*e.g.* pH, ionic strength) used during fabrication can easily alter capsule properties. For example if the intended application mandates a positive surface charge, the surface charge of our capsules can be easily changed to positive by switching the outer layer to a cationic polyelectrolyte (*e.g.* PDADMAC, poly(allylamine)).

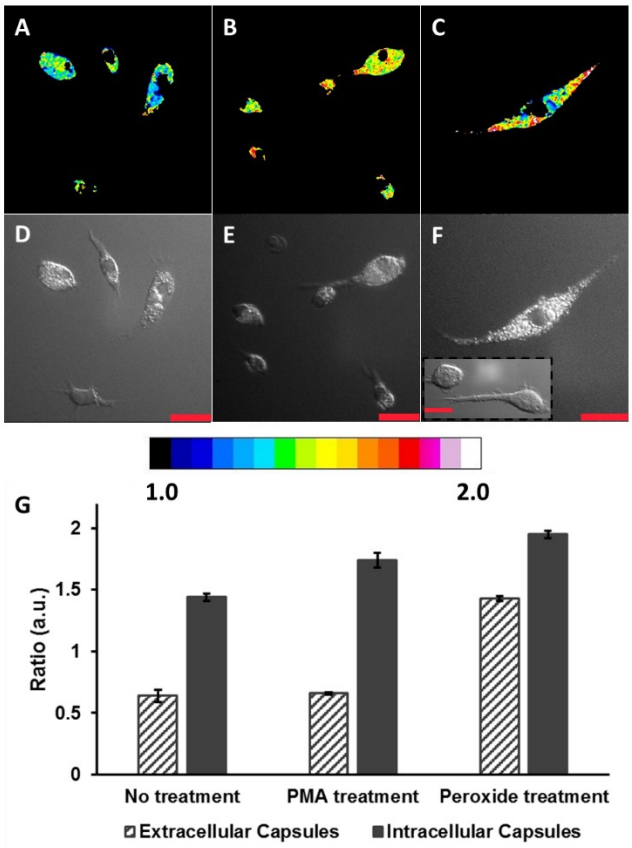

Figure A 3. Confocal fluorescence images of RAW 264.7 macrophage cells. Pseudocolored images represent the ratio of emission intensities collected using 510-540 nm band pass filter and 633 long pass filter, when excited at 445 nm. (A) Cells incubated with microcapsules for 1 h at 37 ^{O}C, (B) microcapsule loaded cells after PMA (2 µg/mL) exposure for 30 min at 37 ^{O}C, and (C) microcapsule loaded cells after H_2O_2 (500 µM) exposure for 30 min at 37 ^{O}C. (D), (E), and (F) DIC images of cells in panel (A), (B), and (C) respectively. Scale bars correspond to 30 µm. (G) Ratiometric response of extracellular (dark grey stripes) and intracellular (dark grey solid) microcapsule sensors. Error bars represent 95% confidence intervals for three separate batches of microcapsule sensors.

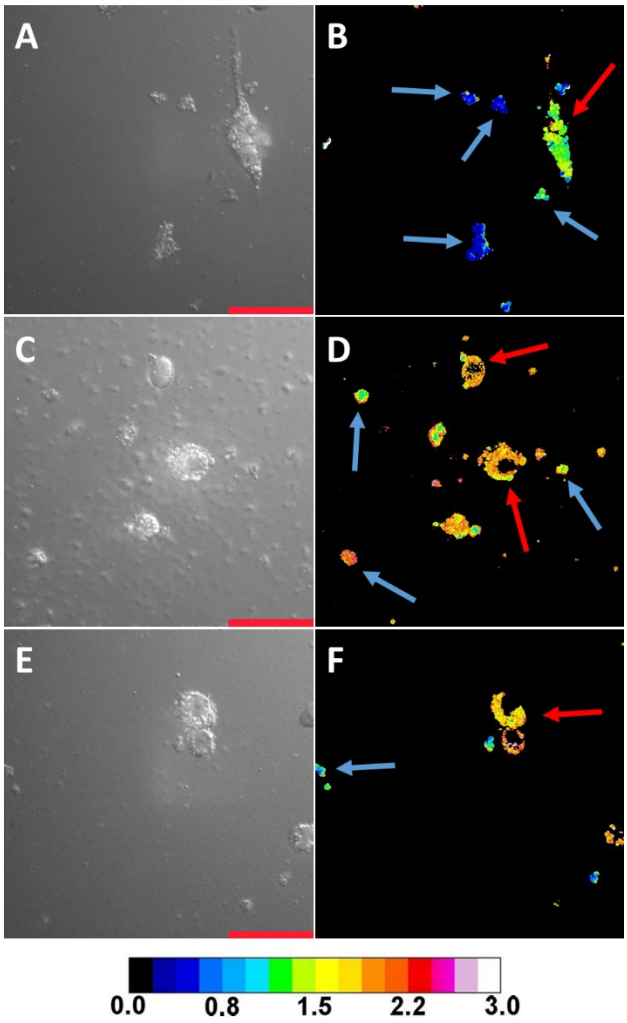

Figure A 4. Confocal ratiometric fluorescence images of RAW 264.7 macrophage cells. Pseudocolored images represent the ratio of emission intensities collected using 510-540 nm band pass filter and 633 long pass filter, when excited at 445 nm. (B) Cells incubated with microcapsules for 1 hr at 37 ^{O}C, (D) microcapsule loaded cells after H_2O_2 (500 µM) exposure for 30 mins at 37 ^{O}C, and (F) microcapsule loaded cells after PMA (2 µg/mL) exposure for 30 mins at 37 ^{O}C. (A), (C), and (E) DIC images of cells in panel (B), (D), and (F) respectively. Scale bars correspond to 50 µm. Blue arrows point to extracellular microcapsule sensors whereas red arrows point to microcapsule loaded cells.